EJBCS

Eurasian Journal of Biological and Chemical Sciences (Eurasian J. Bio. Chem. Sci.)

Cilt: 5 Volume: Suppl. 1 Year: 2022

e-ISSN 2651-5237

EJBCS

Eurasian Journal of Biological and Chemical Sciences

Cilt: 5 Volume: Suppl. 1 Year: 2022

Published Biannually

Corresponding Address

Gaziantep University, Faculty of Arts and Sciences, Department of Biology, Gaziantep, Turkey

E-mail: mtdogan1@gmail.com

Web: http://www.dergipark.org.tr/ejbcs

Owner / Publisher

Muhammet DOĞAN

This journal is peer-reviewed and published twice (June, December) a year.

All responsibility of the articles belongs to the authors.

e-ISSN 2651-5237

EJBCS
Eurasian Journal of Biological and Chemical Sciences

Cilt: 5 Volume: Suppl. 1 Year: 2022

Contents / İçindekiler

RESEARCH ARTICLE
Eurasian J Bio Chem Sci, 5(Suppl 1):105-110, 2022
https://doi.org/10.46239/ejbcs.1139843

EJBCS

Eurasian Journal of Biological and Chemical Sciences

Journal homepage: www.dergipark.org.tr/ejbcs

Perilen Bazlı Serin Pigmentlerin Moleküler Dinamik Simülasyonu ve NIR Bölgesinin Yansımasında Yapısal Özelliklerin İncelenmesi

Güray Kılınççeker[1*], Farhad Zarifi[1]

[*1]Çukurova Üniversitesi, Fen Edebiyat Fakültesi , Kimya Bölümü 01330 Balcalı, Sarıçam, Adana, Türkiye

*Corresponding author : gkilinc@cu.edu.tr
Orcid No: https://orcid.org/0000-0003-3030-4518

Received : 03/07/2022
Accepted : 09/08/2022

Özet: Güneş ışığının etkisini azaltan özel boyalarda kullanılan serin pigmentler genellikle perilenler yardımıyla üretilir. Beyaz boyalar güneş ışığını geniş bir yelpazede yansıtırken, siyah ve diğer koyu renkler geniş bir spektrumu absorbe ettikleri için uygulandıkları malzemelerin ısınmasına etki ederler. "Serin pigmentler" (boyalar) olarak adlandırılan moleküller, koyu renkli olmalarına rağmen güneş ışınlarının NIR bölgesinde çok düşük absorpsiyon göstermeleri nedeniyle ilgi görmektedir. Bu çalışmada, 12 farklı perilen bazlı pigment kuantum hesaplamaları ile analiz edilmiş, yansımaları ve özellikleri arasındaki korelasyonlar incelenmiştir. Hesaplamalarda Hartree-Fock hesaplama yöntemi ve 3-21G temel seti kullanılarak Gaussian 9 Revision D.01 de yapılmıştır. Yardımcı ara yüzey yazılımı olarak Gaussview 5.0.8 kullanılmıştır. Sentezlenen perilenlerin karakterizasyonu FT-IR, NMR, XRD ile yapılmış ve daha önceki çalışmalarda yayınlanmıştır. Simülasyondan elde edilen entalpi, HOMO.LUMO aralığı, simetri ve dipol momentleri karşılaştırılmış ve sonuç olarak NIR yansımasının pigmentlerin dipol momentleri ile ilişkili olduğu tespit edilmiştir.

Anahtar Kelimeler: Serin boyalar, Perilen, Simülasyon, kuantum kimya

Molecular dynamics simulation of perylene-based cool pigments and investigation of structural properties in the reflection of the NIR region

Abstract: Cool pigments used in special paints that reduce the effect of sunlight are generally produced with the help of perylenes. While white paints reflect a wide range of sunlight, black and other dark colors absorb a wide spectrum, so they have an effect on the heating of the materials they are applied to. Molecules called "cool pigments" (dyes) are of interest because they exhibit very low absorption in the NIR region of the sun's rays, although they are dark in color. In this study, 12 different perylene-based pigments were analyzed with quantum calculations and the correlations of their reflections and properties were examined. Hartree-Fock method and 3-21G basis set were applied in the calculations and Gaussian 9 Revision D.01 and Gaussview 5.0.8 were used as interface. The characterization of the synthesized perylenes has been done with Ft-IR, NMR, XRD and has been published in previous studies. The enthalpy, HOMO.LUMO gap, symmetry and dipole moments obtained from the simulation were compared and as a result it was determined that the NIR reflection was related to the dipole moments of the pigments.

Keywords: Cool dyes, Perylene, Simulation, Computational chemistry

1. Giriş

Perilen, yaklaşık bir asır önce tanımlanmış kahverengi bir katıdır ve türevleri küp boya olarak kullanılmıştır. Perilen şekil 1'deki kimyasal yapıya sahiptir. Görüldüğü gibi bu madde, tüm karbon atomlarının sp^2 formunda olduğu ve bunun sonucunda tüm molekülün bir düzlem şeklinde yatay olduğu polisiklik aromatik bir bileşiktir. Bu madde ısıya karşı çok yüksek bir stabilizeye sahiptir ve aynı zamanda çevresel ve ışık stabilitesi de yüksektir. Bu maddenin türevleri de farklı tonlar oluşturabilir. Perilen diimidlerin tonları kırmızı ve şarap kırmızısıyla başlar ve mor, kahverengi ve siyah ile biter. Perilen pigmentleri, kimyasal inertlikleri ve yüksek stabiliteleri nedeniyle düşük toksisiteye sahiptir ve insanlara ve çevreye zarar vermeyen (veya çok az zararı olan) toksik olmayan maddeler olarak bilinirler(Kaur ve ark. 2012; Mazhar ve ark. 2016; Mazhar ve ark. 2017; Meymand ve ark. 2019; Mazhar ve ark. 2020).

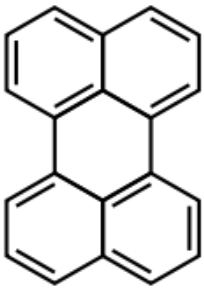

Şekil 1. Perilenin moleküler yapısı

Perilen türevleri otomotiv boya ve elyaf boyama endüstrilerinde yaygın olarak kullanılmasına rağmen, sadece bu endüstrilere sınırlı değildir. Perilen, son zamanlarda, henüz ticarileştirilmemiş olmasına rağmen, güneş pillerinde itme-çekme ve nispeten verimli yapılar oluşturma potansiyelini gösteren pigmentler olarak Boyaya Duyarlı Güneş Pili (DSSC'ler) kullanılmıştır. Pigmente duyarlı güneş pillerinde önemli performans gösteren pigmentler, itme-çekme yapısına sahiptir. Bu pigmentlerin molekülün bir tarafında bir elektron verici grubu ve diğer tarafında bir elektron çekici grubu vardır. Bu yapı, molekülün boşluk bandını azaltmakla birlikte, perilen boyalarının elektronlarını daha iyi verimle TiO_2 nanoparçacıklarına aktarmalarına neden olur. Böyle bir yapı, molekülün LUMO kısmının anhidrit elektron çekici grubuna yakın yerleştirilmesine neden olarak titanyum okside daha iyi yük aktarımı sağlar (Titanyum oksit nanoparçacıklarına pigment bağlanması anhidrit grubu tarafından yapılır)(Mazhar ve ark. 2016; Martini ve ark. 2020; Minei ve ark. 2020; Ferasat ve ark. 2021).

Serin boyalar, alt tabakalarının güneşte daha soğuk kalmasını sağlayan renkleri ifade eder. Güneş radyasyonu, ultraviyole (UV), görünür ışık ve yakın kızıl ötesi (NIR) oluşmaktadır ki insan gözünün yalnızca görünen kısmını algılayabilir. Nesneler bu görünür ışığın bir kısmını emdiğinde, içlerinde renk belirir. UV ve NIR dalgalarının absorpsiyon veya yansıma miktarının malzemenin rengi üzerinde hiçbir etkisinin olmaması dikkat çekicidir. Başka bir deyişle, malzeme bu dalgaları emse de yansıtsa da rengi aynı kalır. Bu bölgelerin absorpsiyon ve yansımasındaki fark, yalnızca o madde tarafından emilen enerji miktarında ortaya çıkar. Yani madde bu alanları emerse iç enerji miktarı artar ve ısınır. Ancak bu alanları yansıtırsa, malzeme tarafından emilen enerji miktarı azalır, bu da daha düşük iç enerji ve sıcaklık ile sonuçlanır. Bu nedenle, amaçlanan uygulamaya bağlı olarak, bu parametre maksimum enerjiyi absorbe etme veya minimum düzeyde absorbe etme kabiliyetine sahip renkleri tasarlamak ve sentezlemek ve yararlanmak için kullanılabilir. Güneş ışığı dalgalarının yaydığı enerji miktarı da Şekil 2'ye bölünmüştür(Mazhar ve ark. 2020).

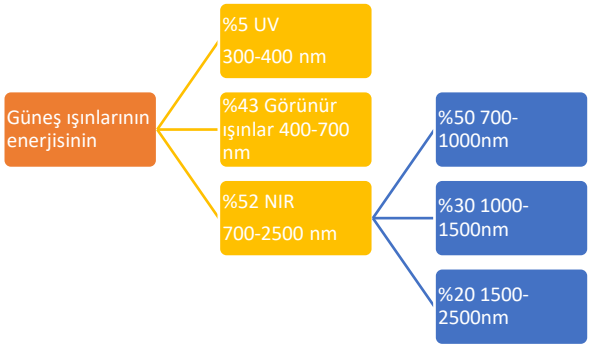

Şekil 2. Güneş spektrumunun bileşenleri ve içerdikleri enerji miktarı

Şekil 2'de gösterildiği gibi, UV ışığı, güneş tarafından yayılan enerjinin küçük bir kısmını oluşturur ve güneş enerjisinin çoğu, görünür ve yakın kızılötesi bölgede bulunur. Belirtildiği gibi, görünür bölgedeki manipülasyon, malzemenin rengini değiştirir ve sabit bir renk için, malzemenin görünür bölgedeki emdiği enerji miktarı değiştirilemez. Bu nedenle, güneş ışığına maruz kalan bir maddenin emdiği enerji miktarını kontrol etmenin tek yolu, güneşten yayılan enerjinin en fazla olduğu (%52) NIR bölgesindeki emilimini kontrol etmektir. Bir renk, bu alanda en az soğurma (veya en fazla yansıma) miktarına sahipse, güneşten mümkün olan en az miktarda enerjiyi (gölgesine göre) alır ve güneş ışığına maruz kaldığında sıcaklığı en düşüktür ve tersi. Bu alanda çok az emilen (veya bu alanda yüksek oranda yansıtılan) renklere serin renkler denir. Bu renkler güneş ışığına maruz kaldıklarında NIR dalgalarını yansıtarak enerjiyi yayarlar ve sıcaklıklarını düşük tutarlar(Mazhar ve ark. 2016).

Son yıllarda kuantum hesaplama yöntemleri, kimya alanında, çok etkili bir rol göstermiştir. Hesaplamalı kimya, moleküllerin ve malzemelerin yapılarını ve özelliklerini incelemek için kuantum kimyasına dayalı ab initio yaklaşımlar ve deneysel yaklaşımlar dahil olmak üzere bilgisayar modelleme ve simülasyonunun kullanımını tanımlar. Hesaplamalı kimya, moleküllerin ve malzemelerin yapısını ve özelliklerini anlamayı amaçlayan hesaplama tekniklerini tanımlamak için de kullanılır. Bu çalışmada önceden sentezlenmiş 12 farklı perilen bazlı boyar maddenin kuantum hesaplama yöntem ile simülasyonu yapılmıştır. Bu boyar maddelerin sentezleme ve karakterizasyonu önceki makalelerde yayınlanmıştır(Ju ve ark. 2020; Wiebeler ve ark. 2021).

1. Materyal ve metot

Simülasyon için Gaussian 9 Revision D.01 ve model hazırlaması için GaussView 5.0.8 kullanılmıştır. Tüm moleküller OPT+FREQ işlemine alınarak optimize edilmiştir. Force Constant optimizasyon aşamasında bir kere hesaplanmıştır. Raman spektrumu incelenmemiştir ve dolayısıyla ROA hesabı da yapılmamıştır. Ayrıca VCD'de ele alınmamıştır. Metot olarak Grand State ve yöntem olarak Hartree-Fock tanımlı spin şeklinde yazılıma girilmiştir. Temel set 3-21G seçilmiş olup ama difüzyon ve hibritleşme seçenekleri hesaplamaya dahil edilmemiştir. Molekülün yükü sıfır ve spini singlet olarak tanımlanmıştır. Bilgisayarın hafıza limitinin 1GB' ı ve işlemcisinin 4 çekirdeği hesaplamada kullanılmıştır. Simülasyonların tamamı çözücüsüz olarak ele alınmıştır.
Simülasyonu yapılmış perilen türevlerinin kimyasal yapıları çizelge 1 de verilmiştir.

Tablo 1. Perilen türevlerinin kimyasal yapıları

Simge	Kimyasal yapı
P1	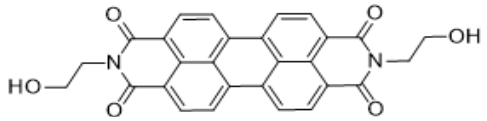
P2	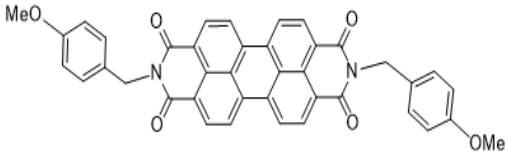
P3	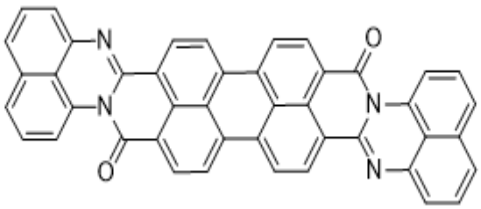
P4	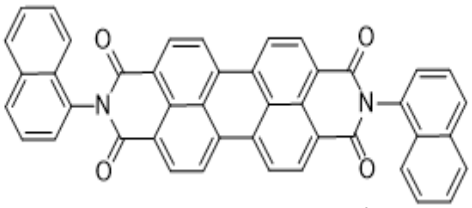
P5	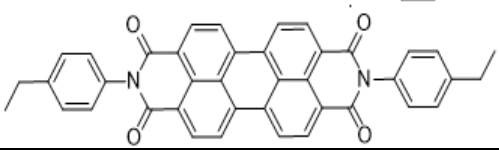
P6	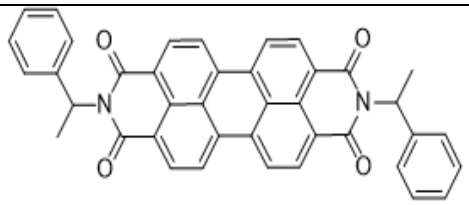
P7	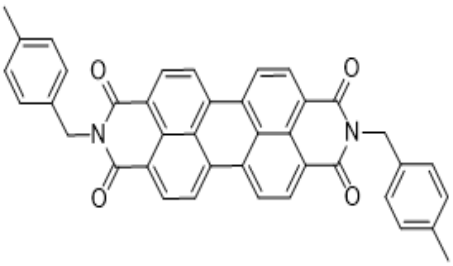
P8	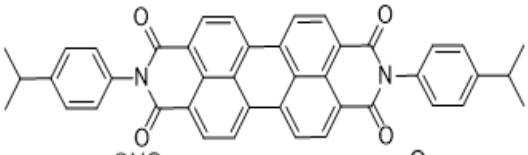
P9	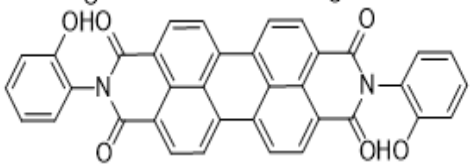
P10	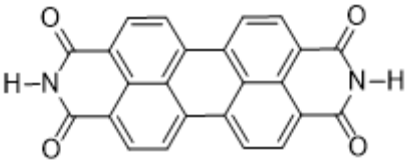
P11	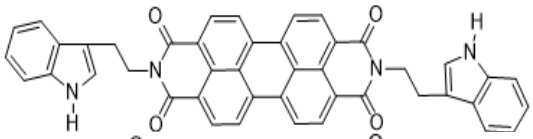
P12	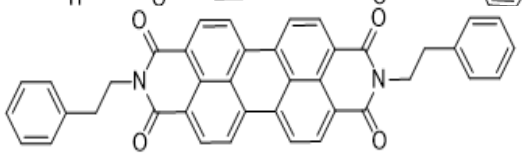

2. Bulgular ve tartışma

Perilen bazlı pigmentler metot bölümünde söylendiği şekilde optimize edildi. Elde edilen optimize moleküler yapılar çizelge 2 de verilmiştir. Daha kolay gözükmek için pigmentler 1'den 12 ye kadar numaralanmışlar.

Tablo 2. Optimize edilmiş pigmentlerin moleküler yapıları

Simge	Optimize edilmiş moleküler yapı
P1	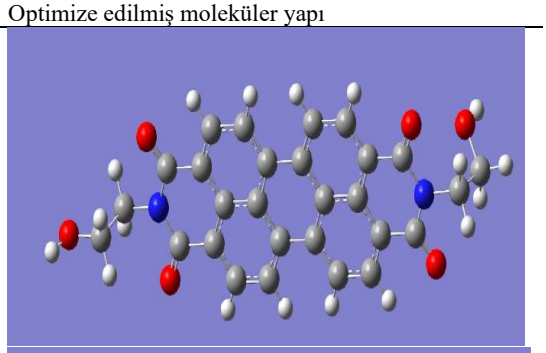
P2	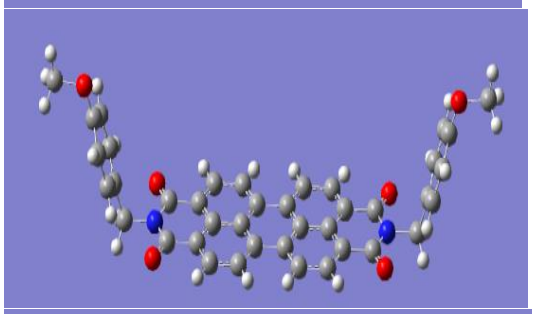
P3	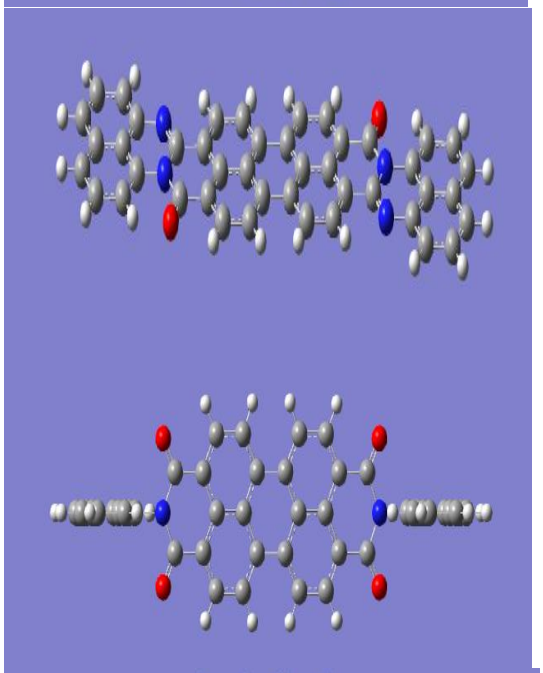
P4	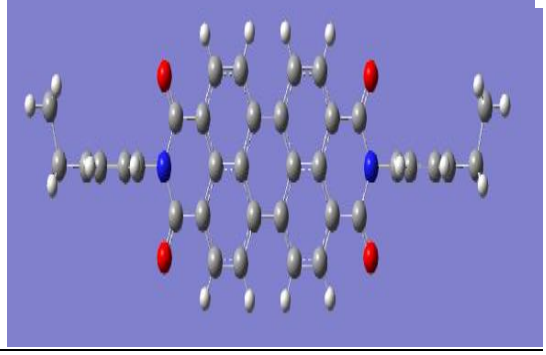
P5	
P6	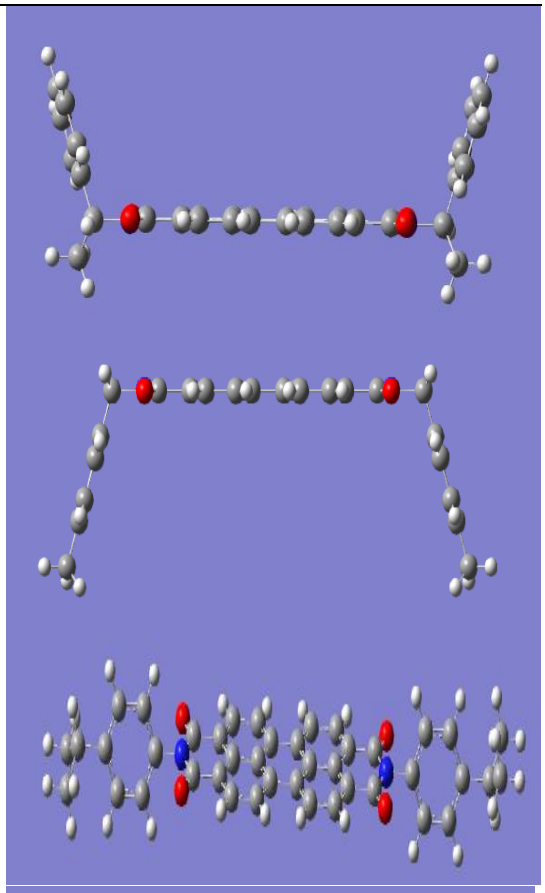
P7	
P8	
P9	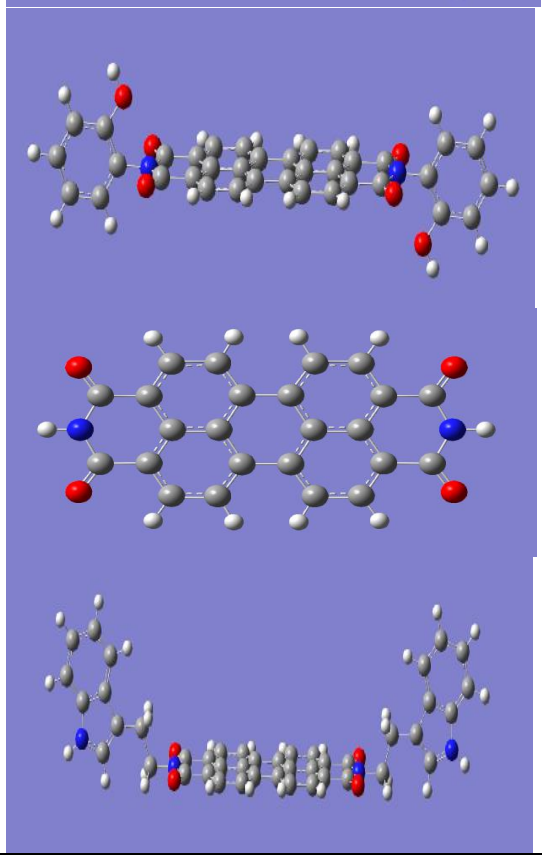
P10	
P11	

P12	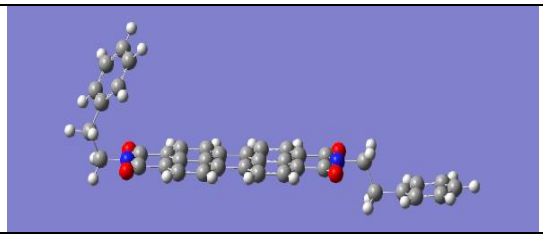

Modellemenin sonunda elde edilen parametrelerin değeri çizelge 3 de verilmiştir.

Tablo 3. Perilen moleküllerinin kuantum hesaplamasının sonucu

Sim	Entalpi	D.M	HOMO	LUMO	Gap
p1	-1619,437	2,8116	-0,28974	-0,01725	0,27249
p2	-2075,7936	2,1177	-0,29237	-0,0203	0,27207
p3	-2033,495	0,001	-0,25392	-0,01421	0,23971
p4	-2075,254	0,0015	-0,29206	-0,0193	0,27276
p5	-1926,926	0,2106	-0,2898	-0,017	0,2728
p6	-1926,933	0,459	-0,2914	0,0194	0,3108
p7	-1926,946	0,4877	-0,2921	-0,0199	0,2722
p8	-2004,502	0,0009	-0,2898	-0,0169	0,2729
p9	-1920,64356	0,0006	-0,28411	-0,01099	0,27312
p10	-1315,44155	0,001	-0,29595	-0,02312	0,27283
p11	-2186,94010	3,158	-0,2841	-0,01967	0,26443
p12	-1926,94074	0,5273	-0,29095	-0,01861	0,27234

Perilen pigmentlerinin deneysel olarak hesaplanan yakın kızıl ötesi yansıtmaları çizelge 4 de belirlenmektedir.

Tablo 4. Perilen pigmentlerinin NIR yansıtmaları

Pigment	NIR yansıtma yüzdesi
p1	17,67
p2	48,72
p3	32,69
p4	48,18
p5	29,36
p6	55,77
p7	43,13
p8	49,12
p9	27,75
p10	29,53
p11	28,25
p12	50,55

Çizelge 4 de belirlendiği gibi P6, P12, P8, P2, P4 ve P7 en etkili olarak NIR yansıtma özelliğini göstermişler. Önceki yayınlanmış çalışmalarda bu etkinin kiristalografi yapısından kaynaklanması açıklanmıştır (Mazhar ve ark. 2016; Mazhar ve ark. 2017). Bu çalışmada kuantum hesaplamaları yöntemini kullanarak simülasyondan elde edilen entalpi, dipol moment, HOMO ve LUMO enerji seviyeleri ve bu seviyeleri arasındaki enerji farkı ele alınmıştır. Çizelge 3 de gözüktüğü gibi HOMO, LUMO ve enerji seviye farkı çok değildir ve dolayısıyla NIR yansıtmasına etkili bir parametre olmadığı tespit edilmiştir. Ayrıca entalpi farkıyla NIR yansıtma arasında doğrusal korelasyon bulunmamaktadır. Pigmentlerin dipol momenti ve geometrileri NIR yansıtmasında etkili parametre olarak kabul edile bilirler (Weyer. 2007). Çizelge 3 de gözüktüğü gibi dipol momentin düşük olması pozitif etki sağlayarak, NIR yansıtmasının artışına sebep olmaktadır. P1 ve P11in dipol momentinin yüksek olması, NIR yansıtmasının düşüşüyle sonuçlanmıştır. Sadece P2 pigmenti 2.1177 Debye dipol momente sahip olarak %48,72 NIR yansıtmasını gösteriyor. P2 de moleküler geometri sonucu etkilemiş ola bilirliği düşünülmektedir. Başka deyişle moleküler geometri ne kadar düz sayfa şekline yaklaştıkça NIR yansıtması da o kadar düşe biliyor. P2, P6 ve P7 kayık geometrisi göstermesinden dolayı NIR yansıtma yüzdesi yüksektir.

3. Sonuç

Bu çalışmada 12 ayrı perilen bazlı pigment kuantum hesaplamaları ile simülasyonu yapılmıştır. Yazılımın çıktısı olarak dipol moment, HOMO ve LUMO ve enerji seviyesi farkı, moleküler geometri ve entalpi verileri değerlendirilmiştir. Perilen pigmentlerinin NIR enerji yansıtmasıyla bu parametrelerin korelasyonu olup olmadığı incelenmiştir. Sonuç olarak NIR yansıtması, dipol moment ve moleküler geometriyle daha çok korelasyonda olduğu anlaşılmıştır.

Teşekkür
Çalışmamıza maddi destek sağlayan Çukurova Üniversitesi Bilimsel Araştırma Projeleri Koordinasyon Birimine (Proje No: FDK-2021-14278) teşekkürlerimizi sunuyorum.

Kaynaklar

Ferasat E, Golshan M, Salami-Kalajahi M & Roghani-Mamaqani H. 2021. Synthesis and properties of fluorescent coumarin/perylene-3, 4, 9, 10-tetracarboxylic diimide hybrid as cold dye. Mater Res Bullet. 144: 111500. https://doi.org/10.1016/j.materresbull.2021.111500

Ju L, Li M, Tian L, Xu P & Lu W. 2020. Accelerated discovery of high-efficient N-annulated perylene organic sensitizers for solar cells via machine learning and quantum chemistry. Mater Comm. 101604. https://doi.org/10.1016/j.mtcomm.2020.101604

Kaur B, Quazi N, Ivanov I & Bhattacharya S. 2012. Near-infrared reflective properties of perylene derivatives. Dyes Pig. 92: 1108-1113. https://doi.org/10.1016/j.dyepig.2011.06.011

Martini F, Minei P, Lessi M, Contiero L, Borsacchi S, Ruggeri G, Geppi M, Bellina F & Pucci A. 2020. Structural order and NIR reflective properties of perylene bisimide pigments: Experimental evidences from a combined multi-technique study. Dyes Pig. 179: 108401. https://doi.org/10.1016/j.dyepig.2020.108401

Mazhar M, Abdouss M, Gharanjig K & Teimuri-Mofrad R. 2016. Synthesis, characterization and near infra-red properties of perylenebisimide derivatives. Prog Org Coat. 101: 297-304. https://doi.org/10.1016/j.porgcoat.2016.08.018

Mazhar M, Abdouss M, Gharanjig K, Teimuri-Mofrad R & Zargaran M. 2017. Effects of isomerism on near infrared properties of perylene bisimide derivatives. J Coat Tech. 14: 207-214. https://doi.org/10.1007/s11998-016-9843-z

Mazhar M, Abdouss M, Zarifi F & Zargaran M. 2020. Effectiveness of perylene pigment on the reduction of energy demand of a building. Pig Resin Tech. https://doi.org/10.1108/PRT-08-2019-0076

Meymand F M, Mazhar M & Abdouss M. 2019. Investigation of substituent effect on cool activity of perylene bisimide pigments. J Coatings Tech. 16: 439-447. https://doi.org/10.1007/s11998-018-0122-z

Minei P, Lessi M, Contiero L, Borsacchi S, Martini F, Ruggeri G, Geppi M, Bellina F & Pucci A. 2020. Boosting the NIR reflective properties of perylene organic coatings with thermoplastic hollow microspheres: Optical and structural properties by a multi-technique approach. Sol Energ. 198: 689-695. https://doi.org/10.1016/j.solener.2020.02.017

Weyer L (2007). Practical guide to interpretive near-infrared spectroscopy, CRC press.

Wiebeler C, Vollbrecht J, Neuba A, Kitzerow H-S & Schumacher S. 2021. Unraveling the electrochemical and spectroscopic properties of neutral and negatively charged perylene tetraethylesters. Sci Rep. 11: 1-11. https://doi.org/10.1038/s41598-021-95551-0

RESEARCH ARTICLE
Eurasian J Bio Chem Sci, 5(Suppl 1):111-118, 2022
https://doi.org/10.46239/ejbcs.1040161

EJBCS

Eurasian Journal of Biological and Chemical Sciences

Journal homepage: www.dergipark.org.tr/ejbcs

Tamoxifen Delivery to Breast Cancer Cells (MCF-7) Via Hydroxyapatite Microspheres

Binnaz Kırbıyık[1], Birgül Mazmanci[1,2], Şeyma Gülnaz Yarlilar[1*], Naz Uğur[3], Kasım Ocakoğlu[3]

[1] *Department of Nanotechnology and Advanced Material, Science Institute, Mersin University, 33363, Mersin, Turkey.*
[2] *Department of Biology, Faculty of Science and Letter, Mersin University, 33363 Mersin, Turkey.*
[3] *Department of Engineering Fundamental Sciences, Faculty of Engineering, Tarsus University, 33400, Tarsus, Turkey*

*Corresponding author : syarlilar@gmail.com
Orcid No: https://orcid.org/0000-0002-0403-3390

Received : 28/12/2021
Accepted : 03/09/2022

Abstract: Drug delivery systems have been used in cancer treatment to increase drug effectiveness. The hydroxyapatite (HAP) based materials used in this area can provide drug transport to the target site without its deterioration. In this study, porous hollow hydroxyapatite microspheres (PHHMs) were produced by using the hydrothermal method. Tamoxifen (TAM) used in the treatment of breast cancer has been covalently attached to the produced microspheres. The obtained microsphere structures (tamoxifen-loaded hydroxyapatite, TAM/H) were successfully characterized by ATR-FTIR, FE-SEM, XRD, and DLS methods. The breast cancer cell line MCF-7 was used to examine the effect of the hybrid structure. The cytotoxic and genotoxic effects of TAM/H were compared with the TAM groups on MCF-7. Our results have showed that, the decrease in cell viability at 24 and 36 hours were still continued at 48 hours only in TAM/H groups. In addition, TAM/H was found to show a genotoxic effect by the increment in genetic damage index (GDI) and damaged cell percentage (DCP%). As a result, use of hydroxyapatite was suitable for the transport of TAM and that covalent binding was suitable for drug particle interaction with hybrid structure and thus controlled drug release occurred.

Keywords: Hydroxyapatite microsphere, Tamoxifen, Hydrothermal method, MCF-7, Cytotoxicity, Genotoxicity.

1. Introduction

Cancer and cancer treatment are a weighty matter in our century. Among other cancer types, breast and lung cancer has been reported to be the most common types (Greenlee et al. 2001). In the medical field, surgery and drug therapy are the leading processes for the treatment of cancer. These methods rely on the removal of the cancerous cells. In chemotherapy, cancer cells are aimed to be annihilated by anti-cancer drugs. Anti-cancer drugs are nonselective and can also damage healthy normal tissues, causing severe side effects such as loss of appetite and nausea. These side effects induced by chemotherapeutic drugs on healthy tissues and organs are a major reason behind the high mortality rate of cancer patients (Senapati et al. 2018).

The side effect of conventional chemotherapy have led to the development of nanoparticle-based drug delivery systems (Yao et al. 2020). Nanoparticle-based drug applications have emerged as promising tools to eliminate the pharmacokinetic interaction associated with traditional drug formulations (Blanco et al. 2015). Commonly used drug carriers are polymeric dendrimers, micelles, microspheres, liposomes, quantum dots, nanoemulsions, gold nanoparticles, and hydrogels (Singh et al. 2017). Nanoparticles for drug delivery include numerous designs in size, shape, and material. Each nanoparticle differs in drug loading capacity, particle and drug stability, drug release rates, and targeted release ability (Haley et al. 2008). Nanoparticles can increase the intracellular concentration of drugs in cancer cells while preventing toxicity in normal cells, using both passive and active target strategies. Besides, the surfaces of the nanoparticles are activated with a higher degree of affinity for cancer cells to bind to cancer cells, rather than healthy cells. Thus, drug concentrations in cancer cells are increased with the effect of nanoparticles, while the undesirable toxic effect that can occur in healthy cells can be minimized (Maeda et al. 2000; Allen et al. 2002).

Today, the production of nanostructured bioceramics and their applications in biomedical fields have become important. Hydroxyapatite (HAP), a bioceramic species, is widely used in different scientific fields such as tissue engineering, drug delivery systems, and chromatographic purification (Jafari et al. 2014). It is a remarkable element of the bioceramics group due to its structural similarity to

the mineral structure of bones and teeth. Because of their good bioactivity and biocompatibility, hydroxyapatite participates in the solid-fluid balance in the environment in which they are placed. In addition, they can directly connect with the bone and other hard tissues and muscles where they are placed (Hench et al. 1993; Pasinli 2004). The reason is that their porous structures offer a high binding affinity for various pharmacological agents such as antibiotics, hormones, enzymes, antibody fragments, steroids (Netz et al. 2001). Concurrently, HAP protects the drug from spoilage until it reaches the physical or chemical target area. At the same time, controlled drug release occurs gradually. Therefore, bioceramics are excellent candidates as promising bio-scaffolds in targeted drug release and tissue engineering (Uskokovic et al. 2014; Andres et al. 2018).

Tamoxifen (TAM) is the most commonly used anti-estrogen drug to treat advanced and early breast cancer and reduce the incidence of breast cancer in high-risk women (Paganini et al. 2000). The drug is classified as a selective estrogen receptor modulator because it is an estrogen agonist/antagonist that alters hormone action by competing with estrogen to bind to the estrogen receptor and partially blocking the endogenous estrogen effect (Bender et al. 2007). Due to its anti-estrogenic effects, TAM was originally used to treat estrogen receptor-positive breast cancers. Nevertheless, TAM (20 mg/day) used in studies to treat breast cancer was shown to inhibit the growth of breast cancer cells (Carlson et al. 2006). Later, the use of the drug was developed to include all types of breast cancer, and more recently it was also used in the prevention of breast cancer for healthy women at high risk (Fisher et al. 1998).

In this study, porous hollow hydroxyapatite microspheres (PHHMs) are successfully synthesized by a hydrothermal method and TAM was covalently bonded to PHHMs. TAM loaded hydroxyapatite microspheres (TAM/H) were obtained. Chemical compositions and properties of TAM/H are determined by Attenuated Total Reflectance-Fourier Transform Infrared Spectroscopy (ATR-FTIR), Field Emission Scanning Electron Microscopy (FE-SEM), X-ray diffraction (XRD), and Dynamic Light Scattering (DLS). In addition, the cytotoxicity and genotoxicity were also explored for bioactivity of TAM/H. A comparison with only TAM was made to test the availability of HAP microspheres in drug delivery.

2. Materials and Methods

2.1. Material

Fetal bovine serum, penicillin-streptomycin, trypsin-EDTA solution, L-glutamine 100X 200mM-100mL were bought from Biowest. Ethylene dinitro tetra acetic acid (EDTA), trizma hydrochloride, ethidium bromide, agarose, agarose-low gelling temperature, trypan blue, poly(sodium 4-styrenesulfonate) (PSS, M_w ~ 16800), calcium chloride, sodium carbonate, disodium hydrogen phosphate, hydrochloric acid were purchased from Sigma-Aldrich. Dimethyl sulfoxide, sodium hydroxide, sodium chloride, triton X-100 were purchased from Merck. All reagents were used without further purification.

2.2 Methods

2.2.1 Synthesis of tamoxifen-loaded hydroxyapatite (TAM/H) microspheres

For a typical synthesis of porous hollow hydroxyapatite microspheres (PHHMs), a previously reported hydrothermal method by Wen Lai and co. workers (Lai et al. 2016) was carried out. Briefly, $CaCO_3$ (vaterite) was synthesized as the first step. For the synthesis of vaterite, 10 mL $CaCl_2$ (0.2 M) solution was mixed with 100 mL PSS and stirred under room temperature with a magnetic stirrer. Subsequently, 10 mL Na_2CO_3 (0.2 M) was added to the solution dropwise and continued to stir for 1 h. The white $CaCO_3$ suspension was washed with ethanol and distilled water, dried in the 60 °C oven for 24 h. 0.2 g vaterite and 0.1 M Na_2HPO_4 were mixed, and NaOH was added until pH 11. Then, the transparent suspension was transferred to Teflon autoclave and hydrothermal reaction continued for 120 °C, 1 h. After the reaction, the obtained porous hollow hydroxyapatite microspheres were centrifuged and washed with absolute ethanol and distilled water then dried in the 60 °C oven for 24 h.

Complex hybrid structures of TAM/H were obtained by integration of TAM to the synthesized porous hollow hydroxyapatite microspheres. The covalent bonding method was applied in the formation of the complex structure. Hybrid structures synthesized at each step have shown in Figure 1.

At the first part (Step 1), 300 mg PHHM was dissolved in 3 mL dry toluene in an inert atmosphere and stirred with a magnetic stirrer at 70 °C. Then, 0.9 mL Triethoxy-3-(2-imidazolin-1-yl)propylsilane was added to the solution and stirred for 24 h. Obtained structure was named PHHM/Si.

At the second step (Step 2), 1.5 mL 1,4-diiodobutane was added to the solution and continued to stir for 24 h in the dark. After, the reaction mixture was filtered and washed five times with diethyl ether. Then, the solid was dried in RT for 48 h in the dark. Obtained structure was named PHHM/SiI. At the third step (Step 3), 50 mg of PHHM/SiI was dissolved in 2 mL dry toluene in an inert atmosphere and stirred with a magnetic stirrer at 90 °C. Then, 100 mg TAM was dissolved in 2 mL dry toluene thereafter, added to the reaction, and continued to stir for 48 h. After the reaction, the obtained material was washed several times with diethyl ether. After, the solid was dried in RT for 48 h in the dark. The final structure was named as TAM/H.

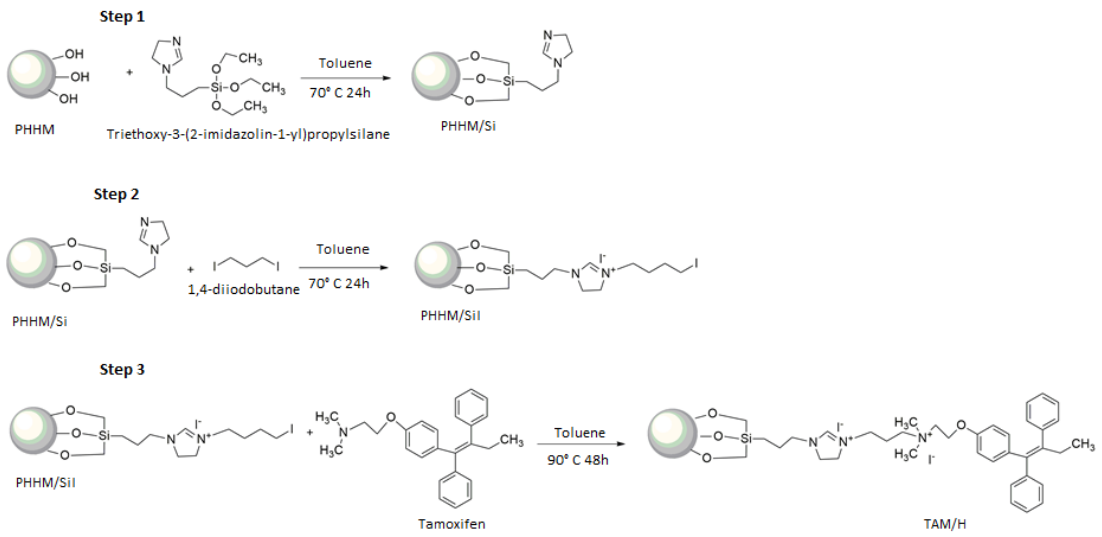

Fig. 1 TAM/H hybrid structure synthesis steps

2.2.2. Characterization

The surface morphology and microstructure of the vaterite and PHHM structures were examined by field emission scanning electron microscopy (FE-SEM, JEOL JSM-6060LV). The structural properties of PHHM were analyzed with a Cu-Kα welded X-ray diffractometer (Bruker D8 Advanced Series) at a scanning rate of 5 ° min^{-1} at wavelength λ = 1.54056 Å, in the range 20-60º. The functional groups in the vaterite, PHHM, PHHM / SiI, TAM structures, the TAM/H microsphere structures were determined by ATR-FTIR (Perkin Elmer Spectrum Two Model). FTIR spectra were collected at room temperature in the 4000-450 cm^{-1} wavelength range.

2.2.3. Bioactivity of TAM/H microspheres

2.2.3.1. Cell culture and treatment

The bioactivity of TAM/H was investigated via cell viability and genotoxicity tests. For this purpose, the human breast cancer cell line MCF-7 was preferred. The breast cancer cell line MCF-7 was obtained from Mersin University, Advanced Technology Laboratory, Turkey.

2.2.3.2. Cell viability testing

Cell viability analysis was performed by xCELLigence system. The xCELLigence system allows for label-free and dynamic monitoring of cellular phenotypic changes in real-time using impedance. Increasing the number of adherent cells and changing conditions in the cell culture alter the impedance. The impedance gives quantitative information about the number, viability, morphology, and migration of the cells (Garcia et al. 2013; Şener et al. 2017).

The cells were placed into tissue culture flasks under humidified 5% CO_2 and 95% air maintained at 37 °C atmosphere in Dulbecco's modified Eagle's medium (DMEM) supplemented with 10% fetal bovine serum (FBS, v/v), 1% penicillin (100 U/ml)-streptomycin (100 mg/ml) and 1% glutamine (100 mg/ml). MCF-7 cells were passaged with 0.25% trypsin and 0.1% ethylene diamine tetraacetic acid (EDTA) after 80% confluency. After seeding 200 µl of the cell suspensions in DMEM containing 10% FBS into the wells (10.000 cells/well) of the E-plate 16. Cells were allowed to adhere to the E-plate for 24 h and subsequently, the media was removed from the well. The cells were treated with different doses (10, 20, 40, 60 µM) of TAM/H. To demonstrate the effectiveness of TAM/H in MCF-7 cells, free tamoxifen (TAM) groups were performed using the same doses of tamoxifen (10, 20, 60 µM). Only the medium was added to the control group (CONT). The changes in the MCF-7 cell proliferation were monitored every 15 min for 92 hours by xCELLigence device. Cell proliferation experiments were performed in triplicate.

2.2.3.3. Comet assay

The comet assay is a single-cell gel electrophoresis method used as a genotoxicity test for measuring DNA damage (Tice et al. 2000). MCF-7 cells were seeded in the tissue-culture plates (2 x 10^5) and incubated for 48h for the cell attachment and subsequently, 4h, the cells were treated with different doses (10, 20, 40, 60 µM) of TAM/H microspheres and different doses (10, 20, 40, 60 µM) of free Tamoxifen (TAM). Cells were harvested by trypsin –EDTA solution. After, washed with PBS and resuspended in ice-cold PBS. About 40 µL of the resuspended cells was mixed with 250 µL of low melting point agarose at 37 °C. Afterward, 100 µL suspension was spread evenly onto a slide. The slides were placed at 4 °C in the dark until gelling had occurred. In the sequel, immersed in chilled lysis buffer at 4 °C for 60 min. After lysis and unwinding, the slides were placed in an electrophoresis tank filled with alkaline electrophoresis buffer. The electrophoresis runs for 20 min at 35 V and 300 mA. After electrophoresis, the slides were transferred into chilled neutralization buffer for 10 min and cold 70% ethanol for 5 min. Thereafter, the slides were air-dried overnight at room temperature and then stained with Ethidium Bromide. The DNA migration was observed using a fluorescence microscope (BX51, Olympus, Tokyo, Japan). H_2O_2 solution was used as a positive

control. For each concentration, 100 randomly selected cells were analyzed. The results were given as Arbitrary Units (AU) values which were used to express the DNA damage. AU values indicating the comet assay results were as: Undamaged, (Type 0); low-level damaged (Type 1); moderately damaged (Type 2); highly damaged (Type 3); ultrahigh-level damaged (Type 4). Two parameters were calculated as genetic damage index (GDI) and damaged cell percent (DCP%) (Çavaş 2011).

2.2.3.4. Statistical analysis

All bioactivity studies were carried out in triplicate and results were expressed as means ± SD. Statistical significance between groups was evaluated using Tukey-HSD for post-hoc multiple comparisons. $p < 0.05$ was considered statistically significant.

3. Results and discussion

3.1. Characterization of Vaterite, PHHM, PHHM/SiI and TAM/H microspheres

The size and morphology of the hydroxyapatite structures were characterized by FESEM and Dynamic Light Scattering (DLS) methods. SEM images of synthesized vaterite ($CaCO_3$) and PHHM are shown in Figure 2a and b. As seen from the SEM images; vaterite structures were obtained in spheres and homogenously dispersed with an average dimension size of around 1000 nm, and this is in line with the results previously reported in the literature (Lai et al. 2016). PHHM was obtained in the form of mesoporous and hollow microspheres with a uniform morphology (Figure 2c and d). The images also revealed that their dimensions are bigger than that of vaterite structures (Lai et al. 2016). According to DLS measurements, it was determined that the particle size distribution of PHHM is between 0.8 - 2.0 µm, and the average diameter is about 1.2 µm (Figure 2e) (Lai et al. 2016). The obtained data were also compatible with SEM analysis.

The XRD pattern of the PHHM structure was shown in Figure 3. The reflections match the characteristic diffraction peaks of the hexagonal hydroxyapatite (JCPDS No. 09-0432). However, the weak calcium carbonate ($CaCO_3$) and calcium hydroxide $Ca(OH)_2$ peaks are seen in the 27-30º range. The calcium carbonate particles were formed by the reaction of the increased calcium hydroxide due to the acidic conditions of hydroxyapatite synthesis with atmospheric carbon dioxide.

An understanding of the surface properties of the synthesized vaterite ($CaCO_3$), PHHM, PHHM/SiI and TAM/H microstructures requires precise characterization of the associated structures. At this point, FTIR spectroscopy which provides important information about surface properties was firstly used. The IR spectrum of the synthesized vaterite was measured between 450-4000 cm^{-1} (Figure 4a). Two absorption bands at 927 cm^{-1} and 798 cm^{-1} and a high level between 1507-1454 cm^{-1} are indicating carbonate (CO_3^{-2}) groups (Wu et al. 2010).

The vibrations of 1021 cm^{-1}, 1414 cm^{-1} and the absorption bands at 562 cm^{-1} and 602 cm^{-1} belonging to the bending vibrations of the phosphate (PO_4^{-3}, P = O) groups of PHHM structures (Figure 4b) (Rocha et al. 2005; Rehman et al. 2016; Taşkın et al. 2018). Besides, the peaks at 872 cm^{-1}, 1414 $cm^{-1,}$ and 1465 cm^{-1} are considered to have a high level of B-type CO_3^{-2} absorption so that CO_3^{-2} is included in the lattice structure (Lai et al. 2016).

Tamoxifen's (TAM) characteristic absorption peaks are shown in Figure 4c. Phenyl ring vibration band (=C-H) at 3027 cm^{-1}; aromatic groups (C=C) at 1556 cm^{-1}, 1521 cm^{-1} and 1460 cm^{-1}; phenyl ring substitution at 770 cm^{-1} and 718 cm^{-1}; methylamine (C-N) at 978 cm^{-1} were characterized (Maji et al. 2014; Nosrati et al. 2017). In Figure 4d, 1655 cm^{-1} peak refers to the -NH strain peaks and the heterocyclic -CH strain p eaks of the imidazole groups in PHHM/SiI structure (Bora et al. 2012; Han et al. 2009). Furthermore, the peak at 502 cm^{-1} is determined to be Si-O strain peak from the silanol group which indicates amine-bonded groups of the silanol groups (Lazarevic et al. 2015). The weak peak at 694 cm^{-1} belongs to C-I vibration band of 1,4-diiodobutane (Simek et al. 2015). The performed characterization studies showed that the complex structure (PHHM/SiI) formed by binding triethoxy-3-(2-imidazolin-1-yl)propylsilane and 1,4-diiodobutane to the PHHM structure was successfully obtained. After the integration of TAM onto the PHHM/SiI complex structure, the vibration bands of TAM representing phenyl ring (C = C) of 1556 cm^{-1} and 1521 cm^{-1} have shifted to 1599 cm^{-1} and 1505 cm^{-1} respectively (Figure 4e). From the obtained data, it was determined that the steps of the covalent bonding of TAM onto the PHHM/SiI structure were successfully carried out.

3.2. Bioactivity

The comparison of cytotoxic effects of TAM/H microspheres and TAM were done in MCF-7 cell line using a real-time cell analyser. As a result of the xCelligence analysis, the time duration / dose interaction was not statistically significant and therefore comparisons were made between dose groups for each time period. The cell index values and percentage cell viability were shown in Table 1.

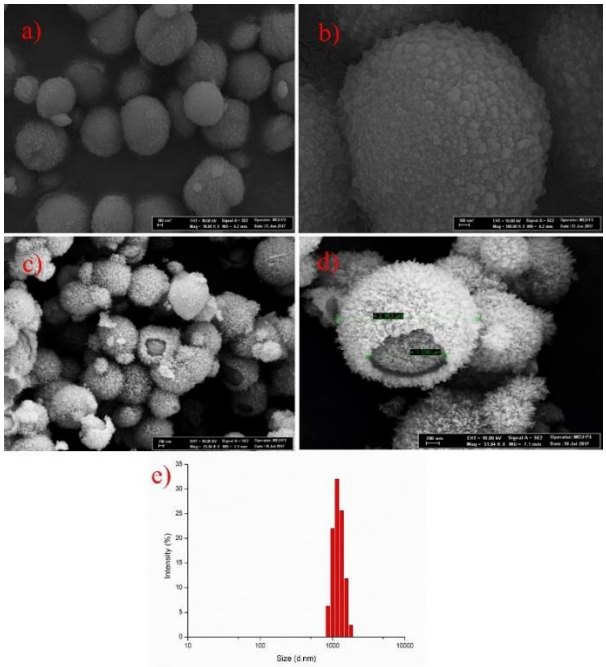

Fig. 2 SEM images of synthesized vaterite ($CaCO_3$) and PHHM

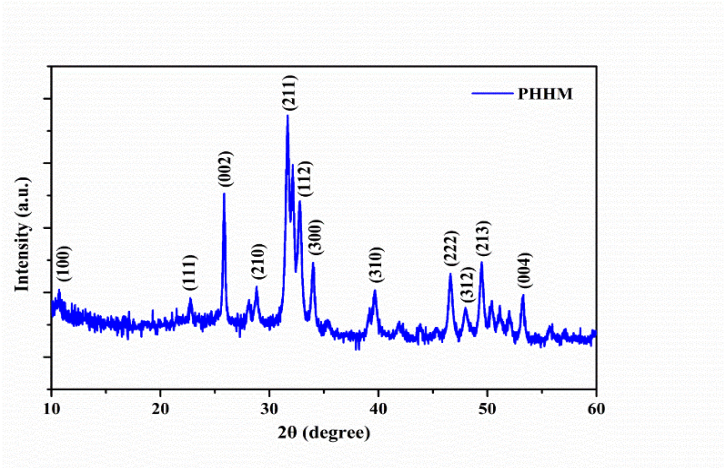

Fig. 3 XRD pattern of the PHHM structure

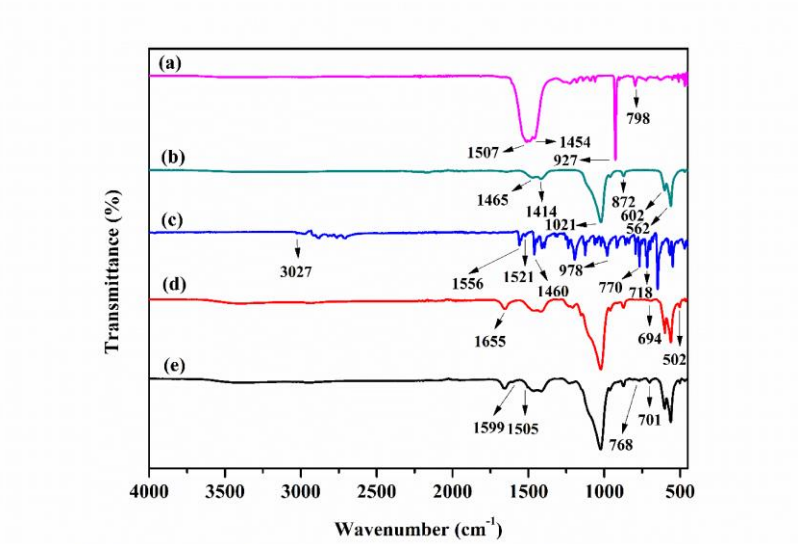

Fig. 4 FTIR spectrum of the synthesized materials.

Table 1: Cell index and cell viability percentages of control and experimental groups

	12 h		24 h		36 h		48 h	
	Cell index	Cell via. (%)	Cell index	Cell via. (%)	Cell index	Cell via. (%)	Cell index	Cell via. (%)
Control	8.58 ± 0.49	100	10.51 ± 0.36	100	10.74 ± 0.29	100	10.60 ± 0.36	100
TAM/H 10	8.80 ± 0.36	102.6	9.45 ± 0.06	89.9	9.15 ± 0.14	85.2	9.00 ± 0.27*	84.9*
TAM/H 20	8.75 ± 0.32	102.0	9.42 ± 0.13	89.6	9.06 ± 0.22	84.4	8.84 ± 0.16*	83.4*
TAM/H 60	8.27 ± 0.94	96.4	9.40 ± 0.22	89.4	9.60 ± 0.61	89.4	9.20 ± 0.61	86.8
TAM 10	9.41 ± 0.55	109.7	9.95 ± 0.57	94.7	10.31 ± 0.41	96.0	11.10 ± 0.46	104.7
TAM 20	9.64 ± 0.76	112.4	8.56 ± 0.24*	81.4*	9.05 ± 0.78*	84.3*	10.54 ± 0.55	99.4
TAM 60	9.58 ± 0.22	111.7	9.86 ± 0.26	93.8	10.37 ± 0.09	96.6	11.18 ± 0.05	105.5

*significant difference compare to control ($p < 0.05$) Values are given mean ± standard deviation.

At the each time period statistical difference was not found significantly (p>0.05) between TAM and TAM/H groups. When TAM and TAM / H groups were compared with the control group, cell index was decreased approximately 5.3-18.6% for TAM groups and 10.1-10.6% for TAM/H groups with compared to the control in 24th h. At 36th hour, the cell index was decreased by 14.8%, 15.6% and 10.6 in the TAM/H 10, TAM/H 20 and TAM/H 60 groups, respectively. At the same time period, cell viability was found to decrease 15.7% in TAM20 group. Decrease of cell index of TAM/H 10, TAM/H 20 and TAM/H 60 groups was reached 15.1%, 16.6% and 13.2% respectively compared to the control at the 48th hour, while cell viability of TAM groups was increased.

Cell viability is an important toxicity assay parameter and is directly associated with the toxic effects of different agents. The xCELLigence system provides real-time monitoring of cells and based on impedance measurements of adherent cells in vitro. Measurement of the electrical impedance gives an idea about adhesion, proliferation and migration of the cells, and it is expressed as the cell index (CI). The CI reflects the cell viability, cell number, attachment quality and cell morphology (Urcan et al. 2010; Öztürk et al. 2018). It was determined that the doses used in this study, both TAM and TAM/H, were toxic to MCF cells. Hassan et al., 2018 reported that the tamoxifen caused a decrease in cell viability in MCF-7 cells and the decrease was dependent on the cell density and tamoxifen concentration (Hassan et al. 2018). Tamoxifen effect by causing loss of cell membrane integrity, down-regulation of telomerase activity, and change in nuclear morphology (Khadka et al. 2015). As a result, cell viability decreased in TAM/H and TAM groups at 24 th and 36 th hours, while the decrease continued in TAM/H group and increased viability in TAM groups at 48 th hours. This shows that TAM was released slowly from tamoxifen-loaded microspheres and the effect of TAM in the hybrid structure is long-term and more effective. Previous study with doxorubicin-loaded microspheres, it has been reported that the porous hydroxyapatite microsphere structures are suitable for drug release (Huang et al. 2020). In this study indicates that porous HAP structures and covalent binding of the drug are suitable for prolonged action.

Comet assay results are shown in Table 2. The DCP% significantly increases in all TAM and TAM/H dose groups compared with the negative control group ($p < 0.05$). Tamoxifen treatment caused DNA damage as well as cytotoxic damage. The maximum increase in the TAM/H and TAM groups is at 20 µM and 40 µM dose, respectively. Increases in DCP% are higher than the PC group. Also, GDI increased in TAM/H and TAM groups compared with the NC group ($p \leq 0.05$). Either damaged cell percentage (DCP%) or genetic damage index (GDI) the increase based on the free TAM and TAM/H microspheres. DCP% and GDI values are higher in loaded groups (TAM/H) than free TAM groups. The study conducted by Wozniak. et al (2007), the DNA damage potential of TAM in peripheral blood lymphocytes and MCF-7 breast cancer cells compared using the comet test. In the data obtained, it has been determined that TAM damages DNA in both normal cells and cancer cells and mainly causes DNA strands to break. TAM has been reported to exhibit genotoxic effects in normal and cancer cells with free radical formation (Wozniak et al. 2007). Melo et al. Reported that the genotoxic effect induced by tamoxifen (TAM) in the MCF-7 cell line was caused by oxidative DNA damage (Melo et al. 2013).

In this study, free TAM as well as covalently bonded TAM to porous structures show that it has genotoxic potential. Mondal et. all has been reported that mesoporous HAp nanostructures have excellent prospects in drug delivery applications due to their high surface area and high pore volume (Mondal et al. 2018). Our results have shown that, TAM/H hybrit structure is effective in breast cancer cells. Studies are in progress regarding the loading capacity or reaction efficiency of tamoxifen to hydroxyapatite microspheres, as well as the tamoxifen release profile.

Table 2. Comet assay results damaged cell percentages (%DCP) and genetic damage index (GDI).

	% DCP	GDI
TAM/H 10	25 ± 8.48	0.97 ± 0.15*
TAM/H 20	38.5 ± 2.12*	1.47 ± 0.02*
TAM/H 40	33.5 ± 4.94*	1.23 ± 0.18*
TAM/H 60	37 ± 0*	1.37±0.07*
TAM 10	24 ± 0	0.89 ± 0
TAM 20	24.5 ± 0.70	0.93 ± 0
TAM 40	38 ±15.55*	1.34 ± 0.54*
TAM 60	31.5 ± 4.94*	1.17 ± 0.16
NC	12.25 ± 4.03[a]	0.44 ± 0.12[a]
PC	28 ± 1*	1.06 ± 0.07

NC: Negative Control; PC: Positive Control.
[*] Statistical difference from NC ($p \leq 0.05$)
[a] Statistical difference from PC ($p \leq 0.05$)
Values are given mean ± SD

Authors' contributions

Experimental planning, design and conducting: Binnaz Kırbıyık, Birgül Mazmancı, Kasım Ocakoğlu.
Writing, original draft preparation: Şeyma Gülnaz Yarlılar, Naz Uğur.
Review of the drafted manuscript: Binnaz Kırbıyık, Birgül Mazmancı, Şeyma Gülnaz Yarlılar, Naz Uğur, Kasım Ocakoğlu.

Declaration of interests

The authors declare that there is no conflict of interests regarding the publication of this paper.

Acknowledgments

This work was supported by Mersin University Scientific Research Project Unit (grant no 2017-1-TP2-2232)

References

Allen TM. 2002. Ligand-targeted therapeutıcs in anticancer therapy. Nat Review Cancer. 2(10): 750-763.

Andres NC, Sieben JM, Baldini M, Rodriguez CH, Famiglietti A, Messina PV. 2018. Electroactive Mg^{2+}-Hydroxyapatite Bender CM, Sereika SM, Brufsky AM, Ryan CM, Vogel VG, Rastogi P, Cohen SM, Casillo FE, Berga SL. 2007. Memory impairments with adjuvant anastrozole versus tamoxifen in women with early-stage breast cancer. Menopause. 14: 995-998.

Blanco E, Shen H, Ferrari M. 2015. Principles of nanoparticle design for overcoming biological barriers to drug delivery. Nature Biotech. 33(9): 941-951.Nanostructured Networks against Drug-Resistant Bone Infection Strains. ACS Appl Mater Interfaces.

Bora DK, Rozhkova EA, Schrantz K, Wyss PP, Braun A, Graule T. Costable EC. 2012. Functionalization of Nanostructured Hematite Thin-Film Electrodes with the Light-Harvesting Membrane Protein C-Phycocyanin Yields an Enhanced Photocurrent. Adv Func Mat. 22: 490–502.

Carlson RW, Hudis CA, Pritchard KI. 2006. Adjuvant endocrine therapy for hormone receptor-positive breast cancer: Evolution of NCCN, ASCO, and St Gallen Recommendations. J Nat Comp Cancer Network. 4(10): 971-979.

Çavaş T. 2011. In vivo genotoxicity evauation of atrizine and atrizine-based herbicide on fish Carassiu auratus using the micronucleus test and the comet assay. Food Chem Tox. 49: 1431-1435.

Fisher B, Costantino JP, Wickerham DL, Redmond CK, Kavanah M, Cronin W M, Vogel V. Robidoux A, Dimitrov N, Atkins J, Daly M, Wieand S, Tan-Chiu E, Ford L, Wolmark N. 1998. Tamoxifen for prevention of breast cancer: report of the National Surgical Adjuvant Breast and Bowel Project P-1 Study. J Nat Cancer Ins. 90: 1371–1388.

Garcia SN, Gutierrez L, McNulty A. 2013. Real-time cellular analysis as a novel approach for in vitro cytotoxicity testing of medical device extracts. J Biomed Mater Res A. 101: 2097-2106.

Greenlee RT, Hill-Harmon MB, Murray T, Thun M. 2001. Cancer statistics. CA Cancer J for Clin. 51(1): 15-36.

Haley B, Frenkel E. 2008. Nanoparticles for drug delivery in cancer treatment. Urologic Oncology: Seminars and Original Investigations. 26: 57–64.

Han L, Park SW, Park D. 2009. Silica grafted imidazolium-based ionic liquids: efficient heterogeneous catalysts for chemical fixation of CO_2 to a cyclic carbonate. Energy Env Sci. 2: 1286–1292.

Hassan F, Mohammed G, Gamal A, El-Hiti GA, Alshanon A, Yousif E. 2018. Cytotoxic effects of tamoxifen in breast cancer cells. J Unexplored Med Data. 3 (3): 2-9

Hench LL, J. Wilson J. 1993. An Introduction to Bioceramics. World Scientific Publishing Co. 139-189.

Jafari S, Adibkia K. 2014. Application of Hydroxyapatite Nanoparticle in the Drug Delivery Systems. J Mol Phar Org Pro Reserch. 03: 01.

Huang H, Du M, Chen J, Zhong S, Wang J. 2020. Preparation and characterization of abalone shells derived biological mesoporous hydroxyapatite microspheres for drug delivery. Mat. Sci Eng C Mater Biol Appl. 113:110969. doi.org/10.1016/j.msec.2020.110969

Khadka NK, Cheng X, Ho CS, Katsaras J, Pan J. 2015. Interactions of the anticancer drug tamoxifen with lipid membranes. Biophys J. 108 (10): 2492-2501.

Lai W, Chen C, Ren X, In-Seop L, Jiang G, Kong X. 2016. Hydrothermal fabrication of porous holl9ow hydroxyapatite microspheres for a drug delivery system. Mat Sci Eng C. 62: 166–172.

Lazarević SS, Janković-Častvan IM, Jokić BM, Janaćković DT, Petrović RD. 2015. Sepiolite functionalized with N-(3(trimethoxysilyl)propyl)-ethylenediamine triacetic acid trisodium salt, Part I: Preparation and characterization, J Serb Chem Soc. 80(9): 1193–1202.

Maeda H, Wu J, Sawa T, Matsumura Y, Hori K. 2000. Tumor vascular permeability and the EPR effect in macromolecular therapeutics: a review. J Cont Rel. 65(1–2): 271–284.

Maji R, ShekharDey N, Satapathy BS, Mukherjee B, Mondal S. 2014. Preparation and characterization of Tamoxifen citrate loaded nanoparticles for breast cancer therapy. Inter J Nanomed. 9: 3107–3118.

Melo MT, de Oliveria IM, Grivicich I, Guecheva TN, Saffi J, Henriques JAP, Rosa RM. 2013. Diphenyl diselenide protects cultured MCF-7 cells against tamoxifen-induced oxidative DNA damage. Biomed Pharma. 67(4): 329–335.

Mondal S, Dorozhkin SV, Pal U. 2018. Recent progress on fabrication and drug delivery applications of nanostructured hydroxyapatite. Nanomed Nanobiotech. 10 (4):1504.

Netz DJA, Sepulveda P, Pandolfelli VC, Spadaro ACC, Alencastre JB, Bentley MVLB, Marchetti JM. 2001. Potential use of gelcasting hydroxyapatite porous ceramic as an implantable drug delivery system, International Journal of Pharmaceutics. 213(1-2): 117-125.

Nosrati H, Rashidi N, Danafar H, Manjili HK. 2017. Anticancer Activity of Tamoxifen Loaded Tyrosine Decorated Biocompatible Fe_3O_4 Magnetic Nanoparticles Against Breast Cancer Cell Lines. J Inorganic and Organomet Poly Mat. 28(3): 1178-1186.

Öztürk E, Karaboğa A, Dokumacı AH, Yerer MB. 2018. Real-time Analysis of Impedance Alterations by the Effects of Vanadium Pentoxide on Several Carcinoma Cell Lines. Turk J Pharm Sci. 15(1): 1-6.

Paganini-Hill A, Clark LJ. 2000. Preliminary assessment of cognitive function in breast cancer patients treated with tamoxifen. Breast Cancer Res Treat. 64(2): 165-7.

Pasinli A. 2004. Biyomedikal alanlarda kullanılan biyomalzemeler. Makine Teknolojileri Elektronik Dergisi. 4: 25-34.

Uskokovic V, Desai TA. 2014. In vitro analysis of nanoparticulate hydroxyapatite/chitosan composites as potential drug delivery platforms for the sustained release of antibiotics in the treatment of osteomyelitis. J Phar Sci. 103(2): 567-579.

Rehman S, Khan K, Mujahid M, Nosheen S. 2016. Synthesis of Nano Hydroxyapatite and its Rapid Mediated Surface Functionalization by Silane Coupling Agent. Mat Sci Eng C Mater Biol Appl. 675–681.

Rocha JHG, Lemos AF. 2005. Hydroxyapatite scaffolds hydrothermally grown from aragonitic cuttlefish bones. J Mater Chem. 15: 5007–5011.

Senapati S, Mahanta AK, Kumar S, Maiti P. 2018. Controlled drug delivery vehicles for cancer treatment and their performance. Signal Transduct Targed Ther. 3:7

Singh SK, SinghS, Lillard JWJr, Singh R. 2017. Drug delivery approaches for breast cancer. Inter J Nanomed. 12: 6205–6218.

Simek P, Klímová K, Sedmidubsky D, Jankovský O, Pumer M, Sofer Z. 2015. Towards graphene iodide: Iodination of graphite oxide. Nanoscale. 7(1): 261-270.

Şener LT, Albeniz G, Dinç B, Albeniz I. 2017. iCELLigence real time cell analysis system for examining the cytotoxicity of drugs to cancer cell lines. Exp Therap Med. 14: 1866-1870.

Taşkın MB, Şahin Ö, Taşkın H, Atakol O, İnal A, Güneş A. 2018. Effect of synthetic nano-hydroxyapatite as an alternative phosphorus source on growth and phosphorus nutrition of lettuce (Lactuca sativa L.) plant. J Plant Nut. 41(9): 1148-1154.

Tice RR, Agurell E, Anderson D, Burlinson B, Hartmann A, Kobayashi H, Miyamae Y, Rojas E, Ryu J-C, Sasaki YF. 2000. Single cell gel/comet assay: guidelines for in vitro and in vivo genetic toxicology testing. Env Mol Mut. 35: 206–221.

Urcan E, Haertel U, Styllou M, Hickel R, Scherthan H, Reichl FX. 2010. Real-time xCELLigence impedance analysis of the cytotoxicity of dental composite components on human gingival fibroblasts. Dent. Mater. 26(1): 51-58.

Wozniak K, Kolacinska A, Blasinska-Morawie M, Morawiec-Bajda A, Morawiec Z, Zadrozny M, ,Blasiak J. 2007. The DNA-damaging potential of tamoxifen in breast cancer and normal cells. Arch Toxicol. 81:519–527. DOI 10.1007/s00204-007-0188-3

Wu Q, Shi J, Wei J, Yang L, Cao S. 2010. In situ functionalization of hollow mesoporous hydroxyapatite with thermal-responsive on-off gates in supercritical CO_2. Royal Soc Chem. 5(86): 70101-70108.

Yao Y, Zhou Y, Liu L, Xu Y, Chen Q, Wang Y, Wu S, Deng Y, Zhang J and Shao A (2020) Nanoparticle-Based Drug Delivery in Cancer Therapy and Its Role in Overcoming Drug Resistance. Front. Mol. Biosci. 7:193.

RESEARCH ARTICLE
Eurasian J Bio Chem Sci, 5(Suppl 1):119-126, 2022
https://doi.org/10.46239/ejbcs.1141865

EJBCS

Eurasian Journal of Biological and Chemical Sciences

Journal homepage: www.dergipark.org.tr/ejbcs

Monoethanolamine Treatment of Fish Wastes and Salmon Guts to Increase Its Palmitoylethanolamide and Anandamide Contents

Lemuel M. Diamante

Seperex Nutritionals Ltd., Center for Innovation, University of Otago, Dunedin, New Zealand

*Corresponding author : lmdiamante2002@yahoo.com
Orcid No: https://orcid.org/0000-0003-1203-7620

Received : 07/07/2022
Accepted : 03/09/2022

Abstract: This study was carried out to determine the palmitoylethanolamide (PEA) and arachidonoylethanolamide (AEA) or anandamide contents in selected fish wastes, treating the fish wastes with highest PEA and AEA with different concentration of monoethanolamine (MEA) solution, incubation temperature and time, as well as the ratio of MEA solution to fish waste to further increase its PEA and AEA contents.Based on the results of the preliminary experiment, a fractional factorial design experiments was done with 4 factors including MEA concentration, incubation time, incubation temperature and dosing ratio (MEA solution:salmon guts). The results showed that the MEA content ranged from 2.25 to 8.06 mg/g sample, the PEA content ranged from 17.4 to 300.2 µg/g sample while the AEA content ranged from 1.3 to 19.0 µg/g sample all on a wet weight basis of all the FD treated samples. The FD treated sample with the highest MEA, PEA and AEA using an MEA solution concentration of 250mM from pure MEA chemical, incubation time of 0.5 hour, incubation temperature of 6oC and a dose ratio of 6 mL MEA solution:100 g salmon guts. The MEA, PEA and AEA contents of the different samples were analysed using the Yates algorithm to determine which of the four factors were more important. The results showed that MEA, PEA and AEA contents were significantly affected by the concentration of MEA solution used in dosing the salmon guts, followed by the incubation time and then a slight effect of dosing ratio while the incubation temperature has no significant effect.

Keywords: Monoethanolamine, HPLC-UV, Palmitoylethanolamide, Anandamide, Fish Wastes, Salmon Guts

1. Introduction

Amide-linked fatty acids occur in nature in the form of ceramides as major components of sphingolipids and as N-acyl constituents of proteins. Among glycerophospholipids they are usually present in trace amounts as N-acylphosphatidylethanolamine (N-acyl PE) and N-acylphosphatidylserine (N-acyl PS) (Schmid et al., 1990). While both N-acyl PE and N-acyl PS may be functionally important components of biological membranes, the major interest in N-acyl PE has been its role as the precursor of N-acyethanolamines (NAEs), especially the endogenous cannabinoid, arachidonoylethanolamide (AEA) or anandamide (Di Marzo, 1998). Schmid (2000) hypothesized that different NAES, including anandamide, can mediate biological processes through targets other than cannabinoid receptors. The cellular levels of both N-acyethanolamines (NAEs) and N-acylphosphatidylethanolamine (N-acyl PE) appear to be tightly regulated under physiological conditions, these are increased in intact cells in response to stress and these are increased massively under conditions of cell and tissue degeneration and membrane degradation (Schmid and Berdyshev, 2002).

The identification and cloning of cannabinoid receptors (Pertwee, 1993; Howlett, 1995) in both brain (cannabinoid 1, CB1) (Matsuda et al., 1990) and peripheral tissues (cannabinoid 2, CB2) (Munro et al., 1993; Bayewitch et al., 1995) facilitated studies in the analgesic effects of cannabinoids. In addition, putative endogenous cannabinoid ligands have been described for both central CB1 (Devane et al., 1992; Fride and Mechoulam, 1993) and peripheral CB2 cannabinoid receptors (Facci et al., 1995). The brain constituent anandamide or AEA, has been shown to be produced by neuronal cells (Di Marzo et al., 1994) and have cannabimimetic effects (Smith et al., 1994; Mechoulam et al., 1996). Agonists at the CB1 receptor site have been shown to exhibit anti-nociceptive activity in models of acute (Smith et al., 1994; Stein et al., 1996) and neuropathic pain (Herzberg et al., 1997). As with endogenous opioid ligands, the duration of activity of AEA is thought to be short (Welch et al., 1995; Stein et al., 1996).

Activation of the CB2 receptor appear to be more involved in downregulation of the inflammatory response (Facci et al., 1995; Mazzari et al., 1996). It has recently become clear that CB2 receptors are expressed on cells of immune origin, including lymphocytes, mast cells and macrophages (Facci et al., 1995; Galiegue et al., 1995). Palmitoylethanolamide or PEA (a candidate for the endogenous ligand at the CB2 receptor) accumulates in inflamed tissue (Natarajan et al., 1982) and has been shown to reduce mast cell degranulation, plasma extravasation and hyperalgesia in a dose dependent manner (Mazzari et al., 1996). It has been proposed that the local production of PEA may lead to inhibition of both inflammation and sensitizing effects of inflammatory products on nociceptive processes (autocoid local inflammation, ALIA) (Levi-Montalcini et al., 1996); this may be a CB2 receptor mediated effect (Jaggar et al., 1998).

PEA is an endogenous fatty acid amide, an analog of the endocannabinoid anandamide (AEA), that belongs to the family of N-acylethanolamines NAE (Hansen, 2010). NAEs are released from cells in response to noxious stimuli. As all NAEs, also the PEA has a local effect, and its tissue levels are closely regulated through the balance of production and degradation activity (Passavanti et al., 2019).

The effects of the PEA are due to its interaction with several pathways: at first, it reduces, via the peroxisome proliferator-activated receptor alpha (PPARα), the recruitment and activation of mast cells at sites of nerve injury and the release of pro-inflammatory mediators from these cells (Costa et al., 2008; Cerrato et al., 2010); secondly, it inhibits the microglia activation and the recruitment of mast cells into spinal cord after peripheral nerve injury, as well as following spinal neuroinflammation or spinal cord injury (Genovese et al., 2008; Esposito et al., 2011). Sugiura et al. (2000) have demonstrated that PEA has just a very low affinity for cannabinoid receptor 2 (CB_2), clarifying why CB_2 antagonists do not inhibit some of its anti-inflammatory effects (Costa et al., 2002). PEA indirectly activates CB_2 and the cannabinoid receptor 1 (CB_1) (Petrosino and Di Marzo, 2017), down-modulating fatty acid amide hydrolase (FAAH), the enzyme responsible of the degradation of AEA, a CB_1 agonist (Di Marzo et al., 2001).

A proprietary method to highly enrich animal tissues with NAEs such as PEA and AEA using the process aid monoethanolamine (MEA) that increases their synthesis in situ was developed by Seperex Nutritionals (2008). In this process, NAEs are synthesized using the tissues own endogenous enzymes (acyltransferases and phospholipases) and phospholipid substrates (phosphatidylethanolamine, PE). Seperex Nutritionals Ltd. had already applied this process to green-lipped mussel meat and recommended its use on fish wastes. In New Zealand, there are several fish wastes from processing plants that this process can be applied like salmon guts, salmon mature and immature roes, hoki guts and hoki roe, as well as squid guts. Knowing the NAEs in these wastes is important since the waste with the highest NAEs would be the best sample to process with MEA to increase further its NAEs. This resulting product can be utilized as a pet food supplement particularly for older dogs and cats suffering from chronic pain and inflammation. Della Rocca and Gamba (2021) pointed out the use of micro-PEA for the chronic pain in dogs and cats.

The problem of fish wastes has increased over the years and becoming a global concern which is affected by several biological, technical, and operational factors as well as socio-economic drivers (Kim and Mendis, 2006; Arvanitoyannis and Kassaveti, 2008). It has been estimated that more than 50% of fish tissues including fins, heads, skin, and viscera are discarded as they are considered wastes. Every year discards from the world's fisheries exceed 20 million tons equivalent to 25% of the total production of marine fishery catch and include "non-target" species, fish processing wastes and by-products (Kim and Mendis, 2006; Mahro and Timm, 2007). Fish wastes and byproducts are increasingly gaining attention, as they offer a significant and sustainable source of high-value bio-compounds, due to their high content of collagen, peptides, chitin, polyunsaturated fatty acids (PUFA), enzymes and minerals, suitable for biotechnological or pharmaceutical applications with high market value (Shahidi et al., 2019; Shavandi et al., 2020). Hence, the process to produce treated fish wastes with high NAEs is an additional technology for fish wastes processing.

Determination of MEA content in samples was needed for the analysis. Several of methods based on the HPLC with refractive index detector (RID) system were published (Supap et al., 2006; Voice and Rochelle, 2013; Zhao et al., 2015) and HPLC with ultraviolet (UV) detector system with derivatization were also reported (Ngim et al., 2007; Larsen and Sansom, 2008; Liu et al., 2009).

Analysis of the PEA and AEA in food samples can be done using the LC-MS system as shown by Cawthron Institute (2009), Abramo et al. (2014) and Esposito et al. (2021).

This study was carried out to determine the PEA and AEA in selected fish wastes and treating the fish wastes with highest PEA and AEA with different concentration of MEA solution, incubation temperature and time, as well as the ratio of MEA to fish waste to further increase its PEA and AEA.

2. Materials and Methods

2.1. Materials

The Sanger reagent (2% 1-fluoro-2,4-dinitrobenzene in acetone), MEA (99.5% pure), sodium bicarbonate, methanol, and hydrochloric acid (HCl) were purchased from the (Sigma-Aldrich, Auckland, New Zealand). The HPLC grade chemicals (99.9%) like Acetonitrile and Formic Acid were procured from Fisher Chemical (Loughborough, UK). The salmon guts, salmon immature and immature roes were obtained from High Country Salmon, Glenbrook, Twizel, New Zealand Salmon while the hoki guts, hoki roe and squid guts from Sanford, Auckland, New Zealand.

2.2. MEA Measurement

The MEA measurement method developed by Larsen and Sansom (2008) was modified in order to use an isochratic pump mode instead of the low-pressure gradient pump mode. The mobile phase used was 50% Acetonitrile and 50% of 0.1% aqueous formic acid solution. After many

evaluations the final method used is summarised as follows. A high-performance liquid chromatography (HPLC) Shimadzu (LC-10AD VP liquid chromatograph) with system controller (SCL-10A VP) equipped with a pump and auto-injector (SIL-10AD VP) and UV-vis detector (SPD-10AV) was used in the analysis of MEA from the hydrolysed fish wastes and standard solutions. The chromatographic column was a Luna 5 µm C18 (2) 100 A, 250 mm x 4.6 mm with a security guard. The detector signal was analysed using the LC Solution software to obtain the integrated area of the peaks from the chromatogram. The mobile phase was a mixture of 50% acetonitrile and 50% of 0.1% aqueous formic acid solution in isochratic pump mode with a flowrate of 0.50 mL/min. HPLC-UVvis measurements were done at room temperature of about 20-25ºC. The UV-vis detector was set with a wavelength of 340 nm for Channel 1 and 254 nm for Channel 2. A 5 µL of the filtered sample was automatically injected into the system for measurement. The retention time and peak area of MEA can be obtained from the print-out of the software. The peak area of various MEA standard solutions was correlated using linear and polynomial regressions. The regression equation with high coefficient of determination (r^2) but at the same time have more realistic values (i.e. no negative values) will was used in converting the peak area of the samples into MEA concentrations (mg/mL). The MEA content of the sample (mg/g sample) was obtained by dividing the MEA concentration with 0.1 g sample which is the amount contained in a 1 mL liquid sample.

The derivatization of the MEA standard solutions and the fish wastes samples followed a modified procedure of Larsen and Samson (2008). The fish wastes samples were prepared by getting 30-40 g and then using the method as follows: a) get 1.0 g of the fish wastes sample and put into a 15-mL plastic container. Add purified water to the 10 mL mark and mix the contents by shaking using a mechanical shaker for 1 min; b) obtain 1 mL each of the mixture into two 1.5 mL Eppendorf tube and centrifuge at 10,000 rpm for 5 minutes; c) a sample of aqueous layer (400 µL) from the each Eppendorf tube was obtained and placed into a 6-mL plastic container, then 400 µL of 2% Sanger's reagent in acetone solution, 400 µL purified water and 160 µL of 1 M sodium bicarbonate solution were added; d) the mixture was mixed by manual shaking the container and then incubating in a water bath at 50ºC for 1 hour; e) at the end of incubation, the container was taken out of the water bath and cooled down at room temperature; f) the mixture was added with 100 µL of 2 M HCl solution and the contents were well mixed; g) obtain 800 µL of this solution and place into another 6-mL plastic container (green top) and dilute with 400 µL of Methanol, and 400 µL of 0.1% aqueous Formic Acid solution; and h) the mixture was mixed well by manual shaking and then filtered thru a 0.45 µm PTFE filter into amber vials for HPLC-UVvis measurement of MEA.

The MEA standard solutions were prepared as follows: a) a stock solution of MEA (10.17 mg/mL) was prepared in methanol. Subsamples of these MEA standard solutions were taken and derivatized to prepare a calibration curve from 0.013 to 1.017 mg/mL which would equate to approximately 0.13 to 10.17 mg/g sample; b) derivatization was done by mixing the MEA standard solution (400 µL), Sanger's reagent in 2% acetone (400 µL), purified water (400 µL) and 1 M sodium bicarbonate solution (160 µL) in a 6-mL plastic container. Then steps (d) to (h) for the sample preparation of fish wastes was followed.

2.3. MEA Treatment of Fish Wastes

A preliminary experiment was done on the treatment of selected fish wastes added with 130 mM concentration of MEA solution and incubated at 10ºC for one hour with a dosing ratio of 4 mL MEA solution: 100 g fish wastes and then was freeze dried. Based on the results of this experiment, 4 factors were identified to be important in the production of NAEs from the MEA-treated fish wastes that gave the highest PEA. The factors include MEA concentration, incubation time, incubation temperature and dosing ratio (MEA Solution:Fish Wastes). A fractional factorial design in 4 factors and 2 levels was carried out as shown in Table 1.

2.4. Moisture Content and Product Yield of the FD Treated Salmon Guts

The initial and final moisture contents of the freeze-dried (FD) treated fish wastes were determined at Cawthron Institute and the product yield was calculated as shown below:

Product Yield = 100 x (Amount of FD Product/Amount of Treated Fish Wastes) (1)

2.5. PEA and AEA Analysis

About 35 g of each freeze dried untreated and MEA-treated fish wastes samples were sent to Cawthron Institute for the determination of their PEA and AEA using the LC-MS method (Cawthron Institute, 2016). All the results were expressed in µg/g of sample.

3. Results and Discussion

3.1. Calibration Curve and Chromatogram of MEA Solution Concentration

Figure 1 shows the calibration curve of MEA with the MEA solution concentration on the y-axis and the HPLC-UV vis area on the x-axis. The separation times for MEA ranged from 7.66 to 8.09 minutes. A linear model can be fitted on the data as shown below:

MEA Concentration (mg/mL) = 0.5143 x (HPLC Area/$1x10^7$) + 0.0026 (r^2 = 0.9933) (2)

The MEA content of the sample was calculated further as shown below,

MEA Content (mg/g sample) = MEA Concentration (mg/mL)/0.1 g sample/mL (3)

The coefficient of determination (r^2) is high at 0.9933 indicating a good fit on the data as also shown in Figure 1.

Table 1. Fractional factorial design in 4 factors and 2 levels for the treatment of fish wastes (with highest PEA content) with different MEA solution concentration, incubation time, incubation temperature and dose ratio (MEA solution:salmon guts) and the resulting MEA, PEA and AEA of freeze-dried products.

Treatment	Factor 1 MEA Concentration	Factor 2 Incubation Time	Factor 3 Incubation Temperature	Factor 4 Dose Ratio
T1	50 mM (-)	0.5 hours (-)	6ºC (-)	2 ml: 100 g (-)
T2	250 mM (+)	0.5 hours (-)	6ºC (-)	6 ml: 100 g (+)
T3	50 mM (-)	5.5 hours (+)	6ºC (-)	6 ml: 100 g (+)
T4	250 mM (+)	5.5 hours (+)	6ºC (-)	2 ml: 100 g (-)
T5	50 mM (-)	0.5 hours (-)	14ºC (+)	6 ml: 100 g (+)
T6	250 mM (+)	0.5 hours (-)	14ºC (+)	2 ml: 100 g (-)
T7	50 mM (-)	5.5 hours (+)	14ºC (+)	2 ml: 100 g (-)
T8	250 mM (+)	5.5 hours (+)	14ºC (+)	6 ml: 100 g (+)

Note: Numbers in parentheses are coded factors where (+) – High Level, (-) – Low Level

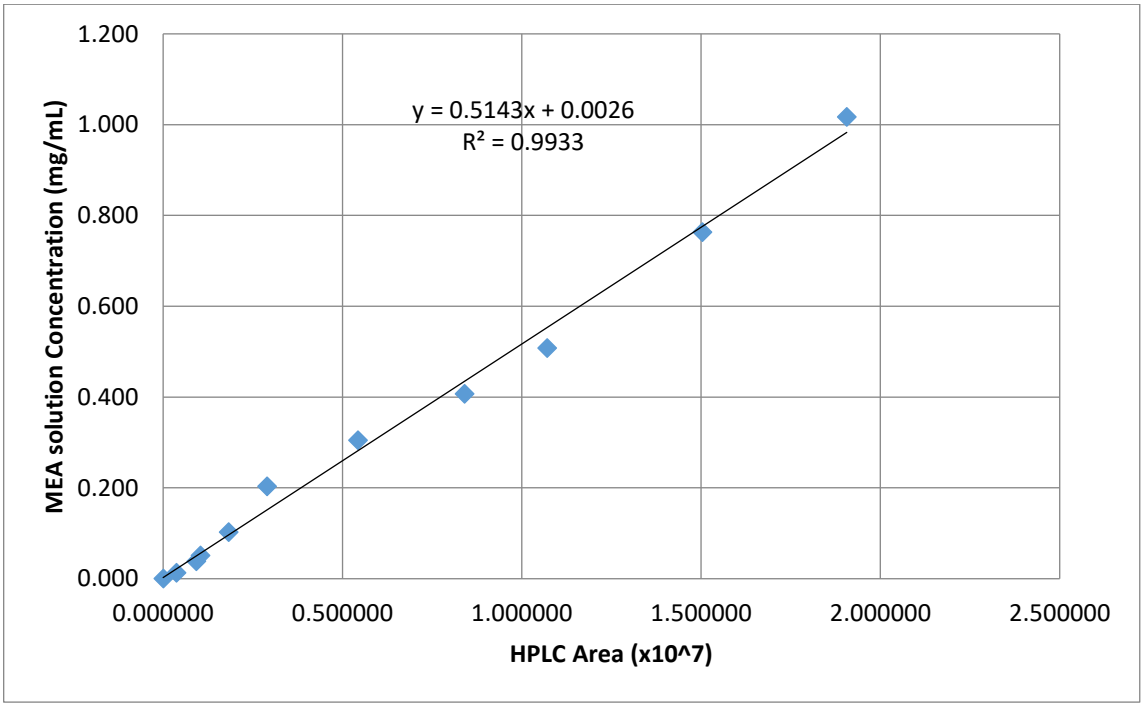

Figure 1. Calibration curve of MEA solution concentration.

The chromatogram of MEA solution with a concentration of 0.508 mg/mL is shown in Figure 2. The peak of the MEA came out at about 7.9 minutes. There were several peaks that also came out later at around 11.0, 13.6 and 14.3 minutes which were due to the mobile phase used. Figure 3 shows the chromatogram of the mobile phase only with 0 MEA concentration. As expected, no peak came out at around t=7.9 mins.

3.2. Preliminary Experiments on the Treatment of Selected Fish Wastes with MEA Solution

A preliminary experiment was done on the treatment of selected fish wastes added with 130 mM concentration of MEA solution and incubated at 10ºC for one hour with a dosing ratio of 4 mL MEA solution:100 g fish wastes and then freeze drying. Table 2 summarises the moisture, PEA and AEA contents of the different freeze-dried samples. The results show that the salmon guts gave the highest PEA (220 µg/g sample) and followed by the squid guts (130 µg/g sample) while the salmon immature roe the highest AEA (38 µg/g sample) and followed by the salmon mature roe (30 µg/g sample). The hoki roe and guts gave the lowest PEA. Based on the results, further experiments on the treatment of salmon guts with different concentration of MEA, incubation time, incubation temperature and dosing ratio (MEA solution:salmon guts).

De Luca et al. (2019) reported the PEA content of different fish meats ranged from 20 to 60 ng/g sample and even considering that fish guts might contain 10 times than the fish meat (~600 ng/g sample = 0.6 µg/g sample), would still be very low compared with the treated fish wastes obtained in this study. It must also be noted that the freeze-dried salmon mature roe gave the lowest moisture content (0.55% w.b.) while the squid guts had the highest moisture content (6.22% w.b.).

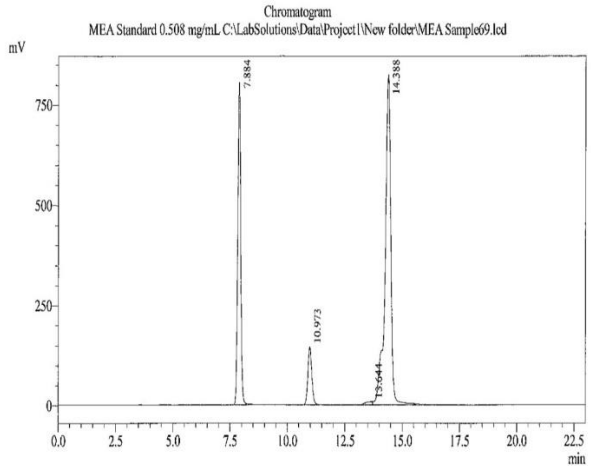

Figure 2. Chromatogram of MEA solution with a concentration of 0.508 mg/mL (MEA is shown at t=7.9 mins).

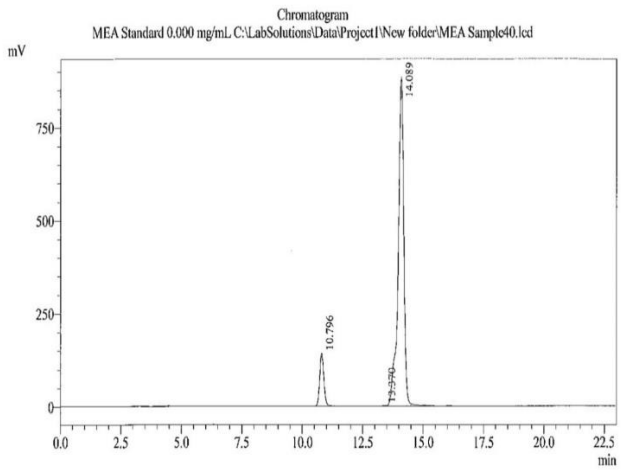

Figure 3. Chromatogram of the mobile phase only with 0 MEA solution concentration (no peak at t=7.9 mins).

3.3. Treatment of Salmon Guts with MEA Solution using a Fractional Factorial Design

Table 3 shows the moisture content, MEA content and percent yield of the different treated and freeze-dried samples using a fractional factorial design. The moisture contents ranged from 2.61 to 3.29 g/100 g sample, the MEA content ranged from 2.25 to 8.06 mg/g sample (wet weight basis) and 2.32 to 8.30 mg/g sample (dry weight basis) and the percent yield from 43.92 to 50.79%. While Table 4 shows the PEA and AEA contents of the different treated and freeze-dried samples. The PEA content ranged from 17.4 to 300.2 µg/g sample while the AEA content ranged from 1.3 to 19.0 µg/g sample.

It must be noted that the LD_{50} of MEA for oral dose in rabbits was at 1.0 to 2.9 g/kg body weight (Knaak et al., 1997). Since, the LD_{50} for dogs was not found, the lower dose of 1.0 g/kg or 1000 mg MEA/kg body weight was assumed to apply for dogs, then all the samples were within the allowable dose even ingesting as much as 100 g of the treated salmon guts for the sample with the highest MEA content. It is worth noting that the highest PEA content of the treated salmon guts increased by 1.5 times of the untreated salmon guts while the AEA increased by 1.7 times.

The MEA, moisture, PEA and AEA contents of the different samples (Tables 3 and 4) were analysed using the Yates algorithm to determine which of the four factors were more important (Myers et al., 2009). The results showed that MEA, PEA and AEA were significantly affected by the concentration of MEA solution used in dosing the salmon guts, followed by the incubation time and then a slight effect of dosing ratio. There is also a high interaction effect between the concentration of MEA solution and incubation time and a slight interaction effect between concentration of MEA solution and dosing ratio. The incubation temperature has no significant effect on all the properties.

Table 2. Moisture, PEA and AEA contents for the different treated fish wastes with 130 mM concentration of MEA solution, dosing ratio of 4 mL MEA solution:100 g fish guts and incubated at 10ºC for one hour and then freeze dried at 60ºC.

Fish Wastes	Moisture Content (% w.b.)	PEA (µg/g sample)	AEA (µg/g sample)
Salmon Mature Roe	0.55	89	30
Salmon Immature Roe	2.02	110	38
Salmon Guts	2.12	220	11
Hoki Roe	2.07	28	3
Hoki Guts	2.57	82	11
Squid Guts	6.22	130	7

Table 3. Moisture content, MEA content and percent yield of the different samples of freeze-dried treated salmon guts in the screening experiments.

Treatment	Moisture Content (g/100g) (wb)	MEA Content (mg/g) (w.w.b.)	MEA Content (mg/g) (d.w.b.)	Percent Yield
T1S	3.14	3.05	3.15	45.83
T2S	2.84	8.06	8.30	43.92
T3S	2.93	2.25	2.32	46.11
T4S	2.61	7.87	8.08	48.68
T5S	3.29	3.18	3.28	44.50
T6S	2.60	7.57	7.77	46.60
T7S	2.62	2.30	2.36	50.79
T8S	2.97	8.05	8.30	46.07

wwb – wet weight basis; dwb – dry weight basis; wb – wet basis

Table 4. PEA and AEA contents on a wet weight basis of the different samples of freeze-dried treated salmon guts in the screening experiments.

Treatment	PEA Content (µg/g) (wet basis)	AEA Content (µg/g) (wet basis)
T1S	17.4	1.3
T2S	300.2	19.0
T3S	34.6	2.4
T4S	120.6	7.0
T5S	28.9	2.4
T6S	252.1	17.5
T7S	44.1	2.8
T8S	138.4	9.1

4. Conclusion

The MEA treated salmon guts gave the highest PEA and followed by the squid guts while the salmon immature roe the highest AEA and followed by the salmon mature roe. The hoki roe and guts gave the lowest PEA.

The MEA, PEA and AEA were significantly affected by the concentration of MEA solution used in dosing the salmon guts, followed by the incubation time and then a slight effect of dosing ratio. There is also a high interaction effect between the concentration of MEA solution and incubation time and a slight interaction effect between concentration of MEA solution and dosing ratio. The incubation temperature has no significant effect on all the properties.

Acknowledgments

The author would like to thank Seperex Nutritionals Ltd. for providing the research funds and facilities.

Authors' contributions:

The article was written by LMD, as well as the data analysis.

Conflict of interest disclosure:

The author declares no conflict of interest on the written article.

References

Abramo F, Campora L, Albanese F, Della Valle MF, Cristino L, Petrosino S, Di Marzo V, Miragliotta V 2014. Increased levels of palmitoylethanolamide and other bioactive lipid mediators and enhanced local mast cell proliferation in canine atopic dermatitis. BMC Veterinary Research. 10: 21-29.

Arvanitoyannis IS, Kassaveti A 2008. Fish industry waste: Treatments, environmental impacts, current and potential uses. Journal of Food Science and Technology. 43: 726-745.

Bayewitch M, Avidor-Reiss T, Levy R, Mechoulam R, Barg J, Vogel, Z 1995. Activation of the peripheral cannabinoid receptor (CB2) inhibits adenyl cyclase. Society of Neuroscience Abstracts. 21: 2608.

Cawthron Institute. 2009. Determination of fatty acid ethanolamides by LC-MS. Cawthron Quality Systems Manual 20 Method 40.113. Nelson, New Zealand. 11 pp.

Cerrato S, Brazis P, Della Valle, MF, Miolo A, Puigdemont A (2010). Effects of palmitoylethanolamide on immunologically induced histamine, PGD2 and TNFα release from canine skin mast cells. Veterinary Immunology and Immunopathology. 133: 9-15.

Costa B, Comelli F, Bettoni I, Coleoni M, Giagnoni G (2008). The endogenous fatty acid amide, palmitoylethanolamide, has anti-allodynic and anti-hyperalgesic effects in a murine model of neuropathic pain: Involvement of CB1, TRPV1 and PPARϒreceptors and neurotrophic factors. Pain. 139: 541-550.

Costa B, Conti S, Giagnoni G, Colleoni M 2002. Therapeutic effect of the endogenous fatty acid amide, palmitoylethanolamide, in rat acute inflammation: Inhibition of nitric oxide and cyclo-oxygenase systems. British Journal of Pharmacology. 137-413-420.

Della Rocca G., Gamba D 2021. Chronic pain in dogs and cats: Is there a place for dietary intervention with micro-palmitoylethanolamide? Animals. 11: 952 (31 pp.). doi.org//10.3390/ani11040952.

De Luca L, Ferracane R, Vitaglione P 2019. Food database of N-acyl-phosphatidylethanolamines, N-acylethanolamines and endocannabinoids and daily intake from a western, a Mediterranean and a vegetarian diet. Food Chemistry. 300: 125218. 9 pp.

Di Marzo V. 1998. Endocannbinoids and other fatty acid derivatives with cannabimemitec properties: biochemistry and

possible physiopathological relevance. Biochimica Biophysics Acta. 1392: 153-175.

Di Marzo V, Fontana A, Cadas H, Schinelli S, Cimino G, Schwartz J, Piomelli D 1994. Formation and inactivation of the endogenous cannabinoid anandamide in central neurons. Nature. 372: 686-691.

Di Marzo V, Melck D, Orlando P, Bisogno T, Zagoory O, Bifulco M, Vogel Z, Petrocellis L 2001. Palmitoylethanolamide inhibits the expression of fatty acid amide hydrolase and enhances the anti-proliferative effect of anandamide in human breast cancer cells. Biochemistry Journal. 348: 249-255.

Esposito E, Paterniti I, Mazzon E, Genovese T, Di Paola R, Galuppo M, Cuzzocrea S 2011. Effects of palmitoylethanolamide on release of mast cell peptidases and neurotrophic factors after spinal cord injury. Brain Behaviour and Immunology. 25: 1099-1112.

Esposito G, Pesce M, Seguella L, Lu J, Corpetti C, Del Re A, De Palma FDE, Esposito G, Sanseverino W, Sarnelli G 2021. Engineered *Lactobacillus paracasei* producing palmitoylethanolamide (PEA) prevents colitis in mice. International Journal of Molecular Sciences. 22: 1-14.

Facci L, Dal Toso R, Romanello S, Buriani A, Skaper SD, Leon A 1995. Mast cell express a peripheral cannabinoid receptor with differential sensitivity to anandamide and palmitoylethanolamide. Proceedings of the National Academy of Science (USA). 92: 3376-3380.

Fride E, Mechoulam R 1993. Pharmacological activity of the cannabinoid receptor agonist, anandamide, a brain constituent. European Journal of Pharmacology. 23: 313-314.

Galiegue S, Mary S, Marchand J, Dussossoy D, Carriere D, Carayon P, Bouaboula M, Shire D, Le Fur G, Casellas P 1995. Expression of central and peripheral cannabinoid receptors in human immune tissues and leukocyte subpopulations. European Journal of Biochemistry. 232: 54-61.

Genovese T, Esposito E, Mazzon E, Di Paola R, Meli R, Bramanti P, Piomelli D, Calignano A, Cuzzocrea S 2008. Effects of palmitoylethanolamide on signaling pathways implicated in the development of spinal cord injury. Journal of Pharmacology and Experimental Therapy. 326: 12-23.

Hansen HS 2010. Palmitoylethanolamide and other anandamide congeners. Propose role in the diseased brain. Experiments in Neurology. 224: 48-55.

Herzberg U, Eliav E, Bennett JG, Kopin IJ 1997. The analgesic effects of R(+)-WIN 55, 212-2 mesylate, a high affinity cannabinoid agonist, in a rat model of neuropathic pain. Neuroscience Letters. 221: 157-160.

Howlett AC 1995. Pharmacology of cannabinoid receptors. Annual Review in Pharmacology and Toxicology. 35: 607-634.

Jaggar SI, Hasnie FS, Sellaturay S, Rice ASC. 1998. The anti-hyperalgesic actions of the cannabinoid anandamide and the putative CB2 receptor agonist palmitoylethanolamide in visceral and somatic inflammatory pain. Pain. 76: 189-199.

Knaak JB, Leung HW, Stott WT, Busch J, Bilsky J 1997. Toxicology of mono-, di- and triethanolamine. Reviews in Environmental Contaminants Toxicology. 149: 1-86.

Kim SK, Mendis E 2006. Bioactive compounds from marine processing by-products – A review. Food Research International. 39: 383-393.

Larsen L, Sansom C 2008. Analysis of MEA in oil: Method development. Commercial Project with Seperex Nutritionals Ltd, Dunedin, New Zealand. 5 pp.

Levi-Montalcini R, Skaper SD, Dal Toso R, Petrelli L, Leon A 1996. Nerve growth factor: from neurotrophin to neurokine. Trends in Neuroscience. 19: 514-520.

Liu N, Yang J, Liu YQ, Qi W 2009. Determination of monoethanolamine by HPLC with pre-column derivatization. Contemporary Chemical Industries. 4.

Mahro B, Timm M 2007. Potential of biowaste from the food industry as a biomass resource. Engineering in Life Sciences. 7: 457-468.

Matsuda LA, Lolait SJ, Brownstein MJ, Young AC, Bonner TI 1990. Structure of a cannabinoid receptor and functional expression of the cloned cDNA. Nature. 346: 561-564.

Mazzari S, Canella R, Petrelli L, Marcolongo G, Leon A 1996. N-(2-Hydroxyethyl) hexadecanamide is orally active in reducing edema formation and inflammatory hyperalgesia by down-modulating mast cell activation. European Journal of Pharmacology. 300: 227-236.

Mechoulam R, Shabat SB, Hanus L, Fride E, Vogel Z, Bayewitch M, Sulcova AE 1996. Endogenous cannabinoid ligands – chemical and biological studies. Journal of Lipid Mediation and Cell Signal. 14: 45-49.

Munro S, Thomas KL, Abu-Shaar M 1993. Molecular characterisation of a peripheral receptor for cannabinoids. Nature. 365: 61-65.

Myers RH, Montgomery DC, Anderson-Cook CM 2009. Response Surface Methodology – Process and Product Optimization Using Designed Experiments. John Wiley & Sons Inc., Hoboken, New Jersey, USA. 681 pp.

Natarajan V, Reddy PV, Schmid PC, Schmid HHO 1982. N-Acylationof ethanolaminephospholipids in canine myocardium. Biochima Biophysica Acta. 712: 342-355.

Ngim KK, Zynger J, Downey B 2007. Analysis of monoethanolamine by derivatization with Marfey's reagent and HPLC. Journal of Chromatographic Science. 45: 126-130.

Passavanti MB, Alfieri A, Pace MC, Pota V, Sansone P, Piccinno G, Barbarisi M, Aurrilio C, Fiore M 2019. Clinical applications of palmitoylethanolamide in pain management: Protocol for a scoping review. Systematic Reviews. 8: 9-12.

Pertwee R 1993. The evidence for the existence of cannabinoid receptors. General Pharmacology. 24: 811-824.

Petrosino S, Di Marzo V 2017. The pharmacology of palmitoylethanolamide and first data on the therapeutic efficacy of some of its new formulations. British Journal of Pharmacology. 174: 1349-1365.

Schmid HHO 2000. Pathways and mechanisms of N-acylethanolamine biosynthesis: can anandamide be generated selectively? Chemistry and Physics of Lipids. 108: 71-87.

Schmid HHO, Berdyshev EV 2002. Cannabinoid receptor-inactive N-acylethanolamines and other fatty acid amides: metabolism and function. Prostaglandins, Leukotrienes and Essential Fatty Acids. 66: 363-376.

Schmid HHO, Schmid PC, Natarjan V. 1990. N-acylated glycerolipids and their derivatives. Progress in Lipid Research. 29: 1-43.

Seperex Nutritionals. 2008. An enrichment process and product – A Method of elevating fatty acid amide levels in cellular tissue and related products. Pending Patent Application WO2008/075978. New Zealand Patents Provisional Specification. 23 pp.

Shahidi F, Varatharajan V, Peng H, Senadheera R 2019. Utilization of marine by-products for the recovery of value-added products. Journal of Food Bioactives. 6: 10-61.

Shavandi A, Hou Y, Carne A, McConnell M, Bekhit AE 2019. Marine waste utilization as a source of functional and health compounds. In Advances in Food and Nutrition Research. Elsevier, Amsterdam, The Netherlands. Volume 87, pp. 187-254.

Smith PB, Compton DR, Welch SP, Razdan RK, Mechoulam R, Martin BR 1994. The pharmacological activity of anandamide,

a putative endogenous cannabinoid, in mice. Journal of Pharmacology and Experimental Therapy. 270: 219-227.

Stein EA, Fuller SA, Edgemond WS, Campbell WB 1996. Physiological and behavioural effects of the endogenous cannabinoid, arachidonylethanolamide (anandamide), in rat. British Journal of Pharmacology. 119: 107-114.

Sugiura T, Kondo S, Kishimoto S, Miyashita T, Nakane S, Kodaka T, Suhara Y, Takayama H, Waku K 2000. Evidence that 2-arachidonoylglycerol but not N-palmitoylethanolamine or anandamide is the physiological ligand for the cannabinoid CB2 receptor: Comparison of the agonistic activities of various cannabinoid receptor ligands in HL-60 cells. Journal of Biological Chemistry. 275: 605-612.

Supap T, Idem R, Tontiwachwuthikul P, Saiwan C 2006. Analysis of monoethanolamine and its oxidative degradation products during CO_2 absorption from flue gases: A comparative study of GC-MS, HPLC-RID and CE-DAD analytical techniques and possible optimum conditions. Industrial Engineering Chemical Research. 45: 2437-2451.

Voice A, Rochelle GT 2013. Products and process variables in oxidation of monoethanolamine for CO_2 capture. International Journal of Greenhouse Gas Control. 12: 472-477.

Welch SP, Dunlow SD, Patrick GS, Razdan RK 1995. Characterisation of anandamide- and fluoroanandamide-induced antinociception and cross tolerance to delta-9-THC after intrathecal administration to mice: blockade of delta-9-THC-induced antinociception. Journal of Pharmacology and Experimental Therapy. 273: 1235-1244.

Zhao Z, Dong H, Huang Y, Cao L, Gao J, Zhang X, Zhang S 2015. Ionic degradation inhibitors and kinetic models for CO_2 manufacture with aqueous monoethanolamine. International Journal of Greenhouse Gas Control. 39: 119-128.

RESEARCH ARTICLE
Eurasian J Bio Chem Sci, 5(Suppl 1):127-134, 2022
https://doi.org/10.46239/ejbcs.1141216

EJBCS

Eurasian Journal of Biological and Chemical Sciences

Journal homepage: www.dergipark.org.tr/ejbcs

Major Phospholipids of Selected Dairy Products as Determined by the HPLC-UVvis and ^{31}P-NMR Methods

Lemuel M. Diamante

Seperex Nutritionals Ltd., Center for Innovation, University of Otago, Dunedin, New Zealand

*Corresponding author : lmdiamante2002@yahoo.com
Orcid No: https://orcid.org/0000-0003-1203-7620

Received : 06/07/2022
Accepted : 03/09/2022

Abstract: This study was carried out to determine the major phospholipids in selected dairy products (Beta Serum, Procream and Phospholipids-Rich Dairy products), evaluate the accuracy of the developed fat extraction method for liquid dairy samples and to compare the major phospholipids of different dairy samples obtained using the HPLC-UVvis and ^{31}P-NMR methods. It was found that the developed fat extraction method can be used to estimate the lipid content of liquid dairy samples were still a bit satisfactory. Using the HPLC-UVvis method, it was found that the sphingomyelin (SM) consists of 2 curves in Beta Serum, Procream and Phospholipid-Rich products. The phosphatidylethanolamine (PE) separated ahead of phosphatidylcholine (PC) and then PC ahead of SM1 and SM2. The results showed that the data of the major phospholipids (PC, PE and SM) in Butter Serum, Procream and Phospholipids-Rich products as determined by the HPLC-UVvis method compared well with those of the ^{31}P-NMR method It must be noted that the analysis temperature for the HPLC-UVvis method was at 40ºC while the ^{31}P-NMR method was at 30ºC, and this might have also contributed to the slight variation of the results. Furthermore, the HPLC-UVvis method is rapid and with cheaper analysis cost compared with the ^{31}P-NMR method.

Keywords: Phospholipids, Phosphatidylcholine, Phosphatidylethanolamine, Sphingomyelin, HPLC-UVvis, ^{31}P-NMR

1. Introduction

Phospholipids are a class of complex polar lipids with an inherent amphiphilic nature due to the presence of a hydrophobic fatty acid tail and a hydrophilic head (Contarini and Povolo, 2013; Donato et al., 2011; Kielbowicz et al., 2013). Phospholipids are subdivided into glycerophospholipids and sphingophospholipids (Donato et al., 2011). Phosphatidylcholine (PC) and phosphatidylethanolamine (PE) are the major glycerophospholipids, while the Sphingomyelin (SM) is the dominant species of sphingophospholipids (Le et al., 2011). Phospholipids may represent only 1-5% of total milk lipids, but are distinctive because of their polar nature that underpins their structural and functional role in the formation of the natural emulsifying layer surrounding fat globules in milk, i.e. the milk fat globule membrane (MFGM) (Contarini and Povolo, 2013). The MFGM has a tripartite structure composed of an inner monolayer of proteins and polar lipid, followed by a 'true' outer bilayer, and originates from the apical plasma membrane of the mammary gland secretory cells (Dewettinck et al., 2008). The amphiphilic nature of phospholipids facilitates the formation of bilayers and, thus, aids in the emulsification of fat in milk (Rombaut and Dewettinck, 2006).

Phospholipids were recently taken more into consideration because of their nutritional and technological characteristics (Dewettinck et al., 2008). Their inhibitory effect on some types of cancer (Kuchta et al., 2012; Castro-Gomez et al., 2016; Verardo et al., 2017), their ability to reduce blood cholesterol levels (Verardo et al., 2017; Duivenvoorden et al., 2006) and enhance brain functioning (Verardo et al., 2017; McDaniel et al., 2003), their anti-bacterial and anti-inflammatory activity (Verardo et al., 2017; Vesper et al., 1999) and their protective effect on gastric mucosa (Kivinen et al., 1992) have been studied. Additionally, their emulsifying properties can be used in several applications in the food, pharmaceutical and cosmetic industry (Lesser et al., 2006).

Dairy products are a good source of these phospholipids (Vesper et al., 1999). The biological membrane of native milk fat globules consists of about one-third phospho- and sphingo-lipids, stabilizing the milk fat globules in the serum phase of milk. Analysis of these lipids can be accomplished by means of ^{31}P-Nuclear Magnetic Resonance (NMR), High Performance Liquid Chromatography (HPLC), Thin Layer

Chromatography (TLC), Fourier Transform Infrared, and by measuring the total phosphorus content (Vanhoutte et al., 2004). Over the course of the past few decades, HPLC has become the preferred method for the determination of phospholipids, as quantitative and qualitative analysis can readily be obtained at a relatively low cost compared to ^{31}P-NMR (Rombaut et al., 2005). For the chromatographic analysis of fats and oils, the use of evaporative light scattering detection is generally preferred (Rombaut et al., 2005; Le et al., 2011), however the detector is very expensive. Rehman et al. (2017) reported a simple and rapid separation and determination of phospholipids by HPLC-UV system and obtained satisfactory results for different phospholipids standards.

Critical points in the analysis of phospholipids in food products are the method of fat extraction, separation, and detection. Often, little attention is given to the first of these. The majority of phospholipids in food products are present in membranous structures, interacting with compounds of a complex food matrix, making them difficult to extract (Rombaut et al., 2005). In order to avoid these problems, a cold-extraction procedures like those of Folch et al. (1957) and Bligh and Dyer (1959) are recommended. Lee et al. (1996) developed a simple and rapid solvent fat extraction for fish tissue based on the two methods mentioned previously and found to have satisfactory results for cod and mackerel samples compared with the Bligh and Dyer method.

There are many commercial dairy products that are obtained from milk processing including Beta Serum and Procream. Beta Serum or Buttermilk is the aqueous phase removed from pasteurized dairy cream after phase inversion during the process of Anhydrous Milk Fat production. Procream or High Fat Retentate is obtained from the microfiltration of whey retentate from the ultrafiltration of cheese whey which is a co-product obtained during manufacture of whey protein isolate (Tetra Pak, 2015).

This study was carried to determine the major phospholipids in selected dairy products (Beta Serum, Procream and Phospholipids-Rich Dairy Product), evaluate the accuracy of the developed extraction method for lipids in dairy samples and to compare the major phospholipids obtained using the HPLC-UVvis and ^{31}P-NMR methods.

2. Material and Method

2.1. Materials

The HPLC grade chemicals (99.9%) like Acetonitrile, Chloroform and Methanol were procured from Fisher Chemical (Loughborough, UK) while the reagent grade Phosphoric Acid (85%) was obtained from Scharlau Laboratory (Sentminat, Spain). The Bovine Phospholipids standards such as Phosphatidylcholine, Phosphatidylethanolamine and Sphingomyelin were procured from Larodan (Solna, Sweden). The Beta Serum powder was obtained from Tatua Dairy Company (Morrinsville, New Zealand) while the Procream powder from Mullins Whey (Mosinee, Wisconsin, USA). The Phospholipids-Rich Products were processed from Procream using a proprietary process at the Pilot Plant of the Institute for Dairy Processing, South Dakota State University, Brookings, South Dakota, USA.

2.2. Solvent Extraction of the Dairy Products Lipids

The solvent extraction method for determining the total lipids in fish tissue of Lee et al. (1996) was adapted for liquid dairy samples and modified as follows: a) weigh out the liquid dairy sample (7.0±0.1 g; record the exact amount) and place into a 100-mL Volumetric Flask with a press fit cover; b) add 70 mL of solvent (2:1 chloroform-methanol if the expected lipid content of the sample will be greater than 6%); c) stir the mixture using a magnetic stirrer set at 750 rpm for 2 minutes; d) filter the homogenate through a coarse filter paper and funnel into a 100 mL glass stoppered graduated cylinder, toward the end of draining, press the filtrate with the round tip of a spatula to moderately squeeze out the remaining solvent. Do not attempt to press all solvent out since there is no need to measure the chloroform layer; e) add 28 mL 0.5% NaCl solution (to prevent emulsion formation) and gently shake by tilting the cylinder 4 times, allow mixture to stand until visible separation occurs (takes about 30 minutes more or less); f) using a glass 10 mL pipet, remove an aliquot (about 9 mL) of the chloroform layer and transfer an exact 7.0 mL into a pre-weighed (to the nearest 1 mg) 40-mL beaker; g) evaporate the solvent using a hot plate set at low setting. Avoid excessive heating and drying (this step requires about 30 minutes); h) reweigh the beaker (to the nearest 1 mg) and calculate the total lipid content using equation 1 as shown below,

$$\text{Lipid content (\%)} = \frac{\text{Lipid extracted (g)}}{\text{Sample weight (g)}} \times \frac{\text{(Chloroform layer+Amounts lost)*}}{\text{7.0 mL}} \times 100 \quad (1)$$

* Use a theoretical calculated volume of 46 mL

i) if the expected lipid content of the sample will be between 2 and 6%, then use 70 mL of solvent (1:1 chloroform-methanol) and then use 35 mL as the theoretical calculated volume in the Lipid Content calculation; j) if the expected lipid content of the sample will be less than 2%, then use 70 mL of solvent (1:2 chloroform-methanol) and then use 23 mL as the theoretical calculated volume in the Lipid Content calculation; and k) transfer the remaining extracted lipid to a dessicator to cool down to room temperature, then close the lid and store until use. Use the extracted lipid for the HPLC-UVvis analysis of the major phospholipids.

2.3. Determination of the Major Phospholipids by the HPLC-UVvis Method

The high-performance liquid chromatography (HPLC) Ultraviolet visible (UVvis) detector method for determining phospholipids of Rehman et al. (2017) was adapted with some modifications as follows. A Shimadzu HPLC with system controller (SCL-10A VP) equipped with a pump system (LC-10 AD VP and FCV-AL) with degasser and auto-injector (SIL-10AD VP) and a UV-vis detector (SPD-10AV) was used in the determination of the major phospholipids (Phospatidylcholine (PC), Phosphatidylethanolamine (PE) and Sphingomyelin (SM)) in the phospholipids standards and dairy samples. The chromatographic column was a Luna 5 µm Silica (2) 100 A, 150 mm x 4.6 mm with a security guard. The detector signal was analysed using the LC Solution software to obtain the

integrated area of the peaks and retention times from the chromatogram. The mobile phase was a mixture of Acetonitrile-Methanol-Phosphoric Acid (85%) (100:10:1.8 v:v:v) in isochratic pump mode with a flowrate of 0.75 mL/min. The mobile phase was degassed by magnetic stirring at 500 rpm under vacuum for about 30 minutes prior to use in the HPLC-UVvis system. The HPLC-UVvis system determination was done at 40ºC by using a ThermaSphere column heater. The temperature of 40ºC was found to give the satisfactory results compared with the 30oC temperature. The detector was set with a wavelength of 203 nm.

The HPLC-UVvis determination were limited to the major phospholipids (PC, PE and SM). A set of stocks solutions of PC, PE and SM standards with a concentration of 2000 µg/mL of solvent were made by oscillating the mixture for 30 seconds at 2000 rpm. The solvent used was a Chloroform-Methanol mixture (1:1 v:v) because the solvent used by Rehman et al. (2017) of n-Hexane:2-Propanol (3:1 v:v) did not fully dissolved the dairy lipids. The phospholipids standards were successively diluted with the solvent to get samples with different concentration from 164 to 1101 µg /mL for PC, from 198 to 1325 µg /mL for PE and from 177 to 600 µg /mL for SM. The samples are filtered through a 0.45 µm PTFE filter and into 1.5-mL amber vials and then loaded into the auto-injector sample holder. A 20 µL of the filtered sample was injected into the HPLC-UVvis System using the auto-injector to obtain the peak area and retention time of the sample. Calibration curves for the different phospholipids standards were obtained and used these in converting the peak areas into the different phospholipids (PC, PE and SM) concentration. For the analysis of liquid dairy samples, first the sample is passed through a 0.45 µm PTFE filter and into 1.5-mL amber vials and then loaded into the auto-injector sample holder.

2.4. Determination of the Major Phospholipids by the ^{31}P-NMR Method

The ^{31}P-NMR method of Mackenzie et al. (2009) was used in the analysis of the different phospholipids in the lipids of the dairy samples. The samples were sent for analysis to the Callaghan Innovation, Lower Hutt, New Zealand where Mackenzie and colleagues are employed.

3. Results and Discussion

3.1. Lipid Contents of the Beta Serum and Procream Products

Table 1 shows the comparison of the calculated and analyzed lipid contents of reconstituted butter serum and Procream with different dilution. The results show that the mean percentage difference between the analyzed and calculated lipid contents had a mean value of 8% for the Beta Serum products and 11% for the Procream products. The results obtained for the reconstituted Procream could probably be improved if samples analyzed were limited to 10% dilution only, since it was observed to have higher percentage difference at 15% dilution. In addition, the higher fat content of the powder (20.55% from Table 1) probably also contributed to the variability of results. This suggests that the developed extraction method for lipids can be used to estimate the lipid content of dairy samples. Considering that the lipid extraction method used was developed for fish tissue the results obtained were still a bit satisfactory.

3.2. Calibration Curves Determination for PC, PE and SM Concentration

Figures 1 to 3 show the calibration curves for PC, PE and SM with the phospholipid concentration on the x-axis and the HPLC-UVvis area under the curve on the y-axis. The separation times for the PC ranged from 7.5 to 9.7 minutes, for the PE ranged from 5.7 to 6.5 minutes and for SM curve 1 (SM1) ranged from 9.7 to 10.8 minutes while SM curve 2 (SM2) ranged from 10.5 to 11.9 minutes. The coefficient of determination (r^2) values of the calibration curves ranged from 0.991 to 0.998 indicating excellent fit of the experimental data from the curve fit. Regression equations to predict the individual phospholipid concentration for the obtained HPLC-UVvis area under the curve were derived from the given calibration curves as shown in Figures 1 to 3 and are shown as equations 2, 3 and 4 below,

PC Concentration = (70.706 x HPLC-UVvis Area) + 172.70 (µg/mL) (r^2 = 0.991) (2)

PE Concentration = (49.611 x HPLC-UVvis Area) + 114.83 (µg/mL) (r^2 = 0.996) (3)

SM Concentration = (50.647 x HPLC-UVvis Area) + 153.52 (µg/mL) (r^2 = 0.998) (4)

3.3. Chromatograms of the Major Phospholipids in Beta Serum and Procream Products

Figures 4 and 5 show the chromatograms of the major phospholipids in Beta Serum and Procream products. The separation times for PC is 8.241 mins, for PE is 5.663 mins, for SM1 is 10.801 mins and for SM2 is 11.982 mins in Beta Serum. While the separation time for PC is 8.213 mins, for PE is 5.632 mins, for SM1 is 10.841 mins and for SM2 is 11.884 mins in Procream. It is expected to have some slight variations in the separation times of the major phospholipids in Beta Serum and Procream because of the difference in their composition and processes undergone. SM usually consists of 2 curves in dairy products as shown by Ferreiro et al. (2017) for milk and Rombaut et al. (2005) for various dairy products. Rehman et al. (2017) in their HPLC-UV determination of various phospholipids standards and Rombaut et al. (2005) in their HPLC-ELSD determination of various dairy products also observed that the PE separated ahead of PC and then PC ahead of SM1 and SM2. The chromatograms also shows that all the major phospholipids can all be obtained within 12 minutes.

Table 1. Calculated and analyzed lipid contents of reconstituted Beta Serum and Procream products with different dilution.

Sample	Calculated Lipid Content*	Analyzed Lipid Content	Percentage Difference
Reconstituted Beta Serum (15% Powder) R1	2.20%	2.25%	2.27%
Reconstituted Beta Serum (15% Powder) R2	2.20%	1.93%	12.27%
Reconstituted Beta Serum (10% Powder) R1	1.47%	1.55%	5.44%
Reconstituted Beta Serum (10% Powder) R2	1.47%	1.41%	4.08%
Reconstituted Beta Serum (10% Powder) R3	1.47%	1.83%	24.49%
Reconstituted Beta Serum (10% Powder) R4	1.47%	1.50%	2.04%
Reconstituted Beta Serum (10% Powder) R5	1.47%	1.50%	2.04%
		Mean	7.52%
Reconstituted Procream (15% Powder) R1	3.08%	2.50%	18.83%
Reconstituted Procream (15% Powder) R2	3.08%	2.14%	30.52%
Reconstituted Procream (9% Powder) R1	1.85%	1.83%	1.08%
Reconstituted Procream (6.5% Powder) R1	1.34%	1.41%	5.22%
Reconstituted Procream (6.5% Powder) R2	1.34%	1.36%	1.49%
		Mean	11.43%

* - calculated lipid content based on the certificate of analysis of the Beta Serum (fat content=14.70%) and Procream (fat content=20.55%) powders

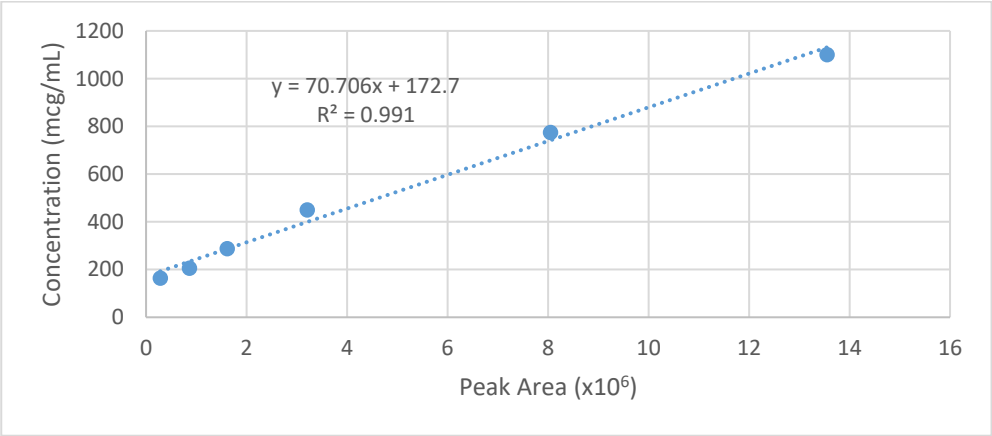

Figure 1. Plot of phosphatidylcholine (PC) concentration against HPLC-UVvis area under the curve (mcg = µg).

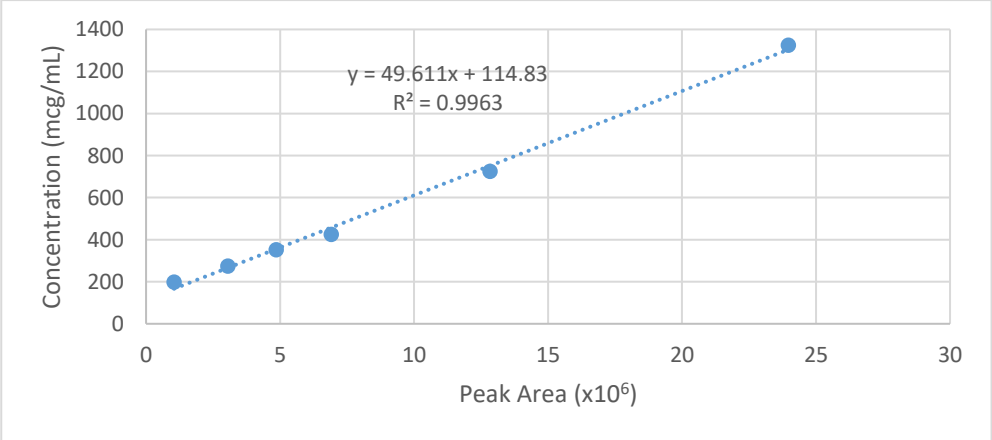

Figure 2. Plot of phosphatidylethanolamine (PE) concentration against HPLC-UVvis area under the curve (mcg = µg).

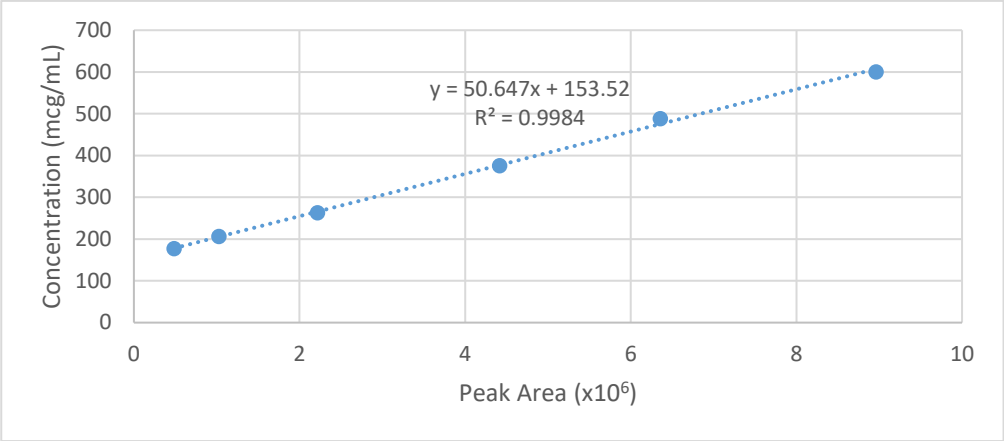

Figure 3. Plot of sphingomyelin (SM) concentration against HPLC-UVvis area under the curve (mcg = µg).

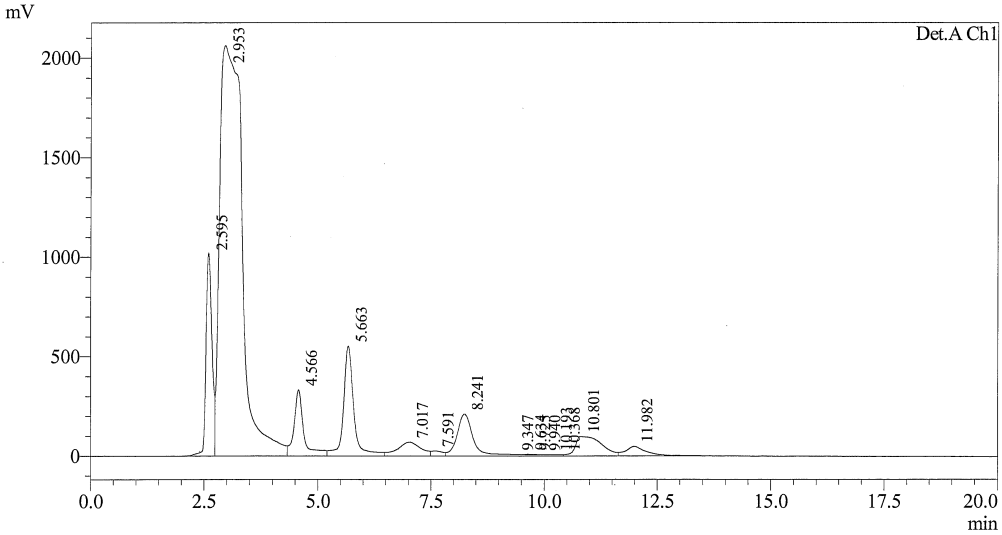

Figure 4. Chromatogram of the major phospholipids in Butter Serum (Separation times: PE= 5.66min; PC=8.24min; SM1=10.80min; and SM2=11.98min).

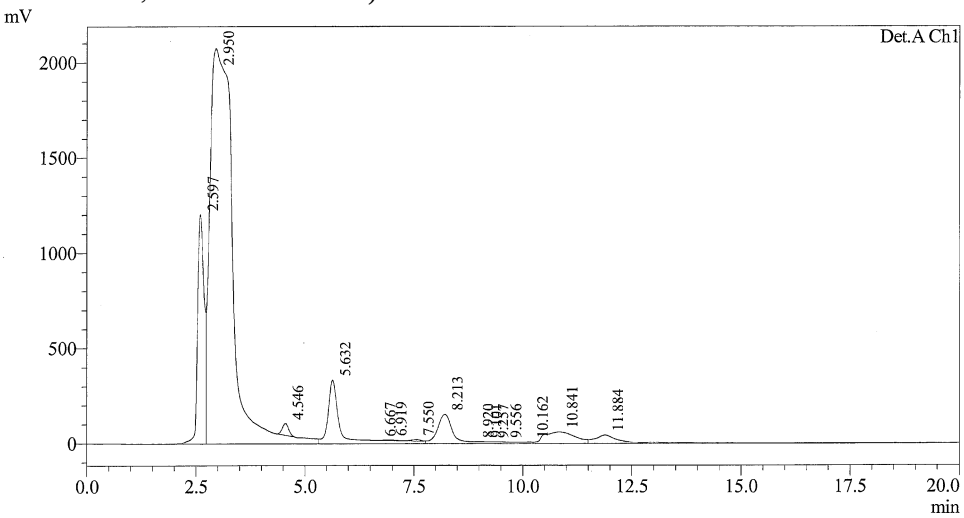

Figure 5. Chromatogram of the major phospholipids in Procream (Separation times: PE=5.63min; PC=8.21min; SM1=10.84min; and SM2=11.88min).

3.4. Amounts of Phospholipids in Beta Serum and Procream Products

Table 2 shows the amounts of PC, PE and SM from the different Beta Serum and Procream products obtained using ^{31}P-NMR and HPLC-UVvis methods. The calculated concentration of the individual phospholipids was determined using equations 2 to 4 from as shown earlier. The results show that for the Reconstituted Beta Serum (15% Powder) gave percentage difference values of 3.3%, 21.0%, 2.2% and 10.0% for PC, PE, SM and Total (PC+PE+SM), respectively between the ^{31}P-NMR and HPLC-UVvis. Only one percentage difference value was above 10% which suggests satisfactory results. On the other hand, the results show that for the Reconstituted Procream (15% Powder) gave percentage difference values of 17.0%, 6.3%, 7.4% and 5.6% for PC, PE, SM and Total (PC+PE+SM), respectively between the ^{31}P-NMR and HPLC-UVvis. Again, only one percentage difference value was above 10% which suggests satisfactory results.

It must be noted that the analysis temperature for the HPLC-UVvis method was at 40°C while the ^{31}P-NMR method was at 30°C, and this might have also contributed to the slight variation of the results. Furthermore, the HPLC-UVvis method is rapid and with cheaper analysis cost compared with the ^{31}P-NMR method.

3.5. Chromatogram of the Major Phospholipids in a Phospholipid-Rich Product (PU 307)

Figure 6 shows the chromatogram of the major phospholipids in a phospholipid-rich product (PU 307). The chromatograms of the PU 305 and PU 306 products were very similar in appearance as the PU 307 product and hence no longer shown. The separation times for PC is 7.538 mins, for PE is 5.131 mins, for SM1 is 10.103 mins and for SM2 is 10.916 mins in the PU 307 product. It is expected to have some slight variations in the separation times of the major phospholipids in the phospholipid-rich products as compared with Beta Serum and Procream products because of the difference in their composition and processes undergone. The chromatogram also shows that all the major phospholipids can all be obtained within 12 minutes.

3.6. Amounts of Phospholipids in Phospholipids-Rich Products

Table 3 shows the amounts of PC, PE and SM from the different phospholipids-rich products (PU305, PU306 and PU307) using ^{31}P-NMR and HPLC-UVvis methods. The calculated concentration of the individual phospholipids was again determined using equations 2 to 4 as before. The results show that for the reconstituted PU 305 product (5% Powder) gave percentage difference values of 3.5%, 7.1%, 9.1% and 4.0% for PC, PE, SM and Total (PC+PE+SM), respectively between the ^{31}P-NMR and HPLC-UVvis. These results are very satisfactory since all the percentage difference values were all below 10%. For the reconstituted PU 306 product (5% Powder) gave percentage difference values of 7.0%, 7.3%, 0% and 0% for PC, PE, SM and Total (PC+PE+SM), respectively between the ^{31}P-NMR and HPLC-UVvis. Lastly, for the reconstituted PU 307 product (5% Powder) gave percentage difference values of 3.3-6.9%, 13.6-20.5%, 3.4-12.5% and 6.8-13.2% for PC, PE, SM and Total (PC+PE+SM), respectively between the ^{31}P-NMR and HPLC-UVvis. The HPLC-UVvis results were closer to the values obtained from direct method of ^{31}P-NMR measurements.

Table 2. Comparison of the amounts of the major phospholipids in the Butter Serum and Procream products using ^{31}P-NMR and HPLC-UVvis methods.

Sample Analysed	^{31}P-NMR Analysis at 30°C (g/100g lipid)				HPLC-UVvis Analysis at 40°C (g/100g lipid)			
	PC	PE	SM	Total*	PC	PE	SM	Total*
Beta Serum								
(BS) Powder via Lipid 12.1	13.8	9.1	35.0					
Reconst. BS (15% Powder) via Lipid					11.7	10.9	8.9	31.5
Percentage Difference **					3.3%	21.0%	2.2%	10.0%
Procream (PRC) Powder via Lipid	8.8	7.9	8.1	24.8				
Reconst. PRC1 (15% Powder) via Lipid					9.4	9.0	7.6	26.0
Reconst. PRC2 (15% Powder) via Lipid					10.2	8.1	7.9	26.2
Reconst. PRC3 (15% Powder) via Lipid					11.3	8.0	7.0	26.3
Mean of Reconst. PRC (15% Powder) via Lipid					10.3	8.4	7.5	26.2
Percentage Difference **					17.0%	6.3%	7.4%	5.6%

Reconst. – Reconstituted * Total (PC+PE+SM) ** Percent Diff = 100 x |^{31}P-NMR – HPLC-UVvis|/^{31}P-NMR

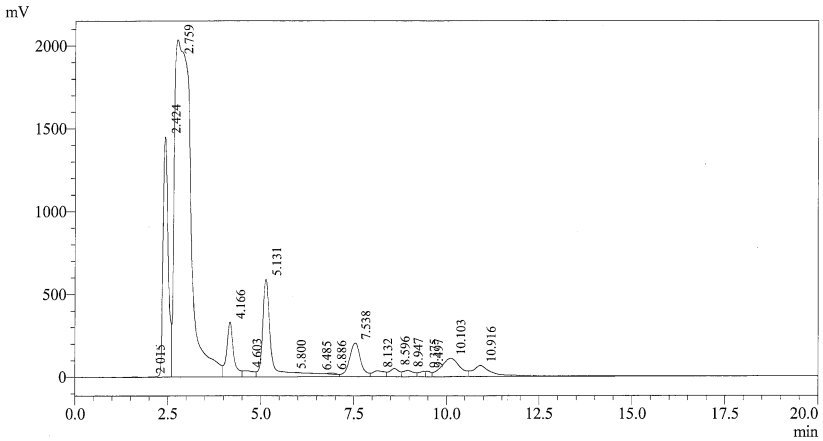

Figure 6. Chromatogram of the major phospholipids in a phospholipid-rich product (PU 307) (Separation times: PE=5.13min; PC=7.54min; SM1=10.10min; and SM2=10.92min).

Table 3. Comparison of the amounts of the major phospholipids in different phospholipids-rich products (PU 305, PU 306 and PU 307) using ^{31}P-NMR and HPLC-UVvis methods.

Sample Analysed	^{31}P-NMR Analysis at 30ºC (g/100g lipid)				HPLC-UVvis Analysis at 40ºC (g/100g lipid)			
	PC	PE	SM	Total*	PC	PE	SM	Total*
PU 305								
Powder via Lipid 8.6	8.4	7.7	24.7					
Reconst. PU 305 (5% Powder) via Lipid					8.3	9.0	8.4	25.7
Percentage Difference**					3.5%	7.1%	9.1%	4.0%
PU 306 Powder via Lipid	8.6	8.2	8.0	24.8				
Reconst. PU 306 (5% Powder) via Lipid					8.0	8.8	8.0	24.8
Percentage Difference**					7.0%	7.3%	0%	0%
PU 307 Powder via Lipid (A)	8.7	8.3	8.0	25.0				
PU 307 Powder Direct Method (B)	9.0	8.8	8.7	26.5				
Reconst. PU 307 (5% Powder) via Lipid					9.3	10.0	9.0	28.3
Percentage Difference (A)**					6.9%	20.5%	12.5%	13.2%
Percentage Difference (B)**					3.3%	13.6%	3.4%	6.8%

Reconst. – Reconstituted * Total (PC+PE+SM) ** Percent Diff = 100 x |^{31}P-NMR – HPLC-UVvis|/^{31}P-NMR

4. Conclusion

A new solvent extraction method for lipids from liquid dairy samples was developed with acceptable results.

Sphingomyelin (SM) consists of 2 curves in Beta Serum, Procream and phospholipid-tich products. The phosphatidylethanolamine (PE) separated ahead of phosphatidylcholine (PC) and then PC ahead of SM1 and SM2.

The developed HPLC-UVvis method can be used for determining the major phospholipids (PC, PE and SM) in dairy products with comparable results with the ^{31}P-NMR method. It must be noted that the analysis temperature for the HPLC-UVvis method was at 40ºC while the ^{31}P-NMR method was at 30ºC, and this might have also contributed to the slight variation of the results. Furthermore, the HPLC-UVvis method is rapid and with cheaper analysis cost compared with the ^{31}P-NMR method.

Acknowledgments

The author would like to thank Seperex Nutritionals Ltd. for providing the research funds and facilities.

Authors' contributions:

The article was written by LMD, as well as the data analysis.

Conflict of interest disclosure:

The authors declare no conflict of interest on the written article.

References

Bligh EG, Dyer WJ 1959. A rapid method of total lipid extraction and purification. Canadian Journal of Biochemistry and Physiology. 37: 911-917.

Contarini G, Povolo M 2013. Phospholipids in milk: composition, biological and technological significance, and analytical strategies. International Journal of Molecular Sciences. 14: 2808-2831.

Castro-Gomez P, Rodriguez-Alcala LM, Monteiro KM, Ruiz AL, Carvalho JE, Fontecha J 2016. Antiproliferative activity of butter milk lipid fractions isolated using food grade and non-food grade solvents on human cancer cell lines. Food Chemistry. 212: 695-702.

Dewettinck, K, Rombaut R, Thienpont N, Le TT, Messens K, van Camp J 2008. Nutritional and technological aspects of milk fat globule membrane material. International Dairy Journal. 18: 436-457.

Donato P, Cacciola F, Chichello F, Russo M, Dugo P, Mondello L 2011. Determination of phospholipids in milk samples by means of hydrophilic interaction liquid chromatography coupled to evaporative light scattering and mass spectrometry detection. Journal of Chromatography.1218: 6476-6482.

Duivenvoorden I, Voshol PJ, Rensen PC, van Duyvenvoorde W, Romijin JA, Emeis JJ, Havekes LM, Nieuwenhuizen W.F.. 2006. Dietary sphinolipids lower plasma cholesterol and triacylglycerol and prevent liver steatosis in APOE*3Leiden mice. American Journal of Clinical Nutrition. 84: 312-321.

Ferreiro T, Gayoso L, Rodriguez-Otero JL 2017. Determination of phospholipids in milk by HPLC with evaporative light scattering detector: Optimization and validation. Journal of Dairy & Veterinary Sciences. 1 (3): 555562. doi: 10.19080/JDVS.2017.01.555562.

Folch JM, Lees M, Sloane-Stanley GH 1957. A simple method for the isolation and purification of total lipids from animal tissues. Journal of Biology and Chemistry. 226: 497-509.

Kielbowicz G, Micke P, Wawrzenczyk C 2013. A new liquid chromatography method with charge aerosol detector (CAD) for the determination of phospholipid classes. Application to Milk Phospholipids. Talanta.105: 28-33.

Kivinen A, Tarpila S, Salminen S, Vapaatalo H 1992. Gastroprotection with milk phospholipids: a first human study. Milchwissenschaft. 47: 694-696.

Kuchta AM, Kelly PM, Stanton C, Devery RA 2012. Milk fat globule membrane – a source of polar lipids for colon health? – A review. International Journal of Dairy Technology. 65: 315-333.

Le TT, Miocinovic J, Nguyen TM, Rombaut R, van Camp J, Dewettinck K 2011. Improved solvent extraction procedure and high-performance liquid chromatography-evaporative light scattering detector method for analysis of polar lipids from dairy materials. Journal of Agricultural and Food Chemistry. 59: 10407-10413.

Lee CM, Trevino B, Chaiyawat M 1996. A simple and rapid solvent extraction method for determining total lipids in fish tissue. Journal of AOAC International. 79: 487-492.

Lesser ME, Sagalowicz L, Michel M, Watzke HJ 2006. Self-assembly of polar food lipids. Advances in Colloid Interface Science. 123: 125-136.

Mackenzie A, Vussotski M., Nekrasov E 2009. Quantitative analysis of dairy phospholipids by ^{31}P NMR. Journal of the American Oil Chemists Society. 86: 757-763.

McDaniel M, Maier S, Einstein G 2003. Brain-specific nutrients: a memory cure? Nutrition. 19: 957-975.

Rehman S, Rehman S, Welter D, Wildenauer D, Ackenheil M 2017. Simple and rapid separation and determination of phospholipids by the HPLC-UV system. Annals of Pharmacology and Pharmaceutics. 2: 1-3.

Rombaut R, Dewettinck K 2006. Properties, analysis and purification of milk polar lipids. International Dairy Journal. 16: 1362-1373.

Rombaut R, Camp JV, Dewettinck K 2005. Analysis of phospho- and sphingolipids in dairy products by a new HPLC method. Journal of Dairy Science. 88: 482-488.

Tetra Pak. 2005. Dairy Processing Handbook. Tetra Pak Processing Systems AB, Lund, Sweden. 482 pp.

Vanhoutte B, Rombaut R, Dewettinck K, van der Meeren P 2004. Phospholipids. In Food Analysis, Volume 1. (M. L. Nollet, ed.), Marcel Dekker, New York, New York. pp. 349-382.

Verardo V, Gomez-Caravaca AM, Arraez-Roman D, Hettinga K 2017. Recent advances in phospholipids from colostrum, milk and dairy by products. International Journal of Molecular Science. 18: 173. doi: 10.3390/ijms18010173.

Vesper H, Schmelz E, Nikolova-Karakashian MN, Dillehay DL, Lynch DV, Merril AH Jr. 1999. Sphingolipids in food and the emerging importance of sphingolipids to nutrition. Journal of Nutrition. 129: 1239-1250.

RESEARCH ARTICLE
Eurasian J Bio Chem Sci, 5(Suppl 1):135-143, 2022
https://doi.org/10.46239/ejbcs.1150114

EJBCS

Eurasian Journal of Biological and Chemical Sciences

Journal homepage: www.dergipark.org.tr/ejbcs

Investigation of the Antibacterial Effect of Astaxanthin and the Prevalence of Virulence and Antimicrobial Resistance Genes of *Aeromonas hydrophila* and *Aeromonas sobria* strains

Jale Korun[1*], Aycan Ulutaş[1]

[*1] *Akdeniz University, Faculty of Fisheries, Department of Aquaculture, Antalya, Türkiye*

*Corresponding author : jalekorun@akdeniz.edu.tr
Orcid No: https://orcid.org//0000-0002-1930-9978

Received : 28/07/2022
Accepted : 09/10/2022

Abstract: In the study, in addition to the antibacterial effect of astaxanthin on *Aeromonas hydrophila* and *A. sobria* strains, the presence of virulence genes (*Aero*, *act*, *ast*, and *hylA*) and antibiotic resistance genes (*tetC* and *sulI*) in the strains was investigated. Antibiotic profiles of the strains were also investigated as part of the study. Strains were identified by conventional biochemical tests and PCR assay using a 16S rDNA primer pair specific for *A. hydrophila*. According to the results of bacteriological and molecular studies, two of the six *Aeromonas* strains were identified as *A. hydrophila* and four of them as *A. sobria.* The *Aero* virulence gene and the *act* virulence gene were found in all strains, while the *ast* and *hylA* virulence genes were detected only in *A. hydrophila* strains. All strains were resistant to chloramphenicol, tetracycline, nalidixic acid, and ampicillin in the standard disk diffusion test. Although all strains showed resistance to tetracycline and moderate resistance to oxytetracycline in the antibiogram tests, *tetC* antibiotic resistance gene was not detected in the strains and *sulI* antibiotic resistance gene was not detected in the strains. In the study, acetone solutions containing 0.1 g and 0.5 g of astaxanthin were found to have an antibacterial effect on *A. hydrophila* strains. Acetone solutions containing 0.1 g, 0.5 g, and 1.0 g of astaxanthin showed antibacterial effects on *A. sobria* strains. It was found that 0.1 g, 0.5 g, and 1.0 g astaxanthin solutions prepared with methanol and distilled water had no antibacterial effects on the strains.

Keywords: *Aeromonas hydrophila*, *Aeromonas sobria*, astaxanthin, virulence genes, antibiotic genes, antibiotics

1. Introduction

The motile *Aeromonas* species, including *Aeromonas hydrophila*, *A. caviae*, *A. sobria*, *A. dhakensis*, *A. jandaei*, and *A. veronii*, also known as mesophilic bacterial species (Ebied et al. 2022), cause motile Aeromonas septicemia (MAS), which can lead to findings such as soft tissue and haemorrhage (Joseph et al. 2013; Hossain and Heo 2020). MAS is observed in farmed and wild fish as well as terrestrial animals and causes up to 80% mortality under farmed conditions (Saharia et al. 2021). The motile *Aeromonas* species *A. hydrophila* and *A. sobria* have been reported to infect freshwater fish species such as tilapia, catfish, carp, and rainbow trout, as well as many tropical or ornamental fish species including goldfish (Elsheshtawy et al. 2019; Yardımcı and Turgay 2021). Also, they have recently been identified as causative agents of intestinal and other infections in humans, e.g., infections associated with natural disasters such as hurricanes and tsunamis, and hospital infections. Therefore, these bacteria are of interest as opportunistic and primary pathogens (Robertson et al. 2014; Hoel et al. 2017).

Members of the genus *Aeromonas* are Gram-negative, rod-shaped, cytochrome oxidase- and catalase-positive, capable of reducing nitrates to nitrites, fermenting glucose, and resistant to the vibriostat agent (2,4-diamino-6, 7-di-iso-propylpteridine phosphate) (Fernández-Bravo and Figueras 2020). *Aeromonas* species are phenotypically divided into two groups: the motile and non-motile groups (Hossain and Heo 2020). The non-motile group consists of psychrophilic *Aeromonas* species that exhibit optimal growth at 22-28 °C. These bacterial species are considered to cause furunculosis, especially in salmonids. The other group is the species that can develop at 35-37 °C and cause motile *Aeromonas* septicemia (MAS) in fish (Hossain and Heo 2020).

So far, a number of potential virulence factors such as pore-forming hemolytic toxins, cytotonic heat-labile (*alt*), cytotonic heat-labile (*ast*), cytotoxic heat-labile enterotoxin (*act*), aerolysin (*Aero*), flagellin (*fla*), elastase (*ela*), serine protease (*ser*), lipase (*lip*), collagenase (*acg*), Dnase (*exu*), and cholesterol acyltransferase (*gcat*) have been identified (Robertson et al. 2014; Guz et al. 2021); however, *ast*, *act*, *alt*, and aerolysin toxin (*Aero*) of mesophilic *Aeromonas* species have been reported as virulence factors that are commonly reviewed in the context of infections (Robertson et al. 2014; Hoel et al. 2017). Robertson et al. (2014) noted

that the aforementioned toxins may be a potential clue for distinguishing pathogenic *Aeromonas* species from non-pathogenic *Aeromonas* species. In addition to virulence factors associated with infection in *Aeromonas* species, another important issue is the detection of multi-antibiotic resistance in these bacteria (Sreedharan et al. 2012; Guz et al. 2021).

Nowadays, the number of studies aimed at determining the antimicrobial profiles of motile *Aeromonas* species, particularly *Aeromonas hydrophila*, *A. caviae*, *A. sobria*, *A. dhakensis*, *A. jandaei*, and *A. veronii*, has increased (Fernández-Bravo and Figueras 2020; Hossain and Heo 2020). The use of antibiotics to treat infections has also been shown to be effective in this situation. Due to the zoonotic properties of motile *Aeromonas* species, the development of antibiotic resistance in these species is of concern not only for fish under farmed conditions, but also for general public health, including fish farmers (Fernández-Bravo and Figueras 2020).

Alternative products of plant origin to antibiotics have been proposed due to the multiantibiotic resistance found in bacteria (Pandey 2018). The ketocarotenoid astaxanthin (AST) (3, 3'-dihydroxy-ß, ß'-carotene-4,4'-dio) is a fat-soluble xanthophyll (Dhankar et al. 2012; Lotfi et al. 2021). It can be naturally synthesized by microorganisms such as the bacterium *Agrobacterium aurantiacum*, the fungus *Xanthophyllomyces dendrorchous* and the green alga *Haematococcus pluvialis* (Olaizola 2007; Dhankhar et al. 2012). In addition, it can be produced synthetically from petrochemicals (Marinho et al. 2021). Today, its human health benefits such as its antioxidant properties, are of interest as it is used as a feed additive for poultry and salmonids. It is also used commercially to color ornamental fish such as goldfish (*Carassius auratus*) and *Pseudochromis fridmani*, and shellfish such as crabs and shrimp (Olaizola 2007; Dhankar et al. 2012; Marinho et al. 2021; Montaya et al. 2021). Although the effects of astaxanthin on reproductive performance, egg production, and egg quality of aquatic animals are well known, increased resistance to bacterial and viral pathogens has also been observed in fish fed astaxanthin-supplemented diets (Lim et al. 2018).

In this study, the antibacterial effect of astaxanthin on *Aeromonas hydrophila* and *A. sobria* strains previously isolated from sick goldfish (*Carassius auratus)*,, antibiotic resistance, and multiple resistance (MAR) of the strains were investigated. The virulence genes (*Aero*, *act*, *ast*, and *hylA*) and antibiotic resistance genes (*tetC* and *sulI*) of the strains were also studied.

2. Materials and Method

2.1. Bacterial strains and phenotypic characterization of the strains

For the study, 6 strains of *Aeromonas* spp. previously isolated from freshly dead goldfish (*Carassius auratus*) showing signs of MAS were used. After an incubation period of 24-28 h at 24 ± 2 °C, bacterial colonies grown on the plates were examined for morphology and color. To determine the morphological and biochemical characteristics of the strains, all strains were tested using conventional identification methods, including hanging drops for motility, Gram stain, cytochrome oxidase (tetramethyl-p-phenylenediamine dihydrochloride), catalase (3% H_2O_2), fermentation test in O/F glucose broth, Voges-Proskauer (VP) and methyl red (MR), citrate utilization in Simmon's Citrate agar, onpg (o-nitrophenyl-β-D-galactopyranoside), vibriostat assay (10 µg and 150 µg, respectively). NaCl tolerance was determined using nutrient broth (NB) spiked with different NaCl concentrations. To determine temperature tolerance, strains were cultured in NB at 4, 25, and 37 °C. H_2S production on Triple Sugar Iron (TSI) agar, gas formation from glucose, hemolysis on blood agar (BA), dihydrolase and decarboxylase assays, acid production from sugars such as glucose, lactose, sorbitol, inositol, fructose, mannose, xylose, galactose, mannitol and sucrose in peptone water, nitrate production, amylase and gelatinase production, and growth on MacConkey agar were studied (Austin and Austin 2007).

2.2. Molecular studies

2.2.1. DNA extractions and PCR studies

For PCR amplification of 16S rDNA, DNA from the strains was extracted using a commercially available kit for purification of bacterial and yeast genomic DNA (Hibrigen, Türkiye). After DNA isolation, samples were stored at -20 °C in the freezer until used for PCR studies (Temizkan and Arda 2004). Prior to testing, the DNA samples were thawed at room temperature. Mytaq HS DNA polymerase kit was used to obtain the PCR products. For this purpose, a standard reaction of 50 µl was prepared. PCR components and amounts are listed in Table 1. For identification of the 16S rDNA, virulence genes (*aero*, *act*, *ast* and *hylA*), and antibiotic resistance genes (*tetC* and *sulI*), the primer pairs used in the study were listed in Table 2 and Table 3.

Table 1 PCR components used in the study

Components	Volume
5xMytaq reaction buffer	10 µl
DNA	5 µl
Primer Fd	1 µl
Primer Rs	1 µl
Mytaq HS DNA polymerase	1 µl
Water (ddH_2O)	32 µl

Table 2 16S rDNA primer sequence for *A. hydrophila* (Gardenia et al. 2010)

Primer	
16S rDNA Fd	
16S rDNA Rs	
Primer sequence	
5´-GAAAGGTTGATGCCTAATACGTA-3´	
5´-CGTGTGGCAACAAAGGACAG-3´	
Annealing	
56 °C	
bp	
685	

Table 3 Primer sequence for DNA amplification of virulence and antibiotic resistance genes

Primer
Aero Fd*
Aero Rs
Primer sequence
5´-CCAAGGGGTCTGTGGCGAAC-3´
5´-TTTCACCGGTAACAGGATTG-3´
bp
209
Primer
act Fd**
act Rs
Primer sequence
5´-GAGAAGGTGACCACCAAGAACA-3´
5´-AACTGACATCGGCCTTGAACTC-3´
bp
232
Primer
ast Fd**
ast Rs
Primer sequence
5´-TCTCCATGCTTCCTTCCACT-3´
5´-GTGTAGCGATTGAAGCCG-3´
bp
331
Primer
hylA Fd**
hylA Rs
Primer sequence
5´-GGCCGGTGGCCCGAAGATACGGG-3´
5´-GGCGGCGCCGGACGAGACGGGG-3´
bp
592
Primer
tetC Fd***
tetC Rs
Primer sequence
5´-AACAATGCGCTCATCGT-3´
5´-GGAGGCAGACAAGGTAT-3´
bp
1138
Primer
sulI Fd***
sulI Rs
Primer sequence
5´-CGGCGTGGGCTACCTGAACG-3´
5´-GCCGATCGCGTGAAGTTCCG-3´
bp
433

*Gardenia et al. (2010), **El-Bahar et al. (2019), ***Duman (2017)

The different thermocyclers were programmed for amplifications of 16S rDNA primer pairs, virulence genes, and antibiotic resistance genes; however, each cycle consisted of an initial denaturation, annealing, extension, and final phase (El-Bahar *et al*., 2019; Duman, 2017; Gardenia *et al*., 2010). The thermocycler programme for each target gene except 16S rDNA is given in Table 4. The PCR cycle for 16S rDNA primer pairs was set to 30 cycles, with initial denaturation for 5 min at 95 °C, 1 min at 94 °C, annealing for 1 min at 56 °C, extension for 1 min at 72 °C. The final stage was incubated for 10 min at 72 °C (Gardenia *et al*., 2010). The thermocycler programme for each target gene except 16S rDNA is given in Table 4.

Table 4 The thermocycler programme for each target gene except 16S rDNA

Thermocycler programme	Target gene	
	*Aero**	*act***
Initial denaturation	95°C/4 min	95°C/4 min
Cycles	30	30
Denaturation	95°C/30 sec	94°C/30sec
Annealing	54°C/45 sec	42°C/30sec
Extension	72°C/30 sec	72°C/1 min
Final stage	72°C/10 min	72°C/10 min
Thermocycler programme	Target gene	
	*Ast***	*hylA***
Initial denaturation	95°C/5 min	94°C/2 min
Cycles	30	35
Denaturation	95°C/1 min	94°C/30 sec
Annealing	55°C/1 min	94°C/30 sec
Extension	72°C/1 min	72°C/1 min
Final stage	72°C/5 min	72°C/5 min
Thermocycler programme	Target gene	
	*tetC****	*sulI****
Initial denaturation	94°C/4min	94°C/4 min
Cycles	35	30
Denaturation	94°C/1 min	94°C/30 sec
Annealing	62°C/2 min	60°C/30 sec
Extension	72°C/3 min	72°C/1 min
Final stage	72°C/7 min	72°C/7min

*Gardenia et al. (2010), **El-Bahar et al. (2019), ***Duman (2017)

2.2.2. Gel electrophoresis

To prepare a 2 % agarose gel, 5 x TBE buffer was diluted 80:20 ml (distilled water: buffer) to 100 ml 1 x TBE buffer. 2 g agarose was added to 1 x TBE buffer and cooled to 50-60 °C at room temperature. Then 2 µl of ethidium bromide solution was added to the cooled agarose. After placing the combs of the electrophoresis apparatus, the prepared gel was poured onto the dish, and the gel was allowed to drain at room temperature. A 100 bp marker was used as a DNA marker. The marker was added to the first well, which contained 5 µl, and 5 µl of the PCR amplification products (4 µl of sample + 1 µl of 6 x dye) were added to the other wells. The test samples were run at 80 V for 60 min. After running the test samples, the bands on the agarose gel were visualised in a U.V. transilluminator.

2.3.1. Preparation of astaxanthin solutions

The commercial form of astaxanthin (Roche, Switzerland) was used for the study. Distilled water, methanol (Merck, Germany) and acetone (Merck, Germany) were used as solvents for the experiments.

2.3.2. Antibacterial effect of astaxanthin by disc diffusion method

To determine the antibacterial activity of astaxanthin, sterile discs were placed on Petri plates containing Mueller-Hinton agar (MHA). 100 µg distilled water, acetone, and methanol solutions containing 0.1g, 0.5g, and 1.0gastaxanthin were added to the empty discs, and zone diameters around the discs were measured at the end of the 16-18 h incubation period at 24 ± 2 °C. Oxytetracycline (OT30, 30 µg) was used as a control antibiotic. The tests were performed in duplicate and the average values were recorded (CLSI M49 2006).

2.4.1. Antibiotic profiles of the strains

Antibiotic resistance of the strains was determined by the standard disc diffusion method (Bauer et al. 1966). Briefly, inoculations from 16-18 hours broth cultures were applied to the surface of Petri plates containing MHA using sterile swabs. Then, the antibiotic-containing discs were placed on the surface of the medium and incubated at 24 ± 2 °C for 16-18 hours. After the incubation period, the diameter of the zone of inhibition around the discs was measured and recorded. The tests were performed in duplicate, and the average of the values was reported. The antibiotics used in the study were ampicillin (AMP10; 10 µg), chloramphenicol (C30; 30 µg), erythromycin (E15; 15 µg), flumequine (UB30; 30 µg), kanamycin (K30; 30 µg), nalidixic acid (NA30; 30 µg), oxytetracycline (OT30; 30 µg), streptomycin (S10; 10 µg), sulfamethoxazole (RL25; 25 µg), tetracycline (TE10; 10 µg), tetracycline (TE30; 30 µg), and trimethoprim (W5; 5 µg). Zone diameter results were interpreted as susceptible ≥ 18 mm, intermediate resistance 13-17 mm and resistance ≤ 13 mm (Odeyemi et al. 2012).

2.4.2. Multi-antibiotic resistance index (MAR)

The multiantibiotic resistance index (MAR) is calculated from the ratio between the number of antibiotics resistant to test organisms and the total number of antibiotics tested. It provides information about the spread of bacterial resistance in populations (Krumperman 1983). The calculated index MAR indicates the presence of environmental strains using multiple antibiotics if it is greater than 0.2 (Ehinmidu 2003).

3. Results

3.1. Phenotypic characterization of the strains

The bacterial colonies were grown between 24 and 48 hours and formed the cream-colored colonies on BHIA. Since the strains were Gram-negative, motile, fermentative, cytochrome oxidase- and catalase-positive, resistant to O/129 vibriostatic agents (10 µg and 150 µg) and reduced nitrate to nitrite, they were classified as putative *Aeromonas* spp. The results of a series of physiological and biochemical tests to further identify putative *Aeromonas* strains are listed below. The isolates produced indole and citrate. They were tolerant to NaCl up to 4% and could grow at 37 °C but not at 4°C. Hydrolysis of urea was negative for all strains. Hydrolysis of gelatin was also negative, but the isolates produced amylase. The strains were able to metabolize lactose, mannitol, mannose, xylose, and galactose. Two strains were able to utilize sucrose, but four strains were unable to utilize sorbitol, inositol, and fructose. The two strains were identified as *Aeromonas hydrophila* (Fig.1)and the 4 strains as *A. sobria*. All phenotypic characteristics of the strains are listed in Table 5.

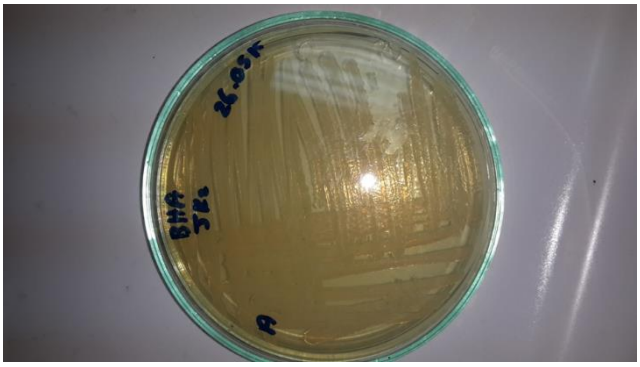

Fig.1. *Aeromonas hydrophila* strain on BHIA

Table 5 Results of morphological, physiological and biochemical tests of the *Aeromonas* strains

Tests	1 (2 strains)	2 (4 strains)	3*	4*
Gram-staining	-	-	-	-
Motility	+	+	+	+
C.oxidase	+	+	+	+
Catalase	+	+	+	+
O/F	F	F	F	F
Indole	+	+	+	+
MR	+	+	-	.
VP	+	+	+	+
H_2S	-	-	-	-
ADH	+	+	+	+
LDC	-	-	V	+
ODC	-	-	-	-
ONPG	+	+	+	+
Citrate	+	+	.	.
Urease	-	-	-	-
Gelatinase	+	+	+	+
Amylase	+	+	+	+
Nitrate red.	+	+	+	+
Growth on MacConkey agar	+	+	.	.
Haemolysis	+, β	+,β	+	+
Growth at:				
37°C	+	+	+	.
4°C	+	+	-	.
Growth in:				
0% NaCl	+	+	+	+
2% NaCl	+	+	+	+
4% NaCl	+	+	+	+
6% NaCl	-	-	-	-
8% NaCl	-	-	-	-
Acid production				
Glucose (acid/gas)	+/+	+/+	+/+	+/+
Lactose	-	-	V	.
Sorbitol	-	-	-	-

Mannitol	+	+	+	+	
Sucrose	+	-	+	+	
Inositol	-	-	-	-	
Fructose	-	-	+	.	
Mannose	+	+	.	.	
Xylose	+	+	-	.	
Galactose	+	+	+	.	
Resistance to Vibriostatic agents					
10 µg		R	R	R	R
150 µg		R	R	R	R

* *A. hydrophila* and *A. sobria* strains from Austin and Austin (2007), +: positive, -: negative, ADH: Arginine dihydrolase, LDC: Lysine decarboxilase, ODC: Ornithine decarboxylase, ONPG: o-nitrophenyl-β-D-galactopyronoside, V: Variable results, .: not stated.

3.2. Molecular studies

According to the results of PCR assays with 16S rDNA, 685 bp amplicons was detected in two of the six *Aeromonas* strains. No amplicons were detected in the four strains. Two of the six strains were found to be *A. hydrophila* strains when the specific-specific 16S rDNA primer pair was used in the PCR studies (Fig.2).

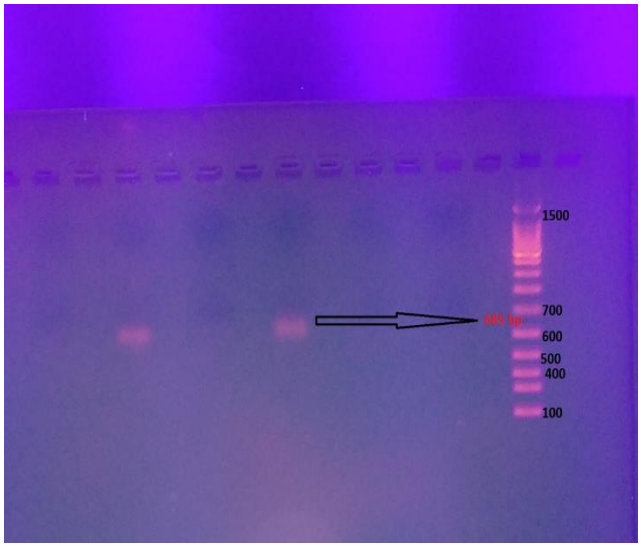

Fig. 2 Result of PCR assay using 16S rDNA pb. M: Marker.

The *aero* virulence gene was detected in 2 strains of *A. hydrophila* and 4 strains of *A. sobria* with a specific band of 209 bp (Fig.3).

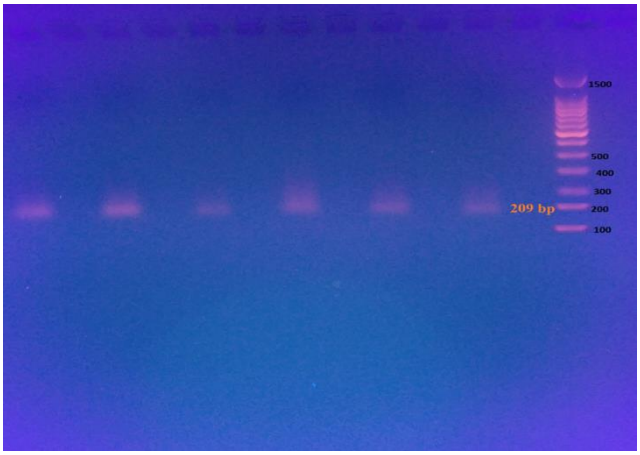

Fig. 3 Result of PCR assay using *Aero* virulence gene. Result of PCR assay using 16S rDNA pb. M: Marker.

In 2 *A. hydrophila* strains, 331 bp amplicons containing the *ast* gene were detected in the PCR assay. However, no amplicons were detected in four *A. sobria* strains (Fig.4). 232 bp amplicons were detected in the 6 strains with the *act* virulence gene (Fig. 5). 592 bp amplicons were observed in 2 *A. hydrophila* strains; however, the 4 *A. sobria* strains had no amplicons for the *hylA* virulence gene (Fig. 6). The antibiotic resistance genes (*tetC* and *sulI*) were not detected in all strains.

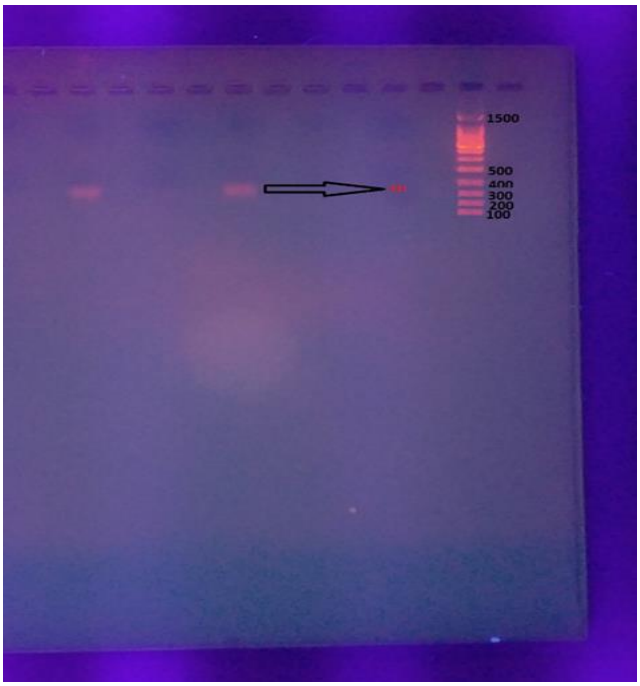

Fig. 4 The amplicons for *ast* gene were detected in two strains of *A. hydrophila*.

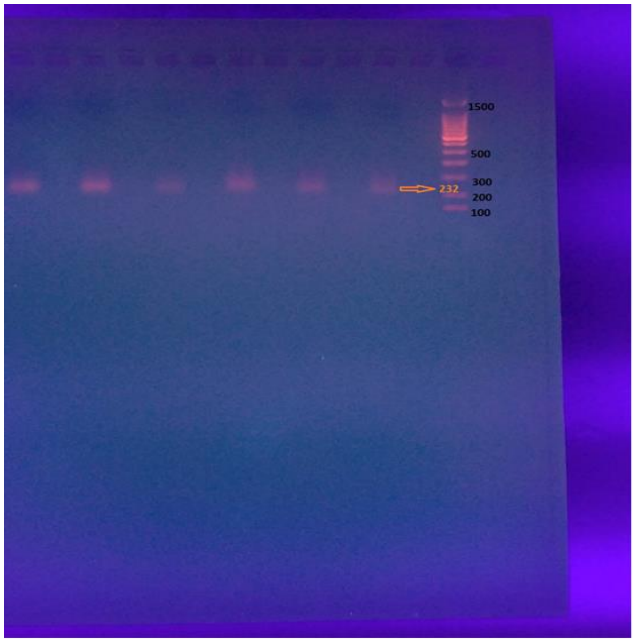

Fig. 5 Result of the PCR assay using the *act* virulence gene.

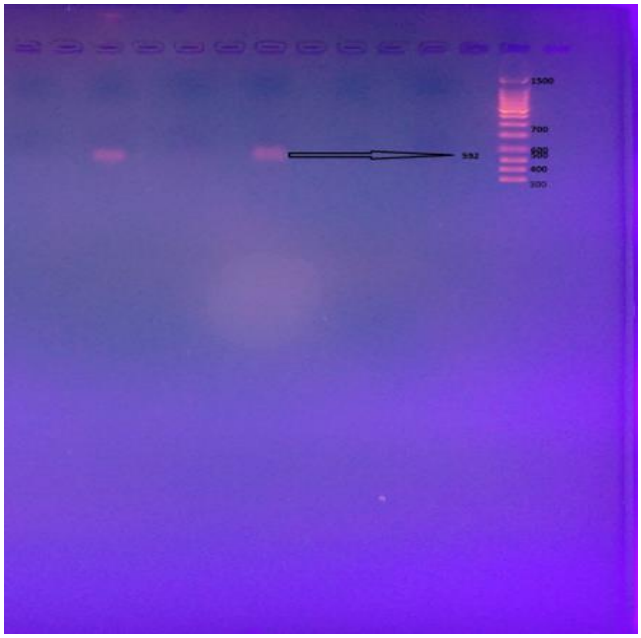

Fig. 6 The amplicons for *hyl A* were detected in 2 *A. hydrophila* strain.

3.3. Results of the antibacterial activity of astaxanthin on *A. hydrophila* and *A. sobria strains*

According to the disc diffusion results, astaxanthin solutions prepared with water and methanol were not effective in *A. hydrophila* and *A. sobria* strains, whereas 0.1g and 0.5g were effective in the strains (Figure 7, Tables 6 and 7); however, 1.0g astaxanthin solutions prepared with acetone were found to be effective in A. sobria strains but not in *A. hydrophila*. *A. hydrophila* strains showed resistance to oxytetracycline, while *A. sobria* strains showed intermediate resistance to OT30, which was used as a control.

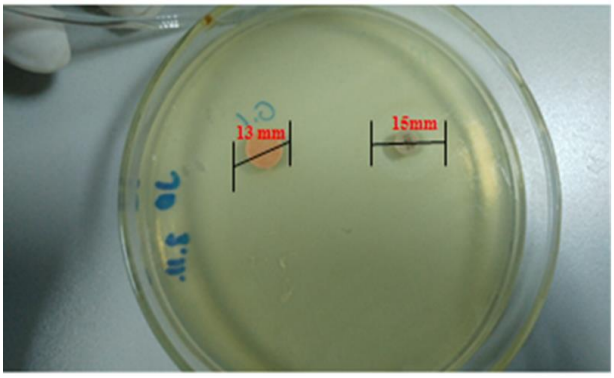

Fig. 7 Effect of acetone solution of astaxanthin on *A. sobria* a: acetone solution containing 0.1g astaxanthin, b: control (OXT 30)

Table 6 Result of disc diffusion test of water, methanol and acetone solutions of astaxanthin on *A. hydrophila* strains

Solvent	Astaxanthin (0.1 g)	Astaxanthin (0.5 g)	Astaxanthin (1.0 g)
Water	R	R	R
Methanol	R	R	R
Acetone	13 mm	18 mm	R
Control (OT30)	R		

R: Resistant

Table 7 Result of disc diffusion test of water, methanol and acetone solutions of astaxanthin on *A. sobria* strains

Solvent	Astaxanthin (0.1 g)	Astaxanthin (0.5 g)	Astaxanthin (1.0 g)
Water	R	R	R
Methanol	R	R	R
Acetone	13 mm	13 mm	16 mm
Control (OT30)		R	

R: Resistance, I. R. : Intermediate Resistnace

3.4. Antibiotic susceptibility profiles of strains

According to the standard disc diffusion technique, the *A. hydrophila* strains were resistant to ampicillin, chloramphenicol, tetracycline, streptomycin, and nalidixic acid. The strains were sensitive to sulfamethoxazole, flumequine, and trimethoprim, while showing intermediate resistance to erythromycin, kanamycin, and oxytetracycline. Strains of *A. sobria* showed resistant to ampicillin, chloramphenicol, sulfamethoxazole, erythromycin, and nalidixic acid, while the strains showed intermediate resistance to flumequine, trimethoprim, kanamycin, and oxytetracycline; strains were not sensitive to any of the antibiotics used in the study. The antibiogram test results of the strains are shown in Table 8.

Tablo 8 Antibiogram profiles of *A. hydrophila and A. sobria* strains against twelve antibiotics used in the study

Species	Antibiotics			
	C30*	RL25	E15	UB30
A.hydrophila (2 strains)	R	18 mm (S)	17 mm (I.R)	22 mm (S)
	Antibiotics			
A.hydrophila (2 strains)	W5 24 mm	TE10 R	S10 R	NA30 R
	Antibiotics			
A.hydrophila (2 strains)	AMP10 R	K30 16 mm (I.R)	TE30 R	OT30 15 mm (I. R)
	Antibiotics			
A.sobria (4 strains)	C30 R	RL25 R	E15 R (I.R)	UB30 17 mm
	Antibiotics			
A.sobria (4 strains)	W5 14 mm (I.R)	TE10 R 12 mm (I.R)	S10 R	NA30
	Antibiotics			
A.sobria (4 strains)	AMP10 R 15 mm (I.R)	K30 R	TE30 15 mm (I.R)	OT30

C30: Chloramphenicol, RL25: Sulfamethaxazole, E15: Erythromycin, UB30: Flumequine, W5: Trimethoprim, TE10: Tetracycline, S10: Streptomycin, NA30: Nalidixic acid, AMP10: Ampicillin, K30: Kanamycin, TE30: Tetracycline, OT30: Oxytetracycline, R: Resistance, S: Susceptibe, I. R: Intermediate Resistance

3.5. Results of MAR Index

The *A. hydrophila* strains proved resistant to 7 of 12 antibiotics used in the study. The strains were found to be intermediate resistance to two antibiotics and sensitive to three antibiotics. *A. sobria* strains were resistant to 7 of the 12 antibiotics. The MAR index value for *A. hydrophila* was 0.5 and the MAR index value for *A. sobria* was 0.6. The results are shown in Table 9.

Table 9 The results of the MAR index for *A. hydrophila* and *A. sobria*

	A.hydrophila	*A.sobria*
Number of the resistant antibiotic disc (a)	6	7
Total number of antibiotics Used in the study (b)	12	12
The MAR index value (a/b)	0.5	0.6

4. Discussion

This study was carried out to determine the antibacterial effect of astaxanthin on *A. hydrophila* and *A. sobria* strains as an alternative to antibiotics. 2 of the 6 strains isolated from goldfish were phenotypically identified as *A. hydrophila* and four as *A. sobria*. PCR study using 16S rDNA-specific primers specific for *A. hydrophila* detected 685 bp amplicons in two of the six strains. The complex pathogenicity mechanism of *A. hydrophila* has been reported to be effective in causing such widespread infections (Ahangarzadeh et al. 2022). Proteinaceous toxins such as hemolysin (*hylA*) and aerolysin (*aerA*) involved in this pathogenicity mechanism, make the *A. hydrophila* strain virulent (Ahangarzadeh et al. 2022). PCR studies using specific primers for the *aerA* and *hylA* virulence genes of *A. hydrophila* strains detected amplicons of 209 bp and 592 bp, respectively, for both strains. Amplicons specific for the *hylA* virulence gene were not detected in four strains defined as *A. sobria*, but amplicons of 209 bp in the PCR study using specific primers for the *aerA* virulence gene were detected in all strains. Robertson *et al*. (2014) reported that the virulence genes hemolysin (*hylA*) and aerolysin (*aerA*) can be useful clues for distinguishing pathogenic *Aeromonas* species from nonpathogenic *Aeromonas* species. A number of conventional microbiological tests are used to determine the phenotypic characteristics of *Aeromonas* spp. Reading the results of these tests can be both time consuming and cause difficulties in accurately identifying bacterial species (Yadav et al. 2014). In the present study, the *hylA* gene was not detected in *A. sobria*, but was detected in *A. hydrophila* strains. The O/129 vibriostat test is important for distinguishing *Aeromonas* and *Vibrio* species. Like this test, the *hylA* virulence gene can also be used to distinguish *A. hydrophila* from other *Aeromonas* species.

Act gene, which belongs to virulence factors, is the most important enterotoxin with hemolytic, cytotoxic, and enterotoxic activities (Sreedharan et al. 2012). Sreedharan et al. (2012) reported that all isolates amplified at least one virulent gene related to the virulent genes of *Aeromonas* species they isolated from ornamental fish culture systems, and 58.3% of *Aeromonas* strains amplified the *act* gene. In the present study, the strains of *A. hydrophila* and *A. sobria* all amplified the *act* gene. The ast gene was detected only in *A. hydrophila* strains.

Antibiotics and other chemicals are used in aquaculture to prevent and treat disease outbreaks. However, the use of antibiotics for therapeutic purposes is not recommended. The development of antimicrobial resistance in pathogenic bacterial species that cause disease affects this condition (Mohd-Aris et al. 2019). *Aeromonas* species play an important role as a source of antimicrobial resistance genes and they can be considered as indicator bacteria for antibiotic resistance detection (Conte et al. 2020). In this study, the antimicrobial resistance genes *tetC* and *sulI* of 6 strains were investigated. No amplification was detected in the PCR study using primers specific for the sulfonamide resistance gene (*sulI*). Similar results were obtained in the PCR study with primers specific for the *tetC* resistance

gene. However, in the antibiogram study using the standard diffusion method, strains were found to be resistant to both 10 µg and 30 µg tetracycline discs. This could be due to the presence of other organisms that cause tetracycline resistance, such as flow pumps, where strains are phenotypically resistant to tetracycline, as noted by Natarajan et al. (2018).

In the study, 6 *Aeromonas* strains were resistant to chloramphenicol. El-Gohary et al. (2020) informed that isolates were highly resistant (80%) to chloramphenicol in their study of *Aeromonas* spp. Hossain et al. (2020) reported that the resistance rate of *Aeromonas* isolates from ornamental guppies (*Poecilia reticulata*) to chloramphenicol was 5.8%. Although chloramphenicol is a broad-spectrum antibiotic, resistance to this antibiotic has been frequently reported (Dinos et al. 2016). Resistance to ampicillin is observed in *Aeromonas* species, with the exception of *Aeromonas trota* and a few strains (Fernández-Bravo and Figueras 2020). In this study, resistance to ampicillin was observed in *A. hydrophila* and *A. sobria*. While *A. hydrophila* strains were moderately resistant to erythromycin in the study, *A. sobria* strains were resistant. Jagoda et al. (2014) investigated the susceptibility of 53 *Aeromonas* isolates from freshwater ornamental fish to 8 antimicrobial agents. In addition to amoxicillin in the beta-lactam antibiotic group, the highest resistance was found to tetracycline at 58.5% and erythromycin at 54.7%. Eid et al. (2022), in their study investigating the resistance of *Aeromonas* isolates isolated from fish and water samples to antibiotics from seven different classes, reported that the isolates showed extremely high resistance (90%) to tetracycline and significant resistance (63.33%) to streptomycin. The isolates showed low resistance to nalidixic acid. In the study, all *Aeromonas* strains showed resistance to 10 µg and 30 µg tetracycline discs. While 2 *A. hydrophila* strains showed intermediate resistance to oxytetracycline, 4 *A. sobria* strains proved resistant. All strains showed resistance to streptomycin and nalidixic acid. In the study, both *A. hydrophila* and *A. sobria* strains showed intermediate resistance to kanamycin.

5. Conclusion

The widespread use of antibiotics in agriculture and aquaculture has led to a global increase in antibiotic resistance. However, because antibiotic resistance arose millions of years before the era of modern antibiotics, it has been shown that the development of antibiotic resistance cannot be completely eliminated (Dinos et al. 2016). In the study, the MAR index value of *A. hydrophila* strains was 0.5; the MAR index value of *A. sobria* strains was 0.6. All strains showed resistance to more than one antibiotic. Strains with multiple resistance to antibiotics, the presence of the *aero* virulence gene and the *act* virulence gene in all strains; this indicates that the treatment of infections that may arise from these pathogenic bacteria will be difficult. Therefore, in this study investigating the antibacterial activity of astaxanthin, it was found that 0.5 g and 0.1 g astaxanthin solutions prepared with acetone effectively showed antibacterial properties in both *A. hydrophila* and *A. sobria* strains. According to the results of the study, it can be assumed that the use of astaxanthin as a feed additive in fish farming has a prophylactic significance in relation to bacterial fish diseases, but there is also a need for more experimental studies that can show the effect of astaxanthin in relation to fish health.

Authors' contributions: The contribution of the authors to the present study is equal.

Conflict of interest disclosure: The authors declared that they have no actual, potential or perceived conflict of interest for this article.

References

Ahangarzadeh M, Najafabadi MG, Peyghan R, Houshmand H, Rohani MS, Soltani M. 2022. Detection and distribution of virulence genes in *Aeromonas hydrophila* isolates causing infection in cultured carps. VRF, 13 (1): 55-60. doi: 10.30466/vrf.2020.115998.2761

Austin B, Austin DA. 2007. Isolation / Detection In: Dobbins P (ed) Bacterial fish pathogens Diseases of farmed and wild fish, 4th edn. Springer-Praxis Edinburgh

Bauer AW, Kirby WM, Sherris JC, Turck M. 1966. Antibiotic susceptibility testing by a standardized single disc method. AJCP. 45, 493-496

Conte D, Palmeiro JK, Bavaroski AA, Rodrigues LS, Cardozo D, Tomaz AP, Camargo JO, Dalla-Costa LM. 2020. Antimicrobial resistance in *Aeromonas* species isolated from aquatic environments in Brazil. JAM, 1-14. doi: 10.1111/jam.14965

CLSI M49. 2006. Methods for broth dilution susceptibility testing of bacteria isolated from aquatic animals: approved guideline. Clinical and Laboratory Standards Institute, USA.

Dhankar J, Kadian SS, Sharma A. 2012. Astaxanthin: a potential carotenoid. JPSR. 3 (5): 1246-1259

Dinos PG, Athanasspoulos CM, Missiri DA, Giannopoulou PC, Ulachogiannis IA, Papadopoulos GE, Papaiannou D, Kalpaxis DL. 2016. Chloramphenicol derivatives as antibacterial and anticancer agents: historic problems and current solutions. Antibiotics, 5(20): 1-21. doi: 10.3390/antibiotics5020020

Duman M. 2017. Gökkuşağı alabalıklarında görülen motil *Aeromonas* (*Aeromonas hydrophila*, *A. sobria*, *A. caviae*), *Yersinia ruckeri* ve *Lactococcus garvieae* bakterilerinin antimikrobiyal duyarlılıkları ve duyarlılıkta rol oynayan genlerin tespiti. Doktora tezi, Uludağ Üniversitesi, Sağlık Bilimleri Enstitüsü Su Ürünleri Hastalıkları ABD, Bursa, 126 sayfa

Ebied MA, Elebshehy EM, Sherif AH, Elgohary M, Turky HA. 2022. Prevalance of antibiotic-resistant *Aeromonas hydrophila* isolated from the farmed striped mullet *Mugil cephalus*. EJABF. 26(2). 383-398

Ehinmidu JO. 2003. Antibiotic susceptibility patterns of urine bacterial isolates in Zaria, Nigeria. TJPR. 2(2): 223-228

Eid HM, El-Mahallawy HS, Shalaby AM, Elsheshtawy HM, Shetewy MM, Eidaroos NH. 2022. Emergency of extensively drug-resistant *Aeromonas hydrophila* complex isolated from *Mugil cephalus* (stripped mullet) and Mediterranean seawater. Vet World, 15(1): 55-64.

El-Bahar MH, Ali GN, Aboyadak MI, Abd El Salam K, Ibrahim SM. 2019. Virulence genes contributing to *Aeromonas*

hydrophila pathogenicity in *Oreochromis niloticus*. Int Microbiol 22: 479-490

El-Gohary FA, Zahran E, El-Gohary AH, Abdelhamid FM, El-Mleeh A, Elmahallawy EK, Elsayed MM. 2020. Investigation of the prevalence, virulence genes, and antibiogram of motile aeromonads isolated from Nile tilapia fish farmers in Egypt and assessment of their water quality. Ani. 10(1432): 1-16. doi: 10.3390/ani/0081432

Elshestawy A, Yehia N, Elkemary M, Soliman H. 2019. Direct direction of unamplified *Aeromonas hydrophila* DNA in clinical fish samples using gold nanoparticle probe-based assay. Aquaculture. 500: 451-457. doi: 10.1016/aquaculture.2018.10.046

Fernández-Bravo A., Figueras MJ. 2020. An update on the genus *Aeromonas*: Taxonomy, epidemiology, and pathogenicicty. Microorganisms. 8(129): 1-39. doi: 10.3390/microorganisms8010129

Gardenia L, Koesharyani I, Supriyadi H, Mufidah T. 2010. Aplikasi deteksi dengan menggunakan polymerase chain reaction (PCR). Prosiding FITA. 877-883.

Guz L, Nowakiewics A, Puk K, Zreba P, Gnat S, Matuszewski L. 2021. Virulence and antimicrobial resistance pattern of *Aeromonas* spp. colonizing European pond turtles *Emys orbicularis* and their natural envirronment. First study from Poland. Animals. 11(2772): 1-14. doi: 10.3390/ani11102772

Hoel S, Vadstein C, Jakobsen AN. 2017. Species distribution and prevalance of putative virulence factors in mesophilic *Aeromonas* spp. isolated from fresh retail sushi. Front. Microbiol. 8(531). doi: 10.3389/fmicb.2017.00931

Hossain S, Heo GJ. 2020. Ornamental fish: a potential source of pathogenic and multidrug resistant motile *Aeromonas* spp. Lett. Appl. Microbiol. 72: 1-12

Hossain S, De Silva BCJ, Dahanayake PS, Zoysa MD, Heo GJ. 2020. Phylogenetic characteristics virulence properties and antibiogram profile of motile *Aeromonas* spp. isolated from ornamental guppy (*Poecilia reticulata*). Arch. Microbiol. 202: 501-509

Joseph AV, Sasidharan RS, Nair NP, Bhat SG. 2013. Occurence of potential pathogenic *Aeromonas* species in tropical seafood, aquafarms and mangroves off Cochin coast in South India. Vet Worl. 6(6): 300-306. doi: 10.5455/vetworld2013

Krumperman PH. 1983. Multiple antibiotic resistance indexing of *Escherichia coli* to identify high-risk sources of fecal contamination of foods. Appl Environ Microbiol. 46: 165-170

Lim KC, Yusoff FMd, Shariff M, Kamarudin MS. 2018. Astaxanthin as feed supplemente in aquatic animals. Rev Aquaculture. 10: 738-773.

Lotfi A, Soleimani M, Ghasemi N. 2021. Astaxanthin reduces demyelination and oligodendrocytes death in a rat model of multiple sclerosis. Cell J. 22(4): 565-571

Marinho YF, Malafaia CB, Araujo KS, da Silva TD, Santos APF, Moraes LB, Gálvaz AO. 2021. Evaluation of the influence of different culture media reon growth, life cycle, biochemical composition, and astaxanthin production in *Haematococcus pluvialis*. Aquac Int. 29: 757-778

Mohd-Aris A, Muhamed Sofie MHN, Zamri-Saad M, Daud HM, Ina-Salwany MY. 2019. Live vaccines against bacterial fish diseases: A review. Vet World. 12 (11): 1806-1815

Montaya JM, Mata SV, Acosta JL, Cabiera BEH, Valdez LGL, Reyes C, Cureño HJB. 2021. Obtaining of astaxanthin from crab exosqueletons and shrimp head shells. Biointerface Res Appl Chem. 11(5): 13516-13523

Natarajan M, Kumar D, Mandal J, Biswal N, Stephen S. 2018. A study of virulence and antimicrobial resistance pattern in diarrhoeagenic *Escherichia coli* isolated from diarrhoeal stool specimens from children and adults in a tertiary hospital, Puducherry, India. J Health Popul Nutr. 37(17): 1-11

Odeyemi OA, Asmat A, Usup G. 2012. Antibiotic resistance and putative virulence factors of *Aeromonas hydrophila* isolated from estuary. J Microbiol Biotechnol Food Sci. 1 (6): 1339-1357

Olaizola M. 2017. The production and health benefits of astaxanthin. Nutraceutical Science and Technology. 321-342.

Pandey G. 2018. Fish pharmacology and toxicology. Day Publishing House, New Delhi, India

Robertson BK, Harden C, Selvaraju SB, Pradhan S, Yadav JS. 2014. Molecular detection, quantificcation, and toxicity profiling of *Aeromonas* spp. in source-and drinking-water. Open Microbiol J. 8: 32-39.

Saharia PK, Hussain IA, Pokhrel H, Kalita B, Borah G, Yasmin R. 2021. Prevalence of motile Aeromonas septicaemia (MAS) in fish culture systems of the central Brahmaputra Valley Zone of Assam, India. Aquac. 52: 1201-1214

Sreedharan K, Philip R, Singh ISB. 2012. Virulence potential and antibiotic susceptibility pattern of motile aeromonads associated with freshwater ornamental fish culture systems: a possible threat to public health. Brz J Microbiol. 754-765.

Temizkan G, Arda N. 2004. Moleküler biyolojide kullanılan yöntemler. BİYOGEM Yayın no: 2. Nobel Tıp Kitapevleri.

Yadav S, Verma DK, Pradhan PK, Dobriyal AK, Sood N. 2014. Phenotypic and genomic identification of *Aeromonas* species from aquatic environment. Int J Fish Aquat Sci. 5(1): 3-20

Yardımcı RE, Turgay E. 2021. Diagnosis of *Aeromonas sobria* and *Saprolegnia* sp. co-infection in rainbow trout fry (*Oncorhynchus mykiss*). Aquat Res. 4(1): 65-72. doi: 10.3153/AR21006

RESEARCH ARTICLE
Eurasian J Bio Chem Sci, 5(Suppl 1):144-150, 2022
https://doi.org/10.46239/ejbcs.1163946

EJBCS

Eurasian Journal of Biological and Chemical Sciences

Journal homepage: www.dergipark.org.tr/ejbcs

Use of onion peels as an economical substrate for microbial inulinase production under solid state fermentation

Özden Canlı Taşar[1*], Gani Erhan Taşar[2]

[1] *High Technology Application and Research Centre, Erzurum Technical University, Erzurum, Türkiye*
[2]*Kahta Vocational High School, Adıyaman University, Adıyaman, Türkiye*

*Corresponding author: ozden.tasar@erzurum.edu.tr
Orcid No: https://orcid.org/0000-0002-4313-5373

Received : 18/08/2022
Accepted : 09/10/2022

Abstract: Onion (*Allium cepa*) is a valuable vegetable and a candidate for sustainable waste management in agri-food industry. The purpose of the current paper was to research the utilization of onion peels to an economical substrate for inulinase production by *Yarrowia lipolytica* ISF7 strain under solid state fermentation (SSF). SSF is preferred to obtain an effective and low-cost inulinase production. The medium designation was optimized using Taguchi design of experiment. For this purpose, Taguchi L_9 orthogonal array layout was applied using the moisture content, initial pH and incubation time as the selected factors at three levels. The results showed that the minimum inulinase activity 22.7 U g^{-1} of dry substrate (ds) was determined using the 6th experimental setup while the highest inulinase activity 292.2 U gds^{-1} was measured from 5th experimental setup. The predicted value was determined as 311.6 U gds^{-1} which was closer to the obtained result (305.1 U gds^{-1}). Consequently, an effective inulinase production can be achieved by *Y. lipolytica* ISF7 using onion peels as an economic substrate under SSF.

Keywords: Solid state fermentation, Taguchi design, enzyme, optimization

1. Introduction

Waste management is going to be more important due to increase at the world population. One of the major challenges of the current age is the conversion of waste materials to valuable products, especially in agri-food industry. The waste materials like egg shells, vegetable peels, coffee grounds have attraction as being candidates for biotechnological applications (Budžaki et al. 2022). The governments investigate policy for food management and safety, decreasing the food loss and evaluation of the non-edible food parts for value-added products. The greatest part of the waste management includes food wastes (Sharma et al. 2022). The onion (*Allium cepa*) is generally cultivated and consumed globally and in terms of economic importance. It is accepted as the second valuable vegetable after tomatoes among all the vegetables. At household kitchen or food industry level, huge amounts of non-edible parts of onions, like peels, top and bottom parts, and corrupted layers are thrown away as garbage (Pathak et al. 2016; Abd-Elsalam et al. 2021; Zhivkova, 2021; Kumar et al. 2022). Furthermore, waste onion parts present environmental problems and cannot be used within animal fodder or fertilizer production depending on its strong aroma (Benítez et al. 2011). An alternative disposal of onion-derived wastes may be used in food ingredients that have positive effects on human health, due to their rich ingredients like dietary fibre, polysaccharides, polyphenols, antioxidants, fructooligosaccharides, alkyl cysteine sulphoxides and flavonoids (Griffiths et al. 2002). Moreover, the onion peels were determined as "suitable" candidates as raw materials for immobilized enzyme carriers; however, a sustainable conversion-production process using these waste materials is not available yet (Budžaki et al. 2022).

Inulin exists the β-2,1-linked D-fructofuranose linear chains residue through a sucrose-type bonding at the reducing end that placed in the roots and tubers. Inulin is a main carbohydrate reserve material and stores energy in many plants like garlic, leek, Jerusalem artichoke, dahlia, chicory, burdock, onion, asparagus, agave, etc. (Van Loo et al. 1995). Onion is an indispensable economic food source and it has been easily available relatively all the time. As a result of regular consumption of this plant for households or food industry, waste onion peels exist in significant amounts every day. It's about 450.000 tonnes of onion wastes exist annually in Europe ('Conversion of

environmentally-unfriendly onion waste into food ingredients', 1999). Bioconversion of the waste materials are considered as economic, environmentally friendly (Bhatnagar et al. 2015). Onion has many valuable contents in its natural structure like, free fat (0.31%), total sugars (4.29%), reducing sugars (3.10%), total dietary fibre (16.02%), digestible carbohydrates (4.7%), crude protein (2.61%), magnesium (1285 mg kg-1), sodium (1021 mg kg-1), phosphorus (881 mg kg-1) and copper (4.58 mg kg-1) (Zhivkova 2021). Besides, the onion contains inulin 2-6% in its natural structure (Van Loo et al. 1995; Rawat et al. 2021). The fructooligosaccharides (FOS) production is made using different enzymes by the transfructosylation of sucrose catalysed by inulinase or β-fructosyltransferase. FOS expands the shelf-life of many products due to their ability (Sangeetha et al. 2005). The disadvantage of microbial inulinase production is its availability in only large quantities at competitive market prices. Thus, the inulinase production by a microorganism should be well optimized using the environmental conditions like pH, incubation temperature and incubation time, content of the medium, etc. (Sguarezi et al. 2009; Tasar, 2020).

Minimum free water content is the main structural property of the SSF. This method has been used since the ancient times for bread and cheese fermentation (Libardi et al. 2017; Soccol et al. 2017). SSF has been used commonly in biotechnological applications like microbial enzyme productions as amylase (Selvam et al. 2016), protease (Kandasamy et al. 2016), laccase (Srinivasan et al. 2019). Although, microbial inulinase production were obtained both of submerged (SmF) and solid-state fermentation (SSF) techniques with different kinds of microorganisms and substrates (Mughal et al. 2009; Erdal et al. 2011; Canli et al. 2013; Tasar, 2020), however, to the best of our knowledge, there have been limited studies using onion peels as substrate for inulinase production under SSF (Ayyachamy et al. 2007; Yazici et al. 2020). SSF method benefits from the low moisture content near or at the surfaces of solid materials for microbial growth and product formation (Selvakumar and Pandey 1999). SmF method needs more energy consumption and labour, besides, SSF presents similar growing condition to the microorganisms with their original habitat with less production cost than SmF (Singhania et al. 2010). Use of statistical optimization designs contributes more efficient fermentation progress, hence, SSF effects were investigated in this study. The researchers applied the optimization methods due to their advantages to enhance the production capacity.

Y. lipolytica is a dimorphic and strict aerobic yeast that has an oleaginous nature. This yeast has ability on the bioconversion of hydrophobic substrates. *Y. lipolytica* has also a GRAS (generally recognized as safe) status, that means this yeast is approved for many applications in food industry by the United States of America Food and Drug Administration (FDA) (Groenewald et al. 2014; Desnos-Ollivier et al. 2020; Fraga et al. 2021; Madzak, 2021). *Y. lipolytica* has a great potential to collect the lipids in large amounts and its whole genome sequencing caused valuable tools for genetic manipulation (Beopoulos et al. 2009; Wang et al. 2013; Hughes et al. 2017; Shi et al. 2018). *Y. lipolytica* is one of the most studied unconventional yeast, however, according to our best knowledge there is not any report for inulinase production using onion peels. This study aimed to research the inulinase production capability of *Y. lipolytica* ISF7 using waste onion peels as substrate under SSF cultivation.

2. Materials and Method

The whole chemicals were purchased and pure inulin (chicory) from Sigma Chemical Co. (USA) and Merck (Germany). Onions were bought from markets in Erzurum, Turkey. Considering the fact that, waste onion peels were needed to be totally free from apparent damage or microbial infections. The washed and dried onion peels were sliced in a blender to 0,5 mm particle-sized fine powder and the main substrate was called as onion peel powder (OPP).

2.1. Microorganism and medium

The microorganism was isolated from 1% inulin enriched-potato dextrose agar containing plates using 0.1 mL cheese whey directly as the microorganism source which was provided from Food Engineering Department Dairy Products, Ataturk University, Turkey. Dairy products are generally contaminated with inulin-hydrolysing microorganisms; thus, cheese whey was used for microorganism isolation target. The best grown isolate named as IN-3 was identified as *Y. lipolytica* ISF7 using 16S rRNA sequence analysis (Fig. 1). The ITS region was amplified under in vitro conditions using universal ITS1 and ITS4 primers. The pGEM-T Easy Vector Systems (Promega UK) was employed for cloning of PCR products and amplification of ITS gene region for sequencing at Macrogen (The Nederlands). The results were determined from the database and were analysed with BioEdit. Y. lipolytica ISF7 was maintained in potato dextrose agar at 4˚C and subcultured. Potato dextrose broth was prepared in 250 mL flasks for the yeast starter culture and one loopful of a 1-d-old *Y. lipolytica* ISF7 was used for the inoculation. The inoculum material was cultivated at 30˚C and 200 rpm for 48 h on an orbital shaking incubator (Zhicheng ZHWY-200B, China). The cell density was adjusted to an absorbance at $1.5_{600\ nm}$ and 1 mL of the suspension was used for the inoculum material. The growth medium contains (g L-1); 3 $(NH_4)_2SO_4$; 5 $NaNO_3$; 0,5 $MgSO_4.7H_2O$; 0,3 $CaCl_2$. 250 mL Erlenmeyer flasks with cotton stoppers were used for cultivation containing five grams of OPP and growth medium. The flasks were autoclaved at 121℃ for 15 min, cooled to room temperature and inoculated. The incubation temperature was adjusted to 35˚C for all experiments.

2.2. Extraction of the enzyme

The crude enzyme was extracted from the medium at the end of the incubation period. For this purpose, 100 mL of sodium acetate buffer (0.1 M pH 5.5) were placed to each flask and incubated in a rotary shaker for 30 min at 150 g at room temperature. The culture filtrates were identified as crude enzyme at the end of centrifugation at 5000 g for 15 min (Hettich Universal).

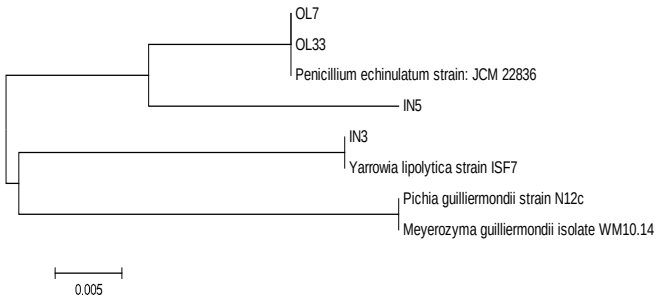

Fig. 1. The phylogenetic tree on the basis of 16S rRNA gene sequence data of *Y. lipolytica* ISF7 strain using neighbour joining method.

2.3. Analytical methods

Extracellular inulinase activity was determined using released reducing sugar from the inulin as described by Pessoni et al. (Pessoni et al. 1999) with some modifications (Ge and Zhang 2005; Mughal et al. 2009). One inulinase unit was determined as the enzyme amount that liberates 1 µmol of fructose from inulin per minute in 1 mL. For this purpose, 100 µL of enzyme source was added to 900 µL sodium acetate buffer (0.1 M pH 5.5) containing 2% (w/v) pure inulin and the glass test tubes were taken to the incubator at 50°C for 15 min. 1 mL of DNS was added to glass test tubes and left for boiling in a water bath for 10 min. Boiling water stopped the enzyme activity. The total volume of the tubes was raised to 8 ml using distilled water and released reducing sugar was measured at 592 nm (Thermo MultiSkan Go, Finland) (Lin and Huang 2000). Distilled water was used as the blank.

2.4. Taguchi DOE methodology and ANOVA analysis

In the current study, there were three efficient factors with three levels, that affect the inulinase production, following; initial pH, the moisture content (%) and incubation time (Table 1). In full factorial design, 27 (3^3) runs of experimental setups would be required. However, Taguchi DOE L_9 design suggests only 9 experimental setups, which is a part of full factorial design. This means less human power, less energy and time consumption that are the main advantages of a production process. This method applies the quadratic loss function to measure the loss for departure of the target Taguchi DOE is based on three different characteristic categories as the bigger-the better, the nominal-the better and the smaller-the better (Hsieh et al. 2005; Tasar, 2022). The bigger-the better criterion was selected to increase the enzyme activity using the equation shown below:

$$S/N = -10 \log10 \left(1/n \sum_{i=1}^{n} \mathbf{1}/\boldsymbol{Yi}^{2}\right)$$

where S/N are performance statistics. The n determines the repetition of the numbers and the Yi is a performance value of the ith experiment in the equation. The calculation of S/N ratio was used for the detection of the maximum yield (Jean and Tzeng, 2003).

Table 1. Optimization parameters and their levels

Levels	Factors		
	pH	Moisture content (%)	Time (d)
1	4.0	55	1
2	5.0	65	2
3	6.0	75	3

Analysis of variance (ANOVA) of the obtained results was used to find out the characteristics variation using the selected factors. Minitab® 19.1.1 Statistical Software (United States) was utilized for all the statistical and experimental analysis. The results were determined as the average value of three runs for each setup.

3. Results and Discussion

The exo-inulinase enzyme catalyses the removing the terminal fructose ending molecules from the non-reducing end of the inulin in one step and the final products exist as fructose and glucose at major and minor ratios, respectively (Zhao et al. 2010). *R. glutinis, A. fumigatus, P. brevicompactum, G. candidum* were studied for inulinase production before (Silva et al. 2011; Canli et al. 2013; Tasar et al. 2015; Tasar, 2020; Rawat et al. 2021).

3.1. Taguchi design results

In the current study, Taguchi DOE was employed for the optimization process of inulinase production by *Y. lipolytica* ISF7. The results showed that the cultivation conditions had great effect on enzyme activity. In a recent paper, it was reported that, use of onion peels, wheat bran and maltose had positive effects on inulinase production by *Rhizopus oryzae* under SSF. The optimization of the temperature, initial pH and incubation time were done using Placket-Burman design, and the obtained results showed that optimal values found as 35˚C, pH of 5.5 and 5 days, respectively (Yazici et al. 2020). However, in the current study, optimal values were found for pH as 6 and 3 days for incubation time. This difference may be resulted from inulinase-producer microorganisms. Onion has been reported for its antioxidant activity as dry onion scales which are thrown away as garbage. In a previous study, extracted onion scales were investigated for their quercetin quantity (Abd-Elsalam et al. 2021). Quercetin is an antioxidant that naturally exists as a free aglycone or glycosidic form as conjugated to one or more sugar molecules (Li and Row 2019).

Table 2. Taguchi L9 orthogonal array and inulinase activity and S/N ratios

Exp. No.	pH	Moisture	Time	Inulinase (U gds^{-1})*	S/N ratios
1	1	1	1	30.6±0.7	29.71
2	1	2	2	43.6±0.51	32.78
3	1	3	3	269.4±5.6	48.60
4	2	1	2	126.6±9.3	42.04
5	2	2	3	292.2±11.4	49.31
6	2	3	1	22.7±0.8	27.12
7	3	1	3	216.2±10.3	46.69
8	3	2	1	23.4±0.5	27.38
9	3	3	2	231.4±12.7	47.28

*Values mean ± standard deviation.

The maximum inulinase activity (292.2 U gds^{-1}) was gained from the 5th experimental setup while the minimum activity 22.7 U gds^{-1} was obtained from the 6th experimental setup (Table 2). It is clear from the Table 2, different environmental conditions combinations caused variation on the results. S/N ratios also approved that the higher inulinase activity had the higher S/N ratio. In a previous study, the INU1 gene encoding exo-inulinase cloned from *Kluyveromyces marxianus* CBS 6556 that was ligated into the surface display plasmid and expressed in *Y. lipolytica*, and the optimal pH was found as 4.5 for the expressed inulinase that was immobilized on the yeast cells. In addition, pH stability was obtained in the pH range of 3-8 (Liu et al. 2010). In another study with the same microorganisms using Jerusalem artichoke extract, the highest inulinase activity was obtained as 41.7 U ml^{-1} at 72th hour of the fermentation, which was similar with the current study (Zhao et al. 2010).

Response data for S/N ratios and their comparison were given. The ranking in Table 2 demonstrates that incubation time had relatively strong impact, while the moisture content and initial pH of the medium had relatively weak impacts on the inulinase production by *Y. lipolytica* ISF7. Taguchi DOE uses the S/N ratio for the deviation of the quality characteristics of the results (Sharma et al. 2005). *Y. lipolytica* is commonly known as an oleaginous yeast and used for biofuel and single cell oil production (Shi et al. 2018; Zhao et al. 2010), however, it's inulinase production capability was investigated before, either naturally or recombinantly (Cui et al. 2011; Liu et al. 2010; Zhao et al. 2010). In a previous study, INU1 gene encoding exoinulinase cloned from *K. marxianus* CBS 6556 into the *Y. lipolytica* ACA-DC 50109 resulted as 41.7 U ml-1 inulinase activity after cell growth for 78 h in a 2-L fermenter with 50.6% (w/w) oil extract from Jerusalem artichoke tubers in its cells within 78 h (Zhao et al. 2010), which was similar to the current study for incubation time (3 days). On the other hand, in a previous study, the optimal pH and temperature were obtained as 4,5 and 50˚C, respectively for *Y. lipolytica* that had the INU1 exo-inulinase gene encoding cloned from *K. marxianus* CBS 6556 (Liu et al. 2010).

Table 3. Response table for means

Level	pH	Moisture	Time
1	114.53	124.47	25.57
2	147.17	119.73	133.87
3	157.00	174.50	259.27
Delta	42.47	54.77	233.70
Rank	3	2	1

Taguchi DOE uses the prediction analysis of the obtained results. Fig. 1 illustrated the main effects plot for S/N ratios. For validation analysis, the proposed experimental methodology, inulinase production was re-designated using the suggested optimal levels. The last step of the study was to predict and verify the optimal conditions using the suggested levels of each individual factors. Using the data showed in Figure 1, the optimal experimental setup was indicated using levels at 3, 3 and 3 that's pH 6, 75% of moisture content, and 3 days for incubation time. The predicted inulinase activity was obtained as 311.6 U gds^{-1} which was closer to the obtained result (305.1 U gds^{-1}).

Fig. 2. Main effects plots for S/N ratios

3.2. ANOVA results

ANOVA table illustrates the influencing factors for the inulinase production by *Y. lipolytica* ISF7 (Table 4). The calculated F values indicated the significance of the factors for inulinase production. As a result of these values, the incubation time had the most significant effect, while the pH had less effects. In a previous study, incubation temperature had the significant effect on inulinase production while the incubation time had less effect (Tasar 2020).

Table 4. Analysis of variance for means.

Source	DF	Seq SS	Adj SS	Adj MS	F	P
pH	2	2965	2965	1483	0.24	0.806
Moisture	2	5525	5525	2763	0.45	0.690
Time	2	82070	82070	41035	6.67	0.130
Residual Error	2	12304	12304	6152		
Total	8	102864				

DF: Degree of freedom; Seq SS: Sequential sum of square; Adj SS: Adjusted sum of square; Adj MS: Adjusted mean of squares; F: F value; P: P value.

ANOVA analysis showed the ranking made on the basis of the amplitude of S/N ratio variation. Figure 2 showed the individual contribution of each factors on inulinase production. It is clear that incubation time had the maximum effect and the initial pH of the medium had the minimum effect on inulinase production. In a prior study, incubation temperature had the greatest impact and the incubation time was the second most effective factor on inulinase production (Tasar 2020).

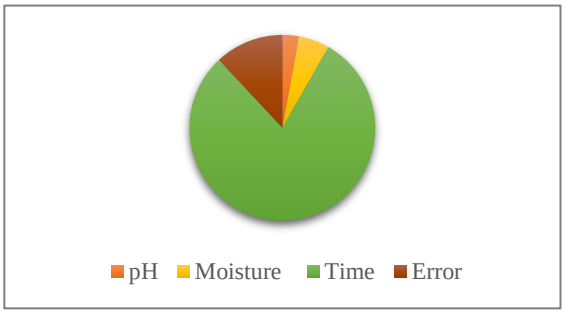

Fig. 3 Contribution of each factor (%)

4. Conclusion

Conclusion

In the current study, the waste onion peels, an important member of the domestic and agri-food industry derived wastes, were employed as an effective, economic and easily available substrate for inulinase production under SSF conditions. SSF commonly presents an economical fermentation for many valuable products like bread and cheese. Taguchi L_9 orthogonal array was utilized for optimization. The obtained results showed that, the environmental conditions have great impact on the fermentation progress. Onion peels can be indicated as a suitable substrate for enhanced inulinase production, besides, optimization of the fermentation is necessary and a powerful tool for effective enzyme production. The moisture content was found as the second effective factor after incubation time on inulinase production. This result is significant because the world stock of the clean water is decreasing day-by-day and there would be a water-crisis in the near future. The next studies can be performed using different agricultural wastes for bio-conversion process of different valuable products.

Acknowledgements

The author would like to thanks to the staff of YUTAM.

Authors' contributions: ÖCT: Methodology, investigation, conceptualization, writing, editing and supervision. GET: Data analysis, software, reading-editing and supervision.

Conflict of interest disclosure:

The author declares that she has no known competing financial interests or personal relationships that could have appeared to influence the work reported in this paper.

Ethics approval and consent to participate

This study does not contain any studies with human participants or animals performed by the author.

Funding

This research received no specific grant from any funding agency in the public, commercial, or not-profit sectors.

References

Abd-Elsalam HAH, Gamal M, Naguib IA, Al-Ghobashy MA, Zaazaa HE, Abdelkawy M. 2021. Development of green and efficient extraction methods of quercetin from red onion scales wastes using factorial design for method optimization: A comparative study. Separations. 8(9): 137. Retrieved from https://doi.org/10.3390/separations8090137

Ayyachamy M, Khelawan K, Pillay D, Permaul K, Singh S. 2007. Production of Inulinase by Xanthomonas campestris pv phaseoli Using Onion (*Allium cepa*) and Garlic (*Allium sativum*) Peels in Solid State Cultivation. Lett. Appl. Microbiol. 45: 439–444.

Benítez V, Mollá E, Martín-Cabrejas MA, Aguilera Y, López-Andréu FJ, Cools K, Esteban RM. 2011. Characterization of Industrial Onion Wastes (Allium cepa L.): Dietary Fibre and Bioactive Compounds. Plant Food Hum. Nutr. 66(1): 48–57. Retrieved from https://doi.org/10.1007/s11130-011-0212-x

Beopoulos A, Cescut J, Haddouche R, Uribelarrea JL, Molina-Jouve C, Nicaud JM. 2009. *Yarrowia lipolytica* as a model for bio-oil production. Prog Lipid Res. 48(6): 375–387. Retrieved from https://doi.org/10.1016/j.plipres.2009.08.005

Bhatnagar A, Sillanpää M, Anna WK. 2015. Agricultural waste peels as versatile biomass for water purification – A review. Chem Eng J. 270: 244–271.

Budžaki S, Velić N, Ostojčić M, Stjepanović M, Rajs BB, Šereš Z, Strelec I. 2022. Waste Management in the Agri-Food Industry: The Conversion of Eggshells, Spent Coffee Grounds, and Brown Onion Skins into Carriers for Lipase Immobilization. Foods, 11(3). Retrieved from https://doi.org/10.3390/foods11030409

Canli O, Tasar GE, Taskin M. 2013. Inulinase production by *Geotrichum candidum* OC-7 using migratory locusts as a new substrate and optimization process with Taguchi DOE. Toxicol Ind Health. 29(8): 704–710. Retrieved from https://doi.org/10.1177/0748233712442737

Conversion of environmentally-unfriendly onion waste into food ingredients. 1999. Retrieved 18 February 2022, from https://cordis.europa.eu/project/id/FAIR961184/results

Cui W, Wang Q, Zhang F, Zhang SC, Chi ZM, Madzak C. 2011. Direct conversion of inulin into single cell protein by the engineered *Yarrowia lipolytica* carrying inulinase gene. Process Biochem. 46(7): 1442–1448. Retrieved from https://doi.org/10.1016/j.procbio.2011.03.017

Desnos-Ollivier M, Letscher-Bru V, Neuvéglise C, Dromer F. 2020. *Yarrowia lipolytica* causes sporadic cases and local outbreaks of infections and colonisation. Mycoses. 63(7): 737–745. Retrieved from https://doi.org/10.1111/myc.13095

Erdal S, Canli O, Algur OF. 2011. Inulinase production by *Geotrichum candidum* using Jerusalem artichoke. Rom Biotechnol Lett. 16(4): 6375–6381.

Fraga JL, Souza CPL, Pereira A da S, Aguieiras ECG, de Silva, LO, Torres AG, Amaral PFF. 2021. Palm oil wastes as feedstock for lipase production by *Yarrowia lipolytica* and biocatalyst application/reuse. 3 Biotech. 11(4): 1–9. Retrieved from https://doi.org/10.1007/s13205-021-02748-1

Ge XY, Zhang WG. 2005. A shortcut to the production of high ethanol concentration from Jerusalem artichoke tubers. Food Technol Biotechnol. 43(3): 241–246.

Griffiths G, Trueman L, Crowther T, Thomas B, Smith B. 2002. Onions a global benefit to health. Phytother Res. 16: 603–615.

Groenewald M, Boekhout T, Neuvéglise C, Gaillardin C, Van Dijck PWM, Wyss M. 2014. *Yarrowia lipolytica*: Safety assessment of an oleaginous yeast with a great industrial potential. Crit Rev Microbiol. 40(3): 187–206. Retrieved from https://doi.org/10.3109/1040841X.2013.770386

Hsieh KL, Tong LI, Chiu HP, Hsin YY. 2005. Optimization of a multi-response problem in Taguchi's dynamic system. Comput Ind Eng. 49 (4): 556–571.

Hughes SR, Qureshi N, López-Núñez JC, Jones MA, Jarodsky JM, Galindo-Leva LÁ, Lindquist MR. 2017. Utilization of inulin-containing waste in industrial fermentations to produce biofuels and bio-based chemicals. World J Microbiol Biotechnol. 33(4): 1–15. Retrieved from https://doi.org/10.1007/s11274-017-2241-6

Jean MD, Tzeng YF. 2003. Use of Taguchi methods and multiple regression analysis for optimal process development of high energy electron beam case hardening of cast iron. Surf Eng. 19(2): 150–156. Retrieved from https://doi.org/10.1179/026708403225002496

Kandasamy S, Muthusamy G, Balakrishnan S, Duraisamy S, Thangasamy S, Seralathan KK, Chinnappan S. 2016. Optimization of protease production from surface-modified coffee pulp waste and corncobs using *Bacillus* sp. by SSF. 3 Biotech. 6(2): 1–11. Retrieved from https://doi.org/10.1007/s13205-016-0481-z

Kumar M, Barbhai MD, Hasan M, Punia S, Dhumal S, Radha Mekhemar M. 2022. Onion (*Allium cepa* L.) peels: A review on bioactive compounds and biomedical activities. Biomed Pharmacother. 146. Retrieved from https://doi.org/10.1016/j.biopha.2021.112498

Li I, Row KH. 2019. Preparation of deep eutectic solvent-based hexagonal boron nitride-molecularly imprinted polymer nanoparticles for solid phase extraction of flavonoids. Microchimica Acta, (186), 1–10.

Libardi N, Soccol CR, Góes-Neto A, Oliveira J, de Vandenberghe, LP, de S. 2017. Domestic wastewater as substrate for cellulase production by *Trichoderma harzianum*. Process Biochem. 57: 190–199. Retrieved from https://doi.org/10.1016/j.procbio.2017.03.006

Lin ZL, Huang XL. 2000. Current Microbiology and Experimental Technology. Beijing Science Press ISBN 7-03-008092-0.

Liu XY, Chi Z, Liu GL, Wang F, Madzak C, Chi ZM. 2010. Inulin hydrolysis and citric acid production from inulin using the surface-engineered *Yarrowia lipolytica* displaying inulinase. Metab Eng. 12(5): 469–476. Retrieved from https://doi.org/10.1016/j.ymben.2010.04.004

Madzak C. 2021. *Yarrowia lipolytica* strains and their biotechnological applications: How natural biodiversity and metabolic engineering could contribute to cell factories improvement. J Fungi. 7(7). Retrieved from https://doi.org/10.3390/jof7070548

Mughal MS, Ali S, Ashiq M, Talish AS. 2009. Kinetics of an Extracellular Exo-Inulinase Production From a 5-Flourocytosine Resistant Mutant of *Geotrichum candidum* Using Two-Factorial Design. Bioresour Technol. 100: 3657–3662.

Pathak PD, Mandavgane SA, Kulkarni BD. 2016. Characterizing fruit and vegetable peels as bioadsorbents. Current Sci. 110(11): 2114–2123.

Pessoni RAB, Figueiredo-Ribeiro RCL, Braga MR. 1999. Extracellular inulinases from *Penicillium janczewskii*, a fungus isolated from the rhizosphere of Vernonia herbacea (Asteraceae). J Appl Microbiol. 87(1): 141–147. Retrieved from https://doi.org/10.1046/j.1365-2672.1999.00805.x

Rawat HK, Soni H, Suryawanshi RK, Choukade R, Prajapati BP, Kango N. 2021. Exo-inulinase production from *Aspergillus fumigatus* NFCCI 2426: purification, characterization, and immobilization for continuous fructose production. J Food Sci. 86(5): 1778–1790. Retrieved from https://doi.org/10.1111/1750-3841.15681

Sangeetha PT, Ramesh MN, Prapulla SG. 2005. Recent trends in the microbial production, analysis and application of Fructooligosaccharides. Trends Food Sci Technol. 16(10): 442–457. Retrieved from https://doi.org/10.1016/j.tifs.2005.05.003

Selvakumar P, Pandey A. 1999. Solid state fermentation for the synthesis of inulinase from *Staphylococcus* sp. and *Kluyveromyces marxianus*. Process Biochem. 34(8): 851–855.

Selvam K, Selvankumar T, Rajiniganth R, Srinivasan P, Sudhakar C, Senthilkumar B, Govarthanan M. 2016. Enhanced production of amylase from *Bacillus* sp. using groundnut shell and cassava waste as a substrate under process optimization: Waste to wealth approach. Biocat Agri Biotechnol. 7: 250–256. Retrieved from https://doi.org/10.1016/j.bcab.2016.06.013

Sguarezi C, Longo C, Ceni G, Boni G, Silva MF, DiLuccio M, Treichel H. 2009. Inulinase production by agro-industrial residues: Optimization of pretreatment of substrates and production medium. Food Bioproc Technol. 2(4): 409–414. Retrieved from https://doi.org/10.1007/s11947-007-0042-x

Sharma A, Kuthiala T, Thakur K, Singh K, Gursharan T, Pawan S. 2022. Kitchen waste: sustainable bioconversion to value - added product and economic challenges. Biomass Convers Biorefin. (0123456789). Retrieved from https://doi.org/10.1007/s13399-022-02473-6

Sharma P, Verma A, Sidhu RK, Pandey OP. 2005. Process parameter selection for strontium ferrite sintered magnets using Taguchi L9 orthogonal design. J Mater Process Technol. 168(1): 147–151. Retrieved from https://doi.org/10.1016/j.jmatprotec.2004.12.003

Shi N, Mao W, He X, Chi Z, Chi Z, Liu G. 2018. Co-expression of Exo-inulinase and Endo-inulinase Genes in the Oleaginous Yeast *Yarrowia lipolytica* for Efficient Single Cell Oil Production from Inulin. Appl Biochem Biotechnol. 185(1): 334–346. Retrieved from https://doi.org/10.1007/s12010-017-2659-1

Silva MF, Freire DMG, De Castro AMH, Di Luccio M, Mazutti MA, Oliveira JV, De Oliveira D. 2011. Concentration, partial characterization, and immobilization of lipase extract from *P. brevicompactum* by solid-state fermentation of babassu cake and castor bean cake. Appl. Biochem. Biotechnol. 164(6): 755–766. Retrieved from https://doi.org/10.1007/s12010-011-9171-9

Singhania RR, Sukumaran RK, Patel AK, Larroche C, Pandey A. 2010. Advancement and comparative profiles in the production technologies using solid-state and submerged fermentation for microbial cellulases. Enzyme Microb Technol. 46: 541–549.

Soccol CR, Costa ESF, da Letti LAJ, Karp SG, Woiciechowski AL, Vandenberghe LP de S. 2017. Recent developments and innovations in solid state fermentation. Biotechnol Res Innov. 1(1): 52–71. Retrieved from https://doi.org/10.1016/j.biori.2017.01.002

Srinivasan P, Selvankumar T, Kamala-Kannan S, Mythili R, Sengottaiyan A, Govarthanan M, Selvam K. 2019. Production and purification of laccase by *Bacillus* sp. using millet husks and its pesticide degradation application. 3 Biotech. 9(11): 1–10. Retrieved from https://doi.org/10.1007/s13205-019-1900-8

Tasar OC. 2022. Glucose oxidase production using a medicinal plant: *Inula viscosa* and optimization with Taguchi DOE. J Food Process Preserv. 46:e16375. Retrieved from https://doi.org/10.1111/jfpp.16375

Tasar ÖC. 2020. Inulinase production capability of a promising medicinal plant: *Inula viscosa*. Commagene J Biol. 4: 67–73. Retrieved from https://doi.org/10.31594/commagene.747618

Tasar OC, Erdal S, Algur OF. 2015. Utilization of leek (Allium ampeloprasum var. porrum) for inulinase production. Prep Biochem Biotechnol. 45(6): 596–604. Retrieved from https://doi.org/10.1080/10826068.2014.940538

Van Loo J, Coussement P, De Leenheer L, Hoebregs H, Smits G. 1995. On the presence of inulin and oligofructose as natural ingredients in the western diet. Crit Rev Food Sci Nutr. 35 (6): 525-552.

Wang LF, Wang ZP, Liu XY, Chi ZM. 2013. Citric acid production from extract of Jerusalem artichoke tubers by the genetically engineered yeast *Yarrowia lipolytica* strain 30 and purification of citric acid. Bioprocess Biosyst Eng. 36(11): 1759–1766. Retrieved from https://doi.org/10.1007/s00449-013-0951-1

Yazici SO, Sahin S, Biyik HH, Geroglu Y, Ozmen I. 2020. Optimization of fermentation parameters for high-activity inulinase production and purification from *Rhizopus oryzae* by Plackett–Burman and Box–Behnken. J Food Sci Technol. 58 (2): 739-751. Retrieved from https://doi.org/10.1007/s13197-020-04591-3

Zhao CH, Cui W, Liu XY, Chi ZM, Madzak C. 2010. Expression of inulinase gene in the oleaginous yeast *Yarrowia lipolytica* and single cell oil production from inulin-containing materials. Metab Eng. 12(6): 510–517. Retrieved from https://doi.org/10.1016/j.ymben.2010.09.001

Zhivkova V. 2021. Determination of Nutritional and Mineral Composition of Wasted Peels from Garlic, Onion and Potato. Carpathian J Food Sci Technol. 134–146. Retrieved from https://doi.org/10.34302/crpjfst/2021.13.3.11

RESEARCH ARTICLE
Eurasian J Bio Chem Sci, 5(Suppl 1):151-156, 2022
https://doi.org/10.46239/ ejbcs.1033670

Eurasian Journal of Biological and Chemical Sciences

Journal homepage: www.dergipark.org.tr/ejbcs

Azol fonksiyonel gözenekli ve içi boş silika nanokompozitlerin karakterizasyonu ve antifungal uygulamaları

Sedef Kaptan Usul[1*], Ayşe Aslan[1], Didem Özçimen[2]

[*1]*Gebze Teknik Üniversitesi, Mühendislik Fakültesi, Biyomühendislik Bölümü, Kocaeli, Türkiye*
[2]*Yıldız Teknik Üniversitesi, Kimya Metalurji Fakültesi, Biyomühendislik Bölümü, İstanbul, Türkiye*

*Corresponding author : sedefkaptan@gtu.edu.tr
Orcid No: https://orcid.org/0000-0002-8178-9343

Received : 07/12/2021
Accepted: 03/10/2022

Özet: Bu çalışmada çok gözenekli (MSN) ve tek gözenekli (HSS) silika nanopartiküllerin yüzeyinde, viniltriazol (VTri) monomerinin polimerizasyon reaksiyonu ile amin grupları oluşturulmuştur. Hazırlanan nanokompozit yapıların karakterizasyonu ve antifungal özelliği incelenmiştir. Nanokompozitlerin karakterizasyonunda MSN ve HSS' nın viniltriazol ile etkileşimini, yüzeydeki azol gruplarının varlığını belirlemek için FTIR ve XRD analizi, termal özelliklerini incelemek için TGA analizi yapılmıştır. Nanokompozitlerin morfolojisini belirlemek için SEM analizi yapılmıştır. Nanokompozit yapıların antifungal özellikleri MİK yöntemi ile kanıtlanmıştır.

Anahtar Kelimeler: Gözenekli silika, tek gözenekli silika, viniltriazol

Characterization and antifungal applications of azole functional mesoporous and hollow silica nanocomposites

Abstract: In this study, mesoporous (MSN) and hollow (HSS) silica nanoparticles were interacted with vinyltriazole to increase the number of amine groups on the surface. The characterization and antibacterial properties of the prepared nanocomposite structures were investigated. In the characterization of nanocomposites, FTIR and XRD analysis was used to determine the interaction of MSN and HSS with vinyltriazole, the presence of azole groups on the surface, and TGA analysis to examine their thermal properties. SEM analysis was performed to determine the morphology of nanocomposites. The antifungal properties of nanocomposite structures have been proven by the MIC method.

Keywords: Mesoporous silica, hollow silica, vinyltriazole

1. Giriş

Çeşitli inorganik nanopartiküller arasında silika partikülleri, mükemmel kimyasal özellikleri nedeniyle büyük ilgi görmektedir. Kararlılıkları, inert yapıları, termal kararlılıkları, düşük yoğunlukları, düşük toksisiteleri ve biyouyumlulukları sayesinde silika nanopartiküller, diğer malzemelerle iyi uyumluluk gösterir ve ayrıca diğer aktif malzemeleri kimyasal olarak bağlamak için kolayca işlevsel eştirilebilmektedir. Gözenekli silika nanopartiküllerin (MSN) geniş yüzey alanları, kararlılıkları ve biyouyumlulukları nedeniyle bu nanopartiküller biyomedikal alanda, eczacılıkta ve biyokimya uygulamalarında kullanılmaktadır. Ayrıca MSN' lerin yapısındaki siloksan bağları (Si-O-Si) sayesinde mekanik olarak kararlı ve mikrobiyal saldırılara karşı dirençlidirler. MSN' lerin sentezi uygun ve az maliyetlidir. Silika metabolik olarak parçalandığında silisik asidin yan ürünlerine ayrılmaktadır. Silisik asit, canlı sistemlerde toksisite azaltma, hastalıklara karşı direnç gibi biyo-uyarıcı görevi görmektedir (Ribes ve ark. 2017; Sattary ve ark. 2020).

İstenilen partikül boyutuna, şekline, gözenekliliğine ve kristalliğine sahip silika nanopartiküller, uygun şekilde tasarlanarak üretilebilmektedir. Sol-jel işlemi ve kalıp destekli sentez, tek gözenekli silikaların (HSS) üretimi için genel olarak kabul edilen yöntemlerdir. Nanopartiküllerin formu, değişen pH veya sıcaklıklar ile değiştirilebilmektedir. Monodisperse fenil grupları içeren HSS' ler, organik çözücülerde çözünüp herhangi bir yapı kullanılmadan üretilmektedir (Derbalah ve ark. 2018; Aslan ve ark. 2019).

Tüm antifungal azollerin (imidazoller, triazoller ve tiyazoller) ana etki mekanizması, sitokrom P450 enzimi olan 14-alfa-demetilazın inhibisyonudur. İnhibisyon, azol grubunun serbest nitrojen atomunun enzimin aktif bölgesindeki hem'in prostetik grubunun demirine

bağlanması nedeniyle oluşmaktadır. Azol içerikli bu yapıların eşsiz özellikleri biyomedikal uygulamalar, kimya ve gıda endüstrisinde kullanımına olanak sağlamaktadır. (Ermakova ve ark. 2012; Stingaci ve ark. 2020). 1-Vinil-1,2,4-triazol (V) en ilginç monomerdir, Antifungal etkisinin yanı sıra termal stabilite ve agresif ortamlara direnç, kompleks oluşturma ve kuaternizasyon yeteneği, biyouyumluluk ve polimerinin kontrol edilebilir molekül ağırlığı gibi bir dizi değerli özelliğe sahiptir (Durmus ve ark. 2011; Pozdnyakov ve ark. 2020).

2. Materyal ve Metot

2.1. Malzemeler

1-vinil-1,2,4-triazol (>97%), Toluen (>99%), Trimethoxymethylsilane (PTMS, %95), Tetraethyl orthosilicate (TEOS, %98), Dimethyl sulfoxide (DMSO, >99), Hexadecyltrimethylammonium bromide (CTAB), (EDMAB), Kamforkinon (Cq) Sigma Aldrich' ten satın alınmıştır.

2.2. Gözenekli silika nanopartiküllerinin sentezi ve modifikasyonu

MSN' ler TEOS ve katyonik yüzey aktif madde CTAB' nin sol-jel reaksiyonu ile sentezlenmiştir. CTAB (0,15 g) ve NH_4F (0,4 g) 100 mL distile suda çözülerek 75◦C ve 1500 rpm'de karıştırıldıktan sonra çözelti şeffaf hale gelince çözeltiye damla damla 2 mL TEOS eklenmiştir. Süt beyazı çökeltiyi ayırmak için santrifüj yapılmıştır. Çökelti 2.5 mL HC1 (%35) ile 150 mL EtOH içinde dağıtılarak 24 saat 75◦C' de bekletilmiştir. Bu prosedür, yüzey aktif maddenin tamamen uzaklaştırılmasını sağlamak için iki kez tekrarlanmıştır (Hachemaoui ve ark. 2020; Son ve Lee 2021).

MSN ve 1-vinil-1,2,4-triazol toluen içinde çözülerek foto polimerizasyonu ile nanokompozit oluşturulmuştur. Başlatıcı olarak Cq (%1 mol) kullanılarak, azot atmosferinde ve sıcaklık 80°C' de 2 saat boyunca reaksiyon bekletilmiştir. MSN-poli(1-vinil-1,2,4-triazol) (MSN-PVTri) nanokompoziti THF ile çöktürüldükten sonra birkaç kez toluen karışımı ile yıkanmıştır. Daha sonra elde edilen nanokompozitler 70 °C vakum altında kurutulmuştur (Çelik ve ark. 2008; Durmus ve ark. 2011).

2.3. Tek gözenekli silika nanopartiküllerinin sentezi ve modifikasyonu

Sol-jel yöntemi silika ve diğer metal oksit partikülleri hazırlamak için kullanılan en yaygın yöntemdir. Bu çalışmada, iki aşamalı sol-jel yöntemiyle tek gözenekli silika partikülleri hazırlanmıştır. Feniltrimetoksisilanın (PTMS) hidrolizi asidik koşullar altında gerçekleştirilmiştir. Hidroliz süresi, içi boş parçacıkların oluşumunda önemli bir rol oynamaktadır. $0.66*10^{-2}$ M HNO_3 sulu çözeltisi 60°C' de su banyosuna yerleştirilmiştir. Çözeltiye PTMS (0.06 M) eklenerek karışım çözeltisi 5 dakika 260 rpm hızında karıştırılmıştır. İkinci aşamada, yoğunlaştırma için elde edilen homojen çözeltiye NH_4OH çözeltisi (1.44 M) ilave edilmiştir. Süt fomuna dönen şeffaf reaksiyon 1 saat boyunca sürekli olarak karıştırılmıştır. Nihai partiküller, santrifüj işlemi ile toplanarak birkaç kez su ve etanol ile yıkanmıştır (Aslan ve ark. 2015; Aslan ve ark. 2019).

HSS ve 1-vinil-1,2,4-triazol toluen içinde çözülerek foto polimerizasyonu ile nanokompozit oluşturulmuştur. Başlatıcı olarak Cq (%1 mol) kullanılarak, azot atmosferinde ve sıcaklık 80°C' de 2 saat boyunca reaksiyon bekletilmiştir. HSS-poli(1-vinil-1,2,4-triazol) (HSS-PVTri) nanokompoziti THF ile çöktürüldükten sonra birkaç kez toluen karışımı ile yıkanmıştır. Daha sonra elde edilen nanokompozitler 70 °C vakum altında kurutulmuştur (Çelik ve ark. 2008; Durmus ve ark. 2011).

2.4. Hazırlanan nanokompozitlerin karakterizasyonu

MSN ve HSS' ların sentezi ile 1-vinil-1,2,4-triazol' ün yüzeyde polimerizasyonu başarılı bir şekilde gerçekleştirilmesini araştırmak için kızılötesi spektroskopi (FTIR) ve X-ışını kırınımı yöntemi (XRD) kullanılmıştır. İlgili fonksiyonel grup absorpsiyonuna dayalı olarak 4000-400 cm^{-1} aralığında MSN ve HSS' lar ile MSN-PVTri ve HSS-PVTri' ler için kaydedilen FTIR spektrumları karşılaştırılarak değerlendirilmiştir. MSN ile MSN-PVTri, HSS ile HSS-PVTri partiküllerinin gözenekli yapıları ve modifikasyonu taramalı elektron mikroskobu (SEM) kullanılmıştır. MSN-PVTri ve HSS-PVTri' nin modifikasyonunu değerlendirmek ve miktarını tahmin etmek için termogravimetrik analiz (TGA) kullanılmıştır. Termogramlar, atmosfer koşullarında 10 °C/dakika ısıtma hızında oda sıcaklığından 800 °C' ye kadar alınmıştır.

2.5. Minimum inhibitör konsantrasyonu (MİK)

Sentezlenen kompozitlerin antifungal aktivitesini değerlendirmek için minimum inhibisyon konsantrasyonu (MİK) yöntemi kullanılmıştır. MİK değerleri, seyreltme yöntemi kullanarak belirlenmiştir. *Saccharomyces cerevisiae (S. Cerevisiae-YPH499 suşu)* bir gün boyunca 28°C' de bir çalkalıyıcı inkübatörde 150 rpm' de 24 saat YPD besiyeri içerisinde kültürlenmiştir. Test suşu nihai yoğunluk $1*10^6$ CFU/mL olacak şekilde YPD besi yerinde süspanse edilerek seyreltilmiştir. DMSO içerisinde çözünen nanokompozitler 24 kuyucuklu plakada belirlenen miktarlarda hazırlanmıştır. Çalışmada 1, 5, 10, 25 ve 50 mg/mL farklı konsantrasyonlarda nanokompozit materyal ile MİK deneyi yapılmıştır. Daha sonra plakaya her kuyucuğa *S. Cerevisiae* süspansiyonu ilave edilerek, plakalar 28°C' de 48 saat çalkalıyıcı inkübatörde inkübasyona bırakılmıştır. Her bir konsantrasyon için üç kopya halinde örnekler hazırlanarak deney üç kez tekrarlanmıştır. Görünür *S. Cerevisiae* büyümesi olamayan en düşük nanokompozit konsantrasyonu MİK olarak kabul edilmiştir (Song ve ark. 2019; Hachemaoui ve ark. 2020; Zhang ve ark. 2021).

3. Bulgular ve Tartışma

3.1. FTIR Analizi

Numunelerin yüzey polimerizasyonu FTIR spektroskopisi kullanılarak analiz edilmiştir. MSN ve MSN-PVTri nanoparçacıklarının kızılötesi spektrumları Şekil 1' de gösterilmektedir. 1064 cm^{-1} ve 800 $cm^{-1'}$ de Si–O–Si bağlarının asimetrik ve simetrik germe titreşimlerini açıkça göstermektedir. 977 cm^{-1} ve 3300 $cm^{-1'}$ deki pikler, sırasıyla Si–OH ve O–H gruplarının germe titreşimlerine atanmaktadır. 2900 cm^{-1} ve 3300 $cm^{-1'}$ deki pikler,

muhtemelen asitle aşındırma işlemiyle çıkarılmayan artık CTAB nedeniyle sırasıyla C–H ve OH bağlarının germe titreşimlerinden kaynaklanmaktadır. Yüzeye viniltriazolün polimerizasyonu ile triazol halkaları, halka gerilmesi (C–N, C=N) titreşimleri nedeniyle 1430–1650 cm^{-1} aralığında birkaç orta güçlü tepe noktası oluşturmaktadır. 1270 $cm^{-1'}$ deki tepe noktası, N–N halkasının gerilmesinden kaynaklanmaktadır. 3430 $cm^{-1'}$ de merkezlenen geniş tepe, bozulmamış PVTri ile etkileşime giren moleküler suyun O-H titreşimine atanmıştır.

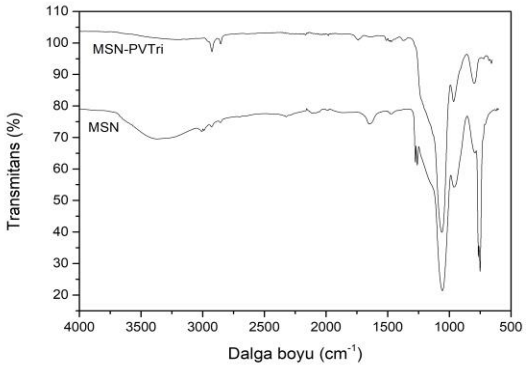

Şekil 1. MSN nanopartikülü ve MSN-PVTri nanokompozitinin FTIR grafiği

HSS ve HSS-PVTri nanoparçacıklarının kızılötesi spektrumları Şekil 2' de gösterilmektedir. HSS spektrumları, Si–O–Si asimetrik gerilmeye ait 1092 $cm^{-1'}$ de güçlü bir absorpsiyon zirvesi göstermektedir. 782 ve 493 $cm^{-1'}$ deki tepe noktaları Si–O'nun simetrik gerilme titreşimine atanabilir ve 936 $cm^{-1'}$ deki tepe noktası Si–OH'nin eğilme titreşiminden kaynaklanabilmektedir. Yaklaşık 3600 $cm^{-1'}$ de zayıf bir ayırt edici Si-OH germe titreşimi gösterilmiştir. 3100 $cm^{-1'}$ deki tepe noktası, HSS'ye bağlı aromatik fenilin C-H gruplarının asimetrik gerilme titreşimine bağlanmaktadır. Bu sonuçlar, HSS oluşturmak için PTMS' nin yoğunlaşma ürününü göstermiştir. Yüzeyde viniltriazolün polimerizasyonu ile triazol halkaları, halka gerilmesi (C–N, C=N) titreşimleri nedeniyle 1430–1650 cm^{-1} aralığında birkaç orta güçlü tepe noktası oluşturmaktadır. 1270 $cm^{-1'}$ deki tepe noktası, N–N halkasının gerilmesinden kaynaklanmaktadır. 3430 $cm^{-1'}$ de merkezlenen geniş tepe, bozulmamış PVtri ile etkileşime giren moleküler suyun O-H titreşimine atanmıştır.

3.2. SEM Analizi

MSN ve MSN-PVTri yüzey morfolojileri SEM ile incelenmiş olunup Şekil 3' te görülmektedir. MSN yüzeyindeki aşılama sonucu oluşan yapıdaki değişiklik Şekil 3' de açıkça görülmektedir. Burada, doğal ve polimer modifiye partiküller karşılaştırılırken belirgin bir fark görülmektedir. Bazı düzensiz şekilli parçacıkların oluşumunda görüldüğü gibi, büyüme de meydana gelmesine rağmen, polimerin parçacık yüzeyini kapladığı açıkça görülmektedir.

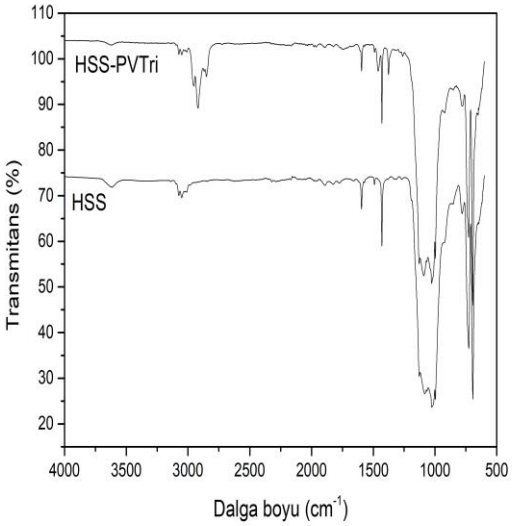

Şekil 2. HSS nanopartikülü ve HSS-PVTri nanokompozitinin FTIR grafiği

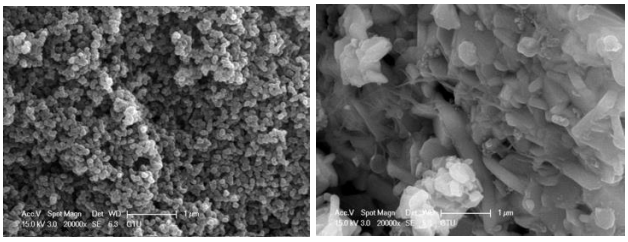

Şekil 3. MSN ve MSN-PVTri SEM görüntüleri

HSS ve HSS-PVTri yüzey morfolojileri SEM ile incelenmiş olunup Şekil 4' te görülmektedir. HSS gözeneklerindeki aşılamanın gerçekleştiği ve gözeneklilik miktarının arttığı Şekil 4' de açıkça görülmektedir.

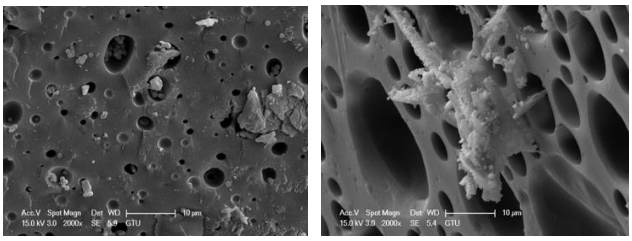

Şekil 4. HSS ve HSS-PVTri SEM görüntüleri

3.3. XRD Analizi

MSN ile MSN-PVTri, HSS ile HSS-PVTri ürünlerinin faz araştırması XRD ile yapılmıştır ve kırınım modeli Şekil 5 ve 6'da sunulmuştur. MSN nanopartikülü 2θ civarında 22°'de görünen bir tepe noktasına sahiptir, amorf formda olduğunu açıkça görülmektedir. Yüzeyin modifikasyonu ile 22°'de yoğunluğun azalması modifikasyonun gerçekleştiğini kanıtlamaktadır.

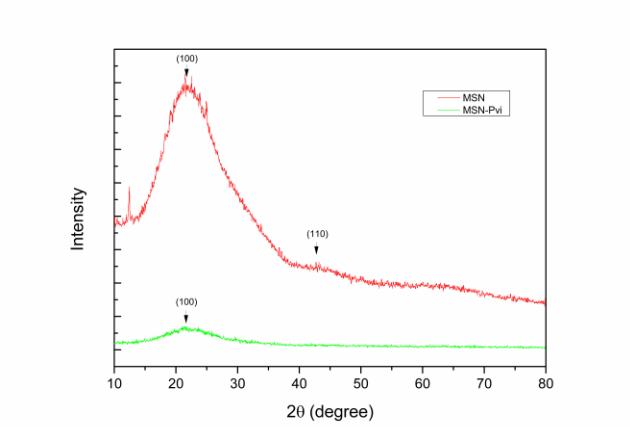

Şekil 5. MSN nanopartikülü ve MSN-PVTri nanokompozitinin XRD grafiği

HSS nanopartikülü 2θ civarında 20°'de görünen bir tepe noktasına sahiptir, amorf formda olduğunu açıkça görülmektedir. Yüzeyin modifikasyonu ile 20°'de yoğunluğun azalması modifikasyonun gerçekleştiğini kanıtlamaktadır.

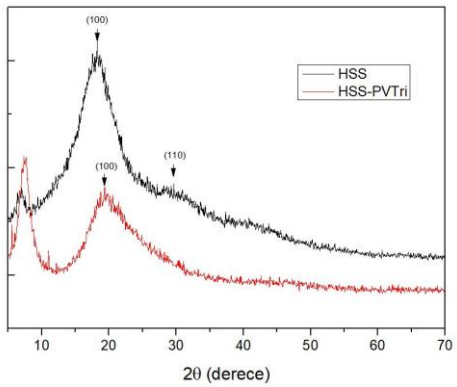

Şekil 6. HSS nanopartikülü ve HSS-PVTri nanokompozitinin XRD grafiği

3.4. TGA Analizi

TGA' nın sıcaklığa karşı ağırlık kaybı grafikleri, nanoparçacıklardan büyütülen polimer miktarının bir tahminini sağlamaktadır. Kaplanmış parçacıklar, hem kalıntıda (polimere bağlı silika) kalan termal olarak kararlı bileşiklerden hem de ağırlık kaybına katkıda bulunan ayrışabilir polimer yapılardan ve başlatıcılardan oluşmaktadır. PVTri polimerinin termal kararlığı 300-350ºC' dir (Sinirlioglu ve ark. 2013). MSN nanopartikülünün yüzeyinde viniltriazol monomerinin büyütülmesinden sonra oluşan MSN-PVTri nanokompozitinin, termal kararlılığının artarak 400 ºC' ye ulaştığı Şekil 7' de görülmektedir. HSS nanopartikülünün yüzeyinde viniltriazol polimerizasyonundan sonra, TGA, %40' lık bir toplam ağırlık kaybı Şekil 8' de görülmektedir.

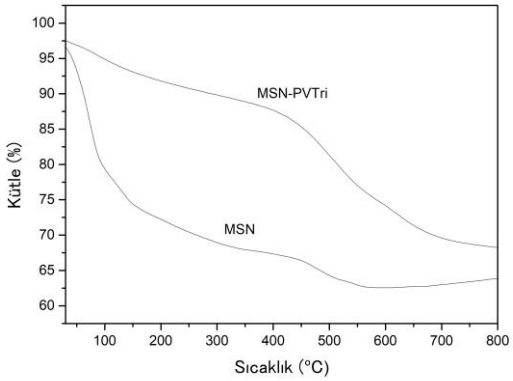

Şekil 7. MSN nanopartikülü ve MSN-PVTri nanokompozitinin TGA grafiği

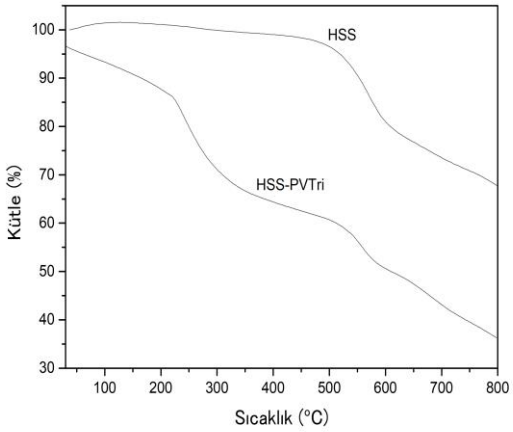

Şekil 8. HSS nanopartikülü ve HSS-PVTri nanokompozitinin TGA grafiği

3.5. Minimum İnhibitör Konsantrasyonu (MİK)

Çalışmada yüzeyleri viniltriazol ile modifiye edilen nanokompozitlerin antifungal özellikleri MİK deneyi ile test edilmiştir. MİK sonuçlarına göre MSN-PVTri MİK değeri 0-1 mg/mL iken HSS-PVTri >8 mg/mL olarak tespit edilmiştir. Buna göre MSN nanopartikülünün HSS' ya göre daha geniş yüzey alanına sahip olması yüzeye daha fazla viniltriazol monomerinin bağlanması sağlamıştır. Şekil 9'da yapılan MİK deneyinin görseli yer almaktadır. Pozitif kontrolde ve HSS-PVTri nanokompozitinin bulunduğu kuyucuklarda *S. Cerevisiae* büyümesi gerçekleşirken, negatif kontrol ve MSN-PVTri nanokompozitinin bulunduğu kuyucuklarda *S. Cerevisiae* büyümesi olmamıştır.

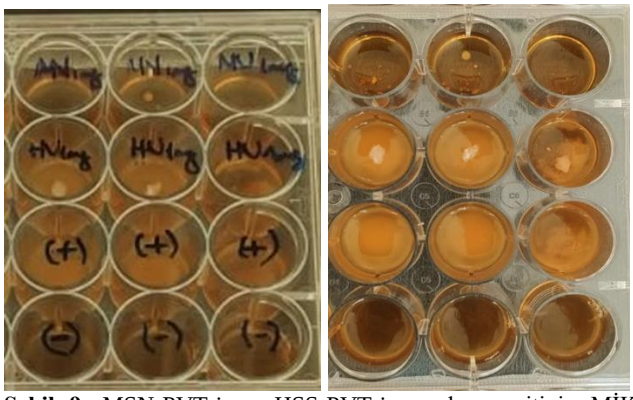

Şekil 9. MSN-PVTri ve HSS-PVTri nanokompozitinin MİK deneyi görseli

Polimerler etkili bir şekilde nanopartikülleri stabilize edebilir, böylece nanokompozitin agregasyonunu önler, suda çözünürlüğü arttırır ve biyolojik aktiviteyi arttırmaktadır (He ve ark. 2021; Prozorova ve ark. 2022; Tsivileva ve ark. 2021). Literatürde yapılan çalışmalar incelendiğinde, vinil triazol monomeri manyetik nanopartiküller ile modifiye edilerek nanokompozitler sentezlenmiştir. Zezin ve ark. (2021) tarafından tasarlanan nanokompozit yüksek antibakteriyel özellik gösterdiği görülmüştür. Zharikov ve ark. (2022) altın nanopartiküller ve vinil triazol ile hazırladıkları nanokompozitler yüksek stabilite ve etkili antibakteriyel özelliklerini göstermiştir. Bizim çalışmamızda farklı olarak manyetik olmayan silika bazlı nanopartiküller kullanılmıştır. Çalışmamızda farklı yöntemler ile üretilen silika nanopartiküller kullanılıp karşılaştırıldığından özgündür.

4. Sonuç

Bu çalışmada sentezlenen MSN-PVTri ve HSS-PVTri nanokompozitlerinin karakterizasyonu ve antifungal etkisi incelenmiştir.

- Nanokompozitlerin modifikasyonu FTIR ve SEM analizi ile kanıtlanmıştır.
- Modifikasyon sonrası MSN-PVTri nanokompozitinin termal kararlığı artan, HSS-PVTri nanokompozitinin azalmıştır.
- XRD analizi sonucunda amorf yapıdaki nanopartikül modifikasyon sonrası zirve değerinde iki nanokompozitte de azalmıştır.
- MSN-PVTri' nin antifungal aktivite gösterdiğini, HSS-PVTri' nin artan konsantrasyon miktarlarına rağmen antifungal aktivite göstermediği MİK deney sonuçlarında görülmüştür.

MSN-PVTri nanokompoziti, HSS-PVTri nanokompozitine göre yüzey gözenekliliğinin ve bağ yapacak gruplarının fazla olması sebebiyle viniltriazol ile etkileşimi daha çok olmuştur. Antifungal özellik gösteren viniltriazol monomerinin MSN-PVTri nanokompozitinde daha fazla bulunması sebebiyle etkili bir antifungal aktivite göstermiştir. MSN-PVTri nanokompozitinin, eşsiz kimyasal, fiziksel ve antifungal özellikleri, antimikrobiyal endüstriyel uygulamalarda kullanılma potansiyeli sunmaktadır.

References

Aslan A, Elanthikkal S, Bozkurt A. 2019. Chitosan/hollow silica sphere nanocomposites for wound healing application. J Mater Res. 34(2):231-239.

Aslan A, Soydan AM, Bozkurt A. 2015. Synthesis and characterization of novel multifunctional polymer grafted hollow silica spheres. J Mater Res. 30(16):2408-2416.

Çelik SÜ, Aslan A, Bozkurt A. 2008. Phosphoric acid-doped poly (1-vinyl-1, 2, 4-triazole) as water-free proton conducting polymer electrolytes. Solid State Ionics. 179(19-20):683-688.

Derbalah A, Shenashen M, Hamza A, Mohamed A, El Safty S. 2018. Antifungal activity of fabricated mesoporous silica nanoparticles against early blight of tomato. Egypt J Appl Sci. 5(2):145-150.

Durmus Z, Unal B, Toprak MS, Aslan A, Baykal A. 2011. Synthesis and characterization of poly (1-vinyl-1, 2, 4-triazole) (PVTri)–barium hexaferrite nanocomposite. Physica B. 406(11):2298-2302.

Ermakova TG, Shaulina LP, Kuznetsova NP, Volkova LI, Pozdnyakov AS, Prozorova GF. 2012. Sorption of noble metal compounds by cross-linked copolymer of 1-vinyl-1, 2, 4-triazole with acrylic acid. Russ J App Chem+. 85(1):35-40.

Hachemaoui M, Boukoussa B, Mokhtar A, Mekki A, Beldjilali M, Benaissa M, Hamacha R. 2020. Dyes adsorption, antifungal and antibacterial properties of metal loaded mesoporous silica: Effect of metal and calcination treatment. Mater Chem Phys. 256:123704.

He, Q, Zhang, D, Zhang, F, Liu, X, Feng, X. 2021. Asymmetric Catalytic Epoxidation of Terminal Enones fort he Synthesis of Triazole Antifungal Agents. Org Lett.23:6961-6966.

Prozorova, GF, Pozdnyakov, AS. 2022. Synthesis, Properties, and Biological Activity of Poly(1-vinyl-1,2,4-triazole) and Silver Nanocomposites Based on It. Polymer Sci C. 1-11.

Pozdnyakov AS, Ivanova AA, Emel'yanov AI, Bolgova YI, Trofimova OM, Prozorova GF. 2020. Water-soluble stable polymer nanocomposites with AuNPs based on the functional poly (1-vinyl-1, 2, 4-triazole-co-N-vinylpyrrolidone). J Organomet Chem. 922:121352.

Pozdnyakov, A, Emel'yanov, A, Ivanova, A, Kuznetsova, N, Semenova, T, Bolgova, Y, Korzhova, S, Trofimova, O, Fadeeva, T, Prozorova, G. 2022. Strong Antimicrobial Activity of Highly Stable Nanocomposites Containing AgNPs Based on Water-Soluble Triazole-Sulfonate Copolymer. Pharmaceutics 14:206.

Ribes S, Ruiz-Rico M, Pérez-Esteve É, Fuentes A, Talens P, Martínez-Máñez R, Barat JM. 2017. Eugenol and thymol immobilised on mesoporous silica-based material as an innovative antifungal system: Application in strawberry jam. Food Control. 81:181-188.

Sattary M, Amini J, Hallaj R. 2020. Antifungal activity of the lemongrass and clove oil encapsulated in mesoporous silica nanoparticles against wheat's take-all disease. Pestic Biochem Phys. 170:104696.

Sinirlioglu D, Muftuoglu AE, Bozkurt A. 2013. 5-(methacrylamido) tetrazole and vinyl triazole based copolymers as novel anhydrous proton conducting membranes. J Polym Res. 20(9):1-10.

Son MJ, Lee SW. 2021. Antibacterial toxicity of mesoporous silica nanoparticles with functional decoration of specific organic moieties. Colloid Surface A. 30:127612.

Song Y, Zhu P, Wu Y, Tan L, Wei W, Liu S, Chen J. 2019. Epsilon-poly-l-lysine decorated ordered mesoporous silica contributes to the synergistic antifungal effect and enhanced solubility of a lipophilic drug. Mater Sci Eng. 99:231-240.

Stingaci E, Zveaghinteva M, Pogrebnoi S, Lupascu L, Valica V, Uncu L, Macaev F. 2020. New vinyl-1, 2, 4-triazole derivatives as antimicrobial agents: Synthesis, biological evaluation and molecular docking studies. Bioorgan Med Chem Lett. 30(17):127368.

Tsivileva, O, Perfileva, AI, Ivanova, AA, Pozdnyakov, A, Prpzprova, GF. 2021. The Effect of Selenium-or Metal-Nanoparticles Incorporated Nanocomposites of Vinyl Triazole Based Polymers on Fungal Growth and Bactericidial Properties. J Polm Env. 29:1287-1297.

Zezin, A, Danelyan, G, Emel'yanov, A, Zharikov, A, Prozorova, G, Zezina, E, Korzhova, S, Fadeeva, T, Abramchuk, S, Shmakova, N, Pozdnyakov, A. 2021. Synthesis of antibacterial polymer metal hybrids in irradiated poly-1-vinyl-1,2,4-triazole complexes with silver ions: pH tuning of nanoparticle sizes. Appl Organomet Chem. 36(4):e6581.

Zhang R, Cui Y, Cheng M, Guo Y, Wang X, Wang J. 2021. Antifungal activity and mechanism of cinnamon essential oil loaded into mesoporous silica nanoparticles. Ind Crop Prod. 171:113846.

Zharikov, AA, Vinogradov, RA, Zezina, EA, Pozdnyakov, AS, Feldman, VI, Vasiliev, AL, Zezin, AA. 2022. The radiation-induced preparation of ultrasmall gold nanoparticles in Au(III) complexes with units of poly(1-vinyl-1,2,4-triazole) and poly(1-vinyl-1,2,4-triazole) – poly(acrylic acid). Colloid Inter Sci Com. 47:100602.

RESEARCH ARTICLE
Eurasian J Bio Chem Sci, 5(Suppl 1):157-161, 2022
https://doi.org/10.46239/ejbcs.1104606

EJBCS

Eurasian Journal of Biological and Chemical Sciences

Journal homepage: www.dergipark.org.tr/ejbcs

Multiresidue chromatographic method for the determination of antibiotic residues in honey by high-performance liquid chromatography with DAD detection

Bouchra Rachid, Ali Jaber*, Edmond Cheble

Laboratoire de Recherche et Développement des Médicaments et des Produits Naturels RDMPN, Faculty of Pharmacy, Lebanese University, Beirut, Lebanon.

*Corresponding author : ali.jaber.2@ul.edu.lb
Orcid No: https://orcid.org/0000-0001-9911-9025

Received : 17/04/2022
Accepted : 23/10/2022

Abstract: Clandestinely, consumers may be exposed to antibiotic (ATB) residues in honey, which could pose a health concern. For the first time, the simultaneous determination of Florfenicol (FF), Penicillin G (PG), and Tetracycline is described in this paper. The multiresidual method was developed and optimized using high-performance liquid chromatography (HPLC) coupled to a diode array detector (DAD). These ATBs were separated on a C18 analytical column after a cleanup process followed by solid-phase extraction (SPE). For the first time, the chromatographic conditions were perfected. After the method validation process, the method was used to assess ATB residues in four Lebanese honey samples. ATBs were separated in less than 15 min with an isocratic elution using a mixture of 80 % potassium dihydrogen phosphate aqueous solution, 20 % acetonitrile. The UV detection was performed at 350 nm for TC, 224 nm for FF, and 230 nm for PG. The proposed method was linear ($R^2 \geq 0.996$) within the concentration ranges of 0.7-17.5 mg.Kg^{-1} for the three compounds. Both intra- and inter-day precision, expressed as RSD, were ≤15 %. The method was subsequently successfully applied to analyze examined ATB residues in honey samples collected from Lebanese beekeeping. The method described could be a valuable tool to conduct a comprehensive survey of honey samples produced in Lebanon, especially in the lack of serious national oversight.

Keywords: Multiresidue, Antibiotics, HPLC-DAD, Honey, SPE.

1. Introduction

Honey is a natural sweet food, produced by *Apis mellifera* bees from the nectar of flowers or secretions from living parts of plants, and insect-secreted products (Majewska et al. 2019). Among few countries over the world, in Lebanon bees feed on natural sources of nectar all year round, providing for a vast range of honey varieties (Lana and Marwan 2016). Figures from the Lebanese Ministry of Agriculture indicate that there are 6.340 beekeepers in Lebanon own approximately 274.390 beehives (Lana and Marwan 2016).

Honey sold as such must not contain any food ingredient, including food additives, or any other substance that is not part of honey. Bees are sensitive to microorganisms and the main bee diseases are American foulbrood, European foulbrood, and Varroosis (Vidal-Naquet 2012). The treatment of bees requires the use of antibiotics, for this the risk of the presence of residues in the honey is not negligible (Johnson and Jadon 2010).

Residues of antibiotics, such as tetracycline (TC), florfenicol (FF), and penicillin G (PG), in foods of animal origin such as honey, as well as their presence in the environment are of increasing interest because low levels of antibiotics can promote proliferation of bacterial resistance to antibiotics (Serwecińska 2020). In honey, their presence causes adverse effects on humans such as allergic reactions, toxic effects, and damage to the central nervous system. In terms of food and human safety, antibiotics are not authorized for the treatment of bees in the European Union (EU) (Lima et al. 2020; Bonerba et al. 2021) as well as in Lebanon, thus no MRLs established for antibiotics in honey (Forsgren 2010). However, in the absence of monitoring in this sector, there is a reasonable possibility to find contaminated honey in the Lebanese markets.

Some countries have established maximum residue limits (MRL) for TCs in honey, for example, 10 µg/kg in Russia and 50 µg/kg in Britain. In contrast, neither Codex Alimentarius nor the European Union (EU) has developed MRLs for veterinary medications in honey, and the use of antimicrobials in beekeeping is illegal in EU member countries (Commıssıon Regulatıon 37/2010 of 22 December, 2009) (European Commission 2010).

The control of antibiotic residues in foodstuffs of animal origin is carried out in two stages the search for an antibiotic effect by a screening method (microbiological, immunological, or physicochemical) and the confirmation of the presence of the antibiotic by a physicochemical method (liquid chromatography coupled with UV detection, fluorimetry or mass spectrometry) (Gaudin 2016).
Screening and detection methods are qualitative methods designed to distinguish positive samples from negative samples. The screening methods must be supplemented by confirmatory methods which are applied to the samples detected positive by the screening methods.
The chromatographic methods and electrophoresis produce precise results on the level of antibiotic residues (Orso et al. 2016; Dawadi et al. 2021).
HPLC is a physicochemical method that allows the detection and quantification of residues of a fairly wide range of antibiotics extending to all families used in human and veterinary medicine.
This is a much more selective and sensitive method than microbiological methods because it allows molecules to be identified separately and therefore avoids possible interference problems between substances (Bensakhria 2016; Peris-Vicente et al. 2022). Thus reversed-phase HPLC (RP HPLC) has become the most common method of separation and analysis (Shabir 2010).

To the best of our knowledge, there is no single HPLC method reported for the simultaneous determination of the selected three antibiotic compounds of three different therapeutic classes including β-lactams, tetracyclines, and amphenicols in honey samples. This work aimed to develop and validate a method for simultaneous determination of TC, FF, and PG residues in honey using HPLC with DAD and a simple sample preparation technique.

2. Materials and Method

2.1. Chemical and Reagents

HPLC gradient grade acetonitrile (ACN) and methanol (MeOH) were purchased from VWR chemicals. Oxalic acid, and potassium dihydrogen orthophosphate anhydrous (KH_2PO_4) were obtained from Analar. Citric acid anhydrous was purchased from HIMEDIA Laboratories. Disodium ethylenediamine tetra acetate (EDTA), Penicillin G potassium salt, and Formic acid (FA) were purchased from Sigma-Aldrich. Tetracycline, and Florfenicol was generously provided by Pharmadex S.a.l. (medicine factory, Beirut, Lebanon). All aqueous solutions were prepared with ultra-pure water (TKA, Micromed, Germany). The solid-phase extraction procedures were carried out using Waters SupelTM-Select HLB cartridge (200 mg, 6 mL) provided by Sigma-Aldrich.

2.2. Apparatus

All chromatographic readings were done using an HP 1100 Series LC system (Hewlett Packard, Palo Alto, CA, USA) equipped with a quaternary pump, a vacuum degasser, a column compartment, an auto sampler, and a diode-array detector, and controlled by the HP Chemstation chromatography software. For the method that will be adopted, the analytical column was Zorbax Eclipse XDB C8, (5 µm, 150 x 4.6 mm) (from Hewlett Packard, Palo Alto, CA, USA). Other equipments such as pH meter CG 820 (SCHOTT GERATE, made in West Germany), electronic weighing balance (RADWAG Wagi Electronic, Poland), Spectrafuge 6C compact centrifuge (Edtexison, NJ USA), Ultrasonic cleaner (BRANSON 200, made in Taiwan) and vortex made by Daihan Scientific Co. (Korea) are also used in this study.

2.3. Preparation of Standard Solutions

In order to obtain a final concentration of $1 mg.mL^{-1}$, a stock standard solution of FF, TC, and penicillin was prepared by dissolving 1 mg of the compound in 1 mL of ACN, MeOH, water/ACN (*v/v*; 1/1) respectively. The solutions were stored in dark vials at + 4 °C until further use. Working solutions were prepared daily by appropriate dilution of aliquots of the standard stock solutions in ultra-pure water. The working solutions were used for sample spiking for the preparation of calibration curves of 6 different concentrations.

2.4. Chromatographic conditions

The elution was conducted using a mobile phase system consisting of a mixture of KH_2PO_4/ACN (80:20). The mobile phase was mixed and sonicated for 5 min and then vacuum filtered through a 0.45 µm nylon filter.
Chromatographic separation of the analytes was achieved on Zorbax Eclipse C18 column, under isocratic mode allowing complete analysis in less than fifteen minutes. The flow rate was adjusted at 1 mL/min and the column thermostat was set at 35 °C. The injection volume was 25 µL, and the final run time of the method was 15 min. Detection wavelengths were set at 224 nm for FF, 230 nm for PE, and 350 nm for TC. While data analysis was performed utilizing the Hewlett-Packard ChemStation software.

2.5. Extraction and clean-up procedure

Extraction and clean–up procedures for samples were performed following the protocol of Kumar et al. (2020) with slight modifications. An aliquot of the honey sample (2.5 g) was taken in a 50 mL centrifuge tube. Then samples were dissolved in10 mL of 0.1M EDTA-McIlvaine buffer (pH 4.0) (prepared as described by Cinquina et al. (2003) followed by vigorous shaking for 5 min. The sample was then centrifuged at 6000 rpm for 10 min. The supernatant was collected and passed through a disposable Whatman membrane filter 0.45 µm (Whatman, Maidstone, UK) to remove any remaining milk flakes. Clean up of the extract was done by using SPE method. The filtrate was loaded on a Supel Select HLB (Hydrophilic-Lipophilic Balance) cartridge preconditioned with 3 mL of methanol followed by 2 mL of ultra-pure water under pressure. The antibiotics were eluted with 1.5 mL of MeOH after the sample cartridge was rinsed with 2 mL of water. The elute was collected and filtered through a 0.45 µm syringe filter before being kept in vials for further analysis.

2.6. Method validation

Before the validation steps, an optimization step was conducted, chromatographic parameters, including composition and flow rate of the mobile phase, gradient elution, injection volume, and column temperature, were studied in order to find the optimum conditions for chromatographic separation of all chemicals in a short amount of time.
The characteristics and the procedures used for validation were performed following the recommendations from the Commission Decision 2002/657/EC of the EU (2002), for the parameters selectivity, linearity, recovery (accuracy), decision limit (CCα), detection capacity (CCβ), and precision. The LOD and LOQ were calculated according to the guideline of the International Conference of Harmonization (ICH) Guidelines (Abraham, 2010). For the validation studies, the work solution was prepared by spiking the appropriate volume of working FF, PE, and TC standards in a blank honey sample (antibiotic-free).

2.7. Statistical analysis

All analyses were performed using Microsoft Excel 2016 (Microsoft Corporation, Redmond, WA, USA). Mean, standard deviations, range, R^2, % RSD, etc. were calculated for each targeted analyte using descriptive statistics.

3. Results and discussion

3.1. Optimization of chromatographic conditions

To achieve satisfactory chromatographic separation and high sensitivity, different solvent systems, to design suitable mobile phases, and columns were optimized. An aqueous mobile phase consisting of potassium dihydrogenophosphate (0.05 M) was the best system, with ACN and MeOH being examined as organic solvents to increase the sensitivity. Improved ATBs identification using ACN may be linked to MeOH's role in TC degradation. Liang et al. (1998) found that the degradation of TC is increased in MeOH solutions via functional group substitutions or additions to TC. The results of this study agreed with findings from these previous studies. This mobile phase still contains relatively high amounts of salts 80 % KH_2PO_4 to be used in conventional reversed-phase analytical columns. The initial mobile phase tests were conducted using a brand C18 column Hypresil-ODS, but the separation efficiency decreased in a short period of use. Thus, it was decided to use a column that resists mildly acidic conditions (Zorbax Eclipse Plus C18). for better selectivity, resolution, and to maximize the retention of FF and PG we used the Zorbax Eclipse which displays a good analysis and the peaks are well distinguished and to increase the sensitivity of the column. The mobile phase was tested to evaluate the separation and responses (analyte area) of a 200 µL of stock solution for each antibiotic, fortified blank honey sample with TC, FF, PG, and observations of peaks according to wavelengths respectively 350 nm, 224 nm, 230 nm.

Using the ODS Hypersil C18 column results showed that reducing the modifier component (MeOH and /or ACN) of the mobile phase decreased the retention times of ATBs involved in this study and generally deteriorates the separation among all of them (Table 1).

Table 1. Effect of mobile phase and column on analytes retention times.

%(KH_2PO_4/ ACN/MeOH)	Rts (min)			Column
	TC	PG	FF	
(90 /10/0)	2.8	3.3	9.9	ODS Hypersil C18
(90 /0/10)	2.8	2.8	13.4	ODS Hypersil C18
(80 /20/0)	2.3	3.1	3.6	ODS Hypersil C18
(75 /25/0)	2.6	3.2	3.5	ODS Hypersil C18
(40/40/20)	1.2	1.3	1.2	ODS Hypersil C18
(80/20/0)	3.2	6.6	9.7	Zorbax Eclipse. Plus

3.2. Method validation

The linearity response was examined by the external standard method. For this purpose, triplicate analysis of milk samples fortified with FF, PE, or TC at seven fortification levels ranging from 0.004 to 5 ppm were prepared and injected in triplicates. The standard calibration curves were generated for each analyte by plotting concentrations against the peak area of the analyte. The validating parameters of each calibration curve (slope (a), intercept (b), and correlation coefficient (R^2) are shown in Table 2. The correlation coefficient ranging between 0.9954 and 0.9969, indicates a strong linear relationship between the concentration of the analyte and the area under the peak.

The sensitivity of the method, i.e. the change in response on a measuring instrument divided by the corresponding change in stimulus, was represented by the slope of the calibration curve (Prichard et al. 2001).

The specificity of the method is defined as the ability to distinguish between an analyte and other substances (United Nations Office on Drugs and Crime & Laboratory and Scientific Section 2009). It was investigated by analysis of ten different blank milk samples to determine any interfering peaks from endogenous compounds.
LOD and LOQ established for this method were calculated from the standard deviation (σ) of y-intercepts of regression analysis and the calibration curve slope (m), according to equations 1 and 2 respectively (Abraham 2010).

$$LOD = 3.3\frac{\sigma}{m} \quad \text{(eq. 1)}$$

$$LOQ = 10\frac{\sigma}{m} \quad \text{(eq. 2)}$$

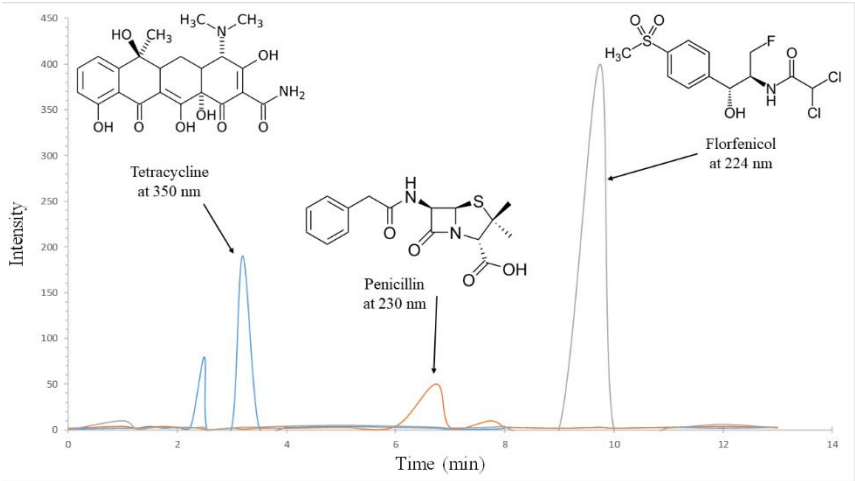

Fig. 1. Chromatograms of fortified honey extract.

Table 2. Regression analysis, LOD, and LOQ of TC, FF, and PG.

Antibiotic	Range ($mg.kg^{-1}$)	Slope	Intercept	Correlation coefficient	LOD ($mg.kg^{-1}$)	LOQ ($mg.kg^{-1}$)
TC	0.7 -17.5	0.0007	-0.2584	0.9969	0.514	1.85
FF	0.7 -17.5	0.01608	-1.5479	0.9963	0.571	1.90
PE	0.7 -17.5	0.0005	0.6675	0.9954	0.606	2.02

The decision limit (CCα) and the detection capability (CCβ) in the case of substances for which no authorized limit has been set, can be determined using the matrix-matched calibration curves. CCα was determined as the "corresponding concentration at the y-intercept plus 2.33 × the standard deviation of RSDR", while CCβ was calculated as the "concentration at the decision limit plus 1.64 × the standard deviation of RSDR" (European Commission 2002). The CCα values ranged from 588 to 863 $\mu g.kg^{-1}$, whereas the CCβ values varied in a range from 457 to 1000 $\mu g.kg^{-1}$. (CCβ) is above the limit of detection in all three antibiotics (

Table **3**).

Table 3. Results for decision limits (CCα), and detection capabilities (CCβ) obtained for the analyzed ATBs in Honey.

ATB	$mg.kg^{-1}$	
	CCα	**CCβ**
TC	0.710	0.609
FF	0.588	0.457
PG	0.863	1

The precision of the method consists of intra-assay precision and inter-assay precision, which was checking the percentage of relative standard deviation (% RSD) of peak areas. The intra-assay precision was confirmed by enriching honey blank sample with antibiotics of interest TC, PG, FF, at a single concentration level respectively (0.02 $mg.mL^{-1}$; 0.015 $mg.mL^{-1}$; 0.0125 $mg.mL^{-1}$) for 3 days (interday), and 11 injections per day (intraday). The data of the repeated analysis are shown in Table 4.

Table 4. Precision test of the method

AC	SD	RSD (%)	Intraday CV (%)	Interday CV (%)
TC	0.324	3.59	2.22	2.53
FF	3.71	4.42	2.23	3.06
PG	0.653	9.87	10.02	11.12

The CV for intraday precision varied from 2.22 % to 10.02 % and the CV for interday precision varied from 2.53 % to 11.12 %. These results are in agreement with the requirements set by the decision 2002/657/EC from the European Union, which is 10 to 20% depending on the concentration of the analyte. % RSD values for peak areas indicate the high precision of the chromatographic system.

3.3. Lebanese honey sample results:

In the absence of any study, to the best of our knowledge, dealing with the residues of antibiotics in honey in Lebanon, we have tried to apply the method to a small sample of honey. Ten honey samples were analyzed. Three of them are gratefully provided by three different farms from the south of Lebanon, the remaining are bought from the Lebanese market. Obtained results show that the samples contain no trace of these three antibiotics at the LODs of the method since chromatograms do not show any peaks on the specific retention times.

It is difficult to refer to Lebanese similar studies in order to compare the numbers we obtained or simply refer to them.

This research paper lays the first building block for a more comprehensive study that will cover all Lebanese regions at a later time, especially in the absence of monitoring and awareness of beekeepers, who are often not subject to any monitoring by the concerned national institutions.

4. Conclusion

To the best of our knowledge, this is the first study in which a fast and reliable method has been developed and validated for simultaneous detection and quantification of FF, PE, and TC in honey. The developed method validated according to recommended criteria of Commission Decision (EC) No 2002/657/EC provided good performance and satisfactory recovery, thus results showed the applicability for routine analysis of honey. Then, the validated method served to detect and quantify FF, PE, and TC residues in two samples from Lebanese farms. The overall results showed the absence of these antibiotics residues in the collected samples. Finally, this validated method can be applied to conduct a comprehensive survey of the whole Lebanese territory by analyzing a sufficient number of samples.

Acknowledgements

The authors are grateful to the Lebanese University; the Faculty of Pharmacy department- Lebanon- for providing all chemicals necessary to carry out this project.

Authors' contributions:

The article is written and designed by A.J., E.C.; Data analyzes were determined by A.J.; Experiments was done by B.R.

Conflict of interest disclosure:

The authors declare that there is no real, potential, or perceived conflict of interest for this article.

References

Abraham J. 2010. International Conference On Harmonisation Of Technical Requirements For Registration Of Pharmaceuticals For Human Use. In Handbook of Transnational Economic Governance Regimes. Brill | Nijhoff, Leiden, pp 1041–1053.

Bensakhria A. 2016. Chromatographie Liquide Haute Performance (HPLC) » Analytical Toxicology. https://www.analyticaltoxicology.com/chromatographie-liquide-haute-performance-hplc. Accessed 22 Sept 2021.

Bonerba E, Panseri S, Arioli F, Nobile M, Terio V, Di Cesare F, Tantillo G, Maria Chiesa L. 2021. Determination of antibiotic residues in honey in relation to different potential sources and relevance for food inspection. Food Chem. 334:127575.

Cinquina AL, Longo F, Anastasi G, Giannetti L, Cozzani R. 2003. Validation of a high-performance liquid chromatography method for the determination of oxytetracycline, tetracycline, chlortetracycline and doxycycline in bovine milk and muscle. J Chromatogr A. 987(1):227–233.

Dawadi S, Thapa R, Modi B, Bhandari S, Timilsina AP, Yadav RP, Aryal B, Gautam S, Sharma P, Thapa BB, Aryal N, Aryal S, Regmi BP, Parajuli N. 2021. Technological advancements for the detection of antibiotics in food products. Processes. 9(9):1500.

European Commission 2002. Commission Decision of 12 August 2002 implementing Council Directive 96/23/EC concerning the performance of analytical methods and the interpretation of results. L221/8:8–36.

European Commission 2010. Commission Regulation (EU) No 37/2010 of 22 December 2009 on pharmacologically active substances and their classification regarding maximum residue limits in foodstuffs of animal origin. 5(470):1–72.

Forsgren E. 2010. European foulbrood in honey bees. J Invertebr Pathol, 103:S5–S9.

Gaudin V. 2016. Caractérisation de la performance et validation des méthodes de dépistage des résidus d'antibiotiques dans les denrées alimentaires. Université Rennes 1. Juin 2016.

Johnson S, Jadon N. 2010. Antibiotic residues in honey. Centre for Science and Environment, New Delhi, September 2010.

Kumar A, Gill JPS, Bedi JS, Chhuneja PK, Kumar A. 2020. Determination of antibiotic residues in Indian honeys and assessment of potential risks to consumers. J Apic Res. 59(1):25–34.

Lana S, Marwan M. 2016. Honey: Lebanons golden elixir (pp. 1–5). BLOMINVEST BANK. https://blog.blominvestbank.com/wp-content/uploads/2016/11/Honey-Lebanons-Golden-Elixir-2.pdf. Accessed 10 Sept 2021.

Liang Y, Denton MB, Bates RB. 1998. Stability studies of tetracycline in methanol solution. J. Chromatogr. A. 827(1):45–55.

Lima CMG, Nora FMD, Seraglio SKT, Da Silva JM, Marzoque HJ, Santana RF, Verruck S, Scussel VM. 2020. Antibiotic residues in honey: A public health issue. Res Soc Dev. 9(11):e1739119604.

Majewska E, Drużyńska B, Wołosiak R. 2019. Determination of the botanical origin of honeybee honeys based on the analysis of their selected physicochemical parameters coupled with chemometric assays. Food Sci Biotechnol. 28(5):1307–1314.

Orso D, Floriano L, Ribeiro LC, Bandeira NMG, Prestes OD, Zanella R. 2016. Simultaneous determination of multiclass pesticides and antibiotics in honey samples based on ultra-high performance liquid chromatography-tandem mass spectrometry. Food Anal Methods. 9(6):1638–1653.

Peris-Vicente J, Peris-García E, Albiol-Chiva J, Durgbanshi A, Ochoa-Aranda E, Carda-Broch S, Bose D, Esteve-Romero J. 2022. Liquid chromatography, a valuable tool in the determination of antibiotics in biological, food and environmental samples. Microchem J. 177:107309.

Prichard FE, Prichard E, Green J. 2001. Analytical measurement terminology: Handbook of terms used in quality assurance of analytical measurement. Royal Society of Chemistry.

Serwecińska L. 2020. Antimicrobials and antibiotic-resistant bacteria: A risk to the environment and to public health. Water. 12(12):3313.

Shabir GA. 2010. Development and validation of a reversed-phase HPLC method for the determination of hydroxybenzene in a cream formulation. Indian J Pharm Sci. 72(3):307–311.

United Nations Office on Drugs and Crime & Laboratory and Scientific Section. 2009. Guidance for the validation of analytical methodology and calibration of equipment used for testing of illicit drugs in seized materials and biological specimens: A commitment to quality and continuous improvement. United Nations.

Vidal-Naquet N. 2012. Les maladies de l'abeille domestique d'élevage, *Apis mellifera* l. Bull Acad Vét France. 165(4):307–316.

REVIEW ARTICLE
Eurasian J Bio Chem Sci, 5(Suppl 1):162-165, 2022
https://doi.org/10.46239/ejbcs.1130645

EJBCS

Eurasian Journal of Biological and Chemical Sciences

Journal homepage: www.dergipark.org.tr/ejbcs

Phenolic compounds that modulate the multi drug resistance through inhibiting of P-glycoprotein encoded by gene ABCB1

Onder Yumrutas[1*], Pınar Yumrutas[2]

[*1] *University of Adıyaman, Faculty of Medicine, Department of Medical Biology, 02200, Adıyaman-Türkiye*
[2] *University of Gaziantep, Faculty of Medicine, Department of Respiratory Disease and Cancer Biology, 27410, Gaziantep-Türkiye*

*Corresponding author : yumrutasonder@gmail.com
Orcid No: https://orcid.org/0000-0001-9657-8306

Received : 15/06/2022
Accepted : 16/10/2022

Abstract: One of the most important challenges in the fight against cancer is acquired/multi drug resistance. P-glycoprotein (P-gp), encoded by gene ABCB1 (or MDR1) in many organs, is one of the important factors involved in the development of drug resistance. P-gp is mainly involved in efflux of toxic substances such as xenobiotics from the cell. Also, it plays a role the efflux of drugs used in the treatment of cancer, and so, it reduces the rate of success in cancer treatment. Phenolic compounds are chemicals that are naturally synthesized in plants and have many biological activities such as especially antioxidant and anticancer. In previous studies, it was determined that in addition to anticancer activities of the phenolic compounds, they modulate the multi drug resistance by inhibiting the expression and function of P-gp. In this review, phenolic compounds that play a role in modulating the multi-drug resistance by inhibiting the activation and expression of P-gp are discussed.

Keywords: Cancer, multi drug resistance, phenolics, P-glycoprotein, ABCB1, MDR1

1. Introduction

Cancer resistance

Cancer is a disease that has been trying to cure for a long time. Millions of people die every year because of the cancer (Sung et al. 2021). In cancer treatment, applications such as chemotherapy, radiotherapy and surgery are basically used. (Jaklitsch et al. 2003; Chabner and Roberts 2005; Kaur et al. 2011). Among these methods, the chemotherapy is used first for the basic inhibition of proliferation, invasion, and metastasis on cancer cells. Despite the positive effects of drugs used for cancer treatments, in some cases there is a resistance to these drugs and the drugs used are excreted from cancer cells by different mechanisms (Gottesman et al. 2002). Because of this efflux, the fight against cancer can be significantly inhibited.

Multi-drug resistance (MDR) pumps serve in the efflux of cancer drugs. These proteins generally play an important defense role when cells are exposed to xenobiotics. While these proteins usually take part in the efflux of toxic substances out of the cell, they can also take part in the removal of different substances (Gottesman et al. 2002). This system also captures the chemotherapeutic agents applied to cancer cells as a foreign substance and immediately sends them out of the cell. Therefore, resistance to chemotherapeutic agents is acquired in cancer cells.

Targeting of P-glycoprotein in modulation of MDR

ATP dependent pumps send many of substrate compounds out of cells to prevent toxicity in many cells (Ford and Beis 2019). The most known of these transporters is P-glycoprotein (P-pg) which is one of the first members described of a large family of ATP-dependent transporters known as the ATP-binding cassette (ABC) family and it is encoded by the ABCB1 (MDR1) gene. P-gp is a protein consisting of two nucleotide binding and two drug binding domains (Gillet and Gottesman 2009; Mollazaleh et al. 2018). There are many studies showing the roles of this efflux pump in cancer resistance (Waghray and Zhang 2017; Shi et al. 2020; Huang et al. 2021).

The P-gp is expressed in most cancer cells. Although P-gp is inhibited by synthetic blocker compounds such as verapamil and cyclosporin (Sikic et al. 1997), undesirable side effects may occur for normal cells due to these compounds. Moreover, it is very interesting that natural compounds and herbal drugs have less side effects than synthetics and have versatile effects at appropriate doses. In previous studies, it has been reported that these transport proteins are suppressed using phytochemicals together with cancer drugs and chemotherapeutic agents remain in cancer cells (Molnár et al. 2010; Teng et al. 2021; Teng et al. 2022).

There are many studies showing the inhibitory effects of plant extracts and phytochemicals on cancer cells (Yumrutas et al. 2015; Yumrutas et al. 2018; Cocelli et al. 2021). It has been proven that isolated phytochemicals are responsible for many biological activities and can also be used in the prevention of cancer by acting on the molecular pathways involved in the pathogenesis of cancer. (Saklani and Kutty 2008). The effects of natural compounds in modulating the multidrug resistance have been discovered as well as inhibition of proliferation of cancer cells, induction of apoptosis, arresting of cell cycle and induction of ROS.

Among the most well-known of these compounds, phenolic compounds have been demonstrated to have biological activities including anticancer (Yumrutas et al. 2018), antioxidant (Erkan et al. 2008), anti-inflammatory (Rocha et al. 2015), antimicrobial (Mandal et al. 2017), wound healing (Ozay et al. 2019). Phenolic compounds include many kind such as flavonoids, lignans, phenolic acids, stilbenes and tannins (Amarowicz and Pegg 2019)

The multi drug resistance can lead to the increased drug absorbance, increased drug efflux, altered drug metabolism, altered treatment target and apoptotic pathway, epigenetic changes, and differences in tumor microenvironment (Holohan et al. 2013; Whang et al. 2019; Zheng et al. 2021). To reduce these effects, it is thought that the increase in the discover of active compounds such as phenolics will significantly support the fight against cancer.

Phenolic compounds that modulates the MDR

Phenolic compounds are secondary compounds synthesized in almost all plants. These compounds are synthesized via the shikimic acid and phenylpropanoid pathway (Laura et al. 2019). Many biological activities of phenolic compounds have been studied for many years. Antioxidant activity is among the most well-known activities (Shahidi and Ambigaipalan, 2015). They exhibit important biological activities by acting on the factors involved in many pathways. Therefore, they exhibit important biological activities (Xu et al., 2021; Roleira et al. 2015; de Oliveira et al. 2021). Phenolic compounds have been determined the roles in modulating of drug resistance in cancer cells and their mechanisms of action on P-gp are mentioned below:

5-hydroxy-7,8-dimethoxyflavanone:5-hydroxy-7,8-dimethoxyflavanone is a flavonoid compound derived from *Fissistigma cupreonitens* (Theng et al., 2021). It was reported that it significantly inhibited function of P-gp at a concentration of 2.5 µg/ml. Therefore, it modulated the MDR inhibiting the efflux of doxorubicin, a drug which being used in cancer treatment, out of the cancer cells. Also, MDR was decreased in the multidrug resistant cervical cancer cell line KB/VIN exposed to Vincristine, Paclitaxel, and Doxorubicin (Theng et al., 2021) in a dose dependent manner.

Kaempferol: It is an important flavonol found in many plants. It suppressed P-gp expression and significantly inhibited its activity in multi-drug resistant cancer cells (KB-V1). However, it increased intracellular drug accumulation. In addition, extracellular efflux of vinblastine was significantly reduced. (Limptrakul et al., 2005).

Cinnamophilin: It is a phenolic lignan obtained from *Cinnamomum philippinense*. In a previous study, when given with drugs such as docetaxel, vincristine, and paclitaxel, it provided modulation of MDR. In addition, the efflux function of p-gb was significantly inhibited and therefore the efflux of doxorubicin was also inhibited (Theng et al. 2021b).

Silychristin A ve 2,3-dehydrosilychristin A: Silychristin A and 2,3-dehydrosilychristin A are the second most abundant derivatives of silymarin. Dose-dependent inhibition of P-gp was observed after administration of silychristin A and 2,3-dehydrosilychristin A. In addition, drug sensitivity was decreased in doxorubicin-resistant ovarian cancer cells. In the same study, the anhydro- and iso- derivatives of silychristin A, In addition to Silychristin A and 2,3-dehydrosilychristin A, not only inhibited the function of P-gp but also reduced its expression (Viktorová et al., 2019).

Caffeic acid: Teng et al (2020) reported that exposure of ABCB1/Flp-InTM-293 and KB/VIN cells with multi-drug resistance to caffeic acid causes inhibition of p-gb protein and reverses MDR resistance. In addition, it was stated that this effect was demonstrated by caffeic acid's binding to P-gp via GLU74 and TRY117 residues.

Procyanidin (catechin-3-O-2-leucocyanidin): It is a polyphenol flavonoid compound found in many fruits and vegetables. In a previous study conducted with human ovarian multidrug resistant subline (A2780) cell line, it was determined that the cell viability was significantly reduced after the application of dose-dependent procyanidin given with paclitaxel and adriamycin. In addition, Procyanidin down-regulated the mRNA and protein expression of MDR1 in resistant A2780 cells through NF-kB inhibition. In addition, MDR1 was suppressed by time-dependent inhibition of YB-1 nuclear translocation through inhibition of the MAP/ERK pathway in A2780/T cells treated with procyanidin (Zhao et al., 2013).

Emodin (1, 3, 8-trihydroxy-6-methylanthra-quinone) and Rhein: Emodin and Rhein are members of anthraquinones, a subgroup of phenolic compounds. (Teng et al, 2022). In a previous study, it observed a decrease the P-gp protein expression in adriamycin-resistant K562/ADM cells. It was stated that P-gp can bind to the R-site, reducing the function of P-gp and reversing MDR (Min et al., 2017). Moreover, Rhein was involved in the correction/modulation of MDR by causing downregulation of P-gp in KB/VIN cells. (Teng et al, 2022).

Conclusion

The roles of phenolics in the elimination of acquired resistance caused by chemotherapeutic agents used in the treatment of cancer have been proven in many studies. In particular, when the effects of phenolics on P-gp expression and function are evaluated, it is thought that the use of these

compounds together with chemotherapeutic agents in the clinic will have important effects. However, most of the studies showing the relationship between phenolic compounds and P-gp have been run by using the cell experiments. In order to evaluate the effects of phenolics on P-gp, the number of in vivo experiments should be also increased. In addition, phenolics can be effluxed by ABC pumps, and this should be taken into account in future studies.

Authors' contributions: ÖY and PY contributed equally to the preparation of this review.

Conflict of interest disclosure: Authors declare no any conflict of interest

References

Amarowicz R, Pegg RB. 2019. Natural antioxidants of plant origin. In Advances in food and nutrition research (Vol. 90, pp. 1-81). Academic Press.

Chabner BA, Roberts TG. 2005. Chemotherapy and the war on cancer. Nat Rev Cancer. 5: 65-72.

Cocelli G, Pehlivan M, Yumrutas O. 2021. Sideritis perfoliata inhibits cell proliferation, induces apoptosis and exhibits cellular antioxidant activity in cervical cancer cells. BLACPMA. 20(4).

de Oliveira EF, Yang X, Basnayake N, Huu CN, Wang L, Tikekar R, Nitin N. 2021. Screening of antimicrobial synergism between phenolic acids derivatives and UV-A light radiation. Journal of Photochemistry and Photobiology B: Biology. 214: 112081.

Erkan N, Ayranci G, Ayranci E. 2008. Antioxidant activities of rosemary (Rosmarinus Officinalis L.) extract, blackseed (Nigella sativa L.) essential oil, carnosic acid, rosmarinic acid and sesamol. Food Chem. 110: 76-82.

Ford RC, Beis K. 2019. Learning the ABCs one at a time: structure and mechanism of ABC transporters. Biochem Soc Trans 47: 23-36.

Gillet JP, Gottesman MM. 2009. Mechanisms of Multidrug Resistance in Cancer. Multi-Drug Resistance in Cancer. 47-76.

Gottesman MM. 2002. Mechanisms of cancer drug resistance. Annu Rev Med. 53: 615-627.

Holohan S, Van Schaeybroeck DB, Longley PG. 2013. Johnston, Cancer drug resistance: an evolving paradigm. Nat Rev. Cancer. 13: 714-726

Huang Y, Zhang J, Zhang Y, Shi L, Qin X, Lu B, Ding Y, Wang Y, Chen T, Yao Y. 2021. P-glycoprotein suppression by photothermal-responsive nitric oxide releasing nanoplatform for triple-combination therapy of multidrug resistant cancer. Mater Des. 211:110160.

Jaklitsch MT, Mery CM, Audisio RA. 2003. The use of surgery to treat lung cancer in elderly patients. Lancet Oncol. 4: 463-471.

Kaur P, Hurwitz MD, Krishnan S, Asea A. 2011. Combined hyperthermia and radiotherapy for the treatment of cancer. Cancers. 3: 3799-3823.

Laura A, Moreno-Escamilla JO, Rodrigo-García J, Alvarez-Parrilla E. 2019. Phenolic compounds. In *Postharvest physiology and biochemistry of fruits and vegetables* (pp. 253-271). Woodhead Publishing.

Limtrakul P, Khantamat O, Pintha K. 2005. Inhibition of P-glycoprotein function and expression by kaempferol and quercetin. J Chemotherapy. 17: 86-95.

Mandal SM, Dias RO, Franco OL. 2017. Phenolic compounds in antimicrobial therapy. J Med Food. 20: 1031-1038.

Min H, Niu M, Zhang W, Yan J, Li J, Tan X, Li B, Su M, Di B, Yan F. 2017. Emodin reverses leukemia multidrug resistance by competitive inhibition and downregulation of P-glycoprotein. PLoS ONE 12: e0187971

Mollazadeh S, Sahebkar A, Hadizadeh F, Behravan J, Arabzadeh, S. 2018. Structural and functional aspects of P-glycoprotein and its inhibitors. Life Sci. 214:118-123.

Molnár J, Engi H, Hohmann J, Molnár P, Deli J, Wesolowska O, Michalak K, Wang Q. 2010. Reversal of multidrug resistance by natural substances from plants. Curr Top Med Chem.10: 1757-1768.

Özay Y, Güzel S, Yumrutaş Ö, Pehlivanoğlu B, Erdoğdu İH, Yildirim Z, Turk BA, Darcan S. 2019. Wound healing effect of kaempferol in diabetic and nondiabetic rats. J Surg Res. 233: 284-296.

Roleira FM, Tavares-da-Silva EJ, Varela CL, Costa SC, Silva T, Garrido J, Borges F. 2015. Plant derived and dietary phenolic antioxidants: Anticancer properties. Food Chemistry. 183: 235-258.

Rocha J, Eduardo-Figueira M, Barateiro A, Fernandes A, Brites D, Bronze R, Duarte CMM, Serra AT, Pinto R, Freitas M, Fernandes E, Silva-Lima B, Mota-Flipe H, Sepodes B. 2015. Anti-inflammatory effect of rosmarinic acid and an extract of Rosmarinus officinalis in rat models of local and systemicinflammation. Basic Clin Pharmacol Toxicol. 116: 398-413.

Saklani A, Kutty SK. 2008. Plant-derived compounds in clinical trials. Drug Discov. Today. 13, 161-171.

Shahidi F, Ambigaipalan P. 2015. Phenolics and polyphenolics in foods, beverages and spices: Antioxidant activity and health effects–A review. Journal of functional foods. 18: 820-897.

Shi X, Valizadeh A, Mir SM, Asemi Z, Karimian A, Majidina M, Safa A, Yosefi B. 2020. miRNA-29a reverses P-glycoprotein-mediated drug resistance and inhibits proliferation via up-regulation of PTEN in colon cancer cells. Eur J Pharmacol: 880:173138.

Sikic BI, Fisher GA, Lum BL, Halsey J, Beketic-Oreskovic L, Chen G. 1997. Modulation and prevention of multidrug resistance by inhibitors of P-glycoprotein. Cancer Chemother Pharmacol. 40: S13-S19.

Sung H, Ferlay J, Siegel RL, Laversanne M, Soerjomataram I, Jemal A, Bray F. 2021. Global cancer statistics 2020: GLOBOCAN estimates of incidence and mortality worldwide for 36 cancers in 185 countries. CA: a cancer journal for clinicians. 71: 209-249.

Teng YN, Huang BH, Huang SY, Wu IT, Wu TS, Lee TE, Hung CC. 2021. Cinnamophilin overcomes cancer multi-drug resistance via allosterically modulating human P-glycoprotein on both drug binding sites and ATPase binding sites. Biomed Pharmacother. 144: 112379.

Teng, YN, Kao MC, Huang SY, Wu TS, Lee TE, Kuo CY, Hung CC. 2022. Novel application of rhein and its prodrug diacerein for reversing cancer-related multidrug resistance through the dual inhibition of P-glycoprotein efflux and STAT3-mediated P-glycoprotein expression. Biomed Pharmacother. 150: 112995.

Teng YN, Lin KI, Lin YC, Thang TD, Lan YH, Hung CC. 2021. A novel flavonoid from Fissistigma cupreonitens, 5-hydroxy-7, 8-dimethoxyflavanone, competitively inhibited the efflux function of human P-glycoprotein and reversed cancer multi-drug resistance. Phytomedicine. 85: 153528.

Teng YN, Wang CC, Liao WC, Lan YH, Hung CC. 2020. Caffeic acid attenuates multi-drug resistance in cancer cells by inhibiting efflux function of human P-glycoprotein. Molecules. 25: 247.

Viktorová J, Dobiasová S, Řehořová K, Biedermann D, Káňová K, Šeborová K, Václavíková R, Valentová K, Ruml T, Křen V, Macek T. 2019. Antioxidant, anti-inflammatory, and multidrug resistance modulation activity of silychristin derivatives. Antioxidants. 8: 303.

Waghray D, Zhang Q. 2017. Inhibit or evade multidrug resistance P-glycoprotein in cancer treatment: miniperspective. J Med Chem. 61:5108-5121.

Xu QN, Zhu D, Wang GH, Lin T, Sun CL, Ding R, Tian WJ, Chen HF. 2021. Phenolic glycosides and flavonoids with antioxidant and anticancer activities from Desmodium caudatum. Natural Product Research. 35: 4534-4541.

Yumrutas O, Oztuzcu S, Pehlivan M, Ozturk N, Poyraz IE, Iğci YZ, Cevik MO, Bozgeyik I, Aksoy AF, Bağış H, Arslan A. 2015. Cell viability, anti-proliferation and antioxidant activities of Sideritis syriaca, Tanacetum argenteum sub sp. argenteum and Achillea aleppica subsp. zederbaueri on human breast cancer cell line (MCF-7). J Appl Pharm Sci. 5: 001-005.

Yumrutaş Ö, Pehlivan M, Güven C, Bozgeyik I, Bozgeyik E, Yumrutas P,Temiz E, Üçkardeş F. (2018). Investigation of cytotoxic effect of salvia pilifera extracts and synthetic chlorogenic and caffeic acids on DU145 prostate cancer cells line. KSÜ Doğa Bilimleri Dergisi. 21:141-147.

Zhao BX, Sun YB, Wang SQ, Dua L, Huo QL, Ren F, Li GF. 2013. Grape seed procyanidin reversal of p-glycoprotein associated multi-drug resistance via down-regulation of NF-κB and MAPK/ERK mediated YB-1 activity in A2780/T cells. PloS ONE. 8: e71071.

EJBCS